Biochemical Analysis of HYAL2: Studies of patient mutations and identification of interacting proteins

by

Promita Ghosh

A Thesis submitted to the Faculty of Graduate Studies of

The University of Manitoba

in partial fulfillment of the requirements of the degree of

Master of Science

Department of Biochemistry and Medical Genetics

Faculty of Health Sciences

University of Manitoba

Winnipeg

ABSTRACT

Hyaluronic acid (HA) is abundantly present in the extracellular matrix (ECM) and reported to have a functional role during embryonic development. Among ECM components, HA has one of the fastest rates of turnover and is facilitated by hyaluronidases (HYALs). HYAL1 and HYAL2 are the predominant HYALs associated with the HA catabolism in somatic tissues. HYAL2 being a GPI-anchored cell-surface hyaluronidase is presumed to generate HA fragments (10-20 kDa) from large-sized extracellular HA (>200 kDa) followed by further degradation in the lysosomes into tetrasaccharides. *Hyal2* knockout (KO) mice displayed craniofacial abnormalities and severe pre-weaning lethality. High frequency ultrasound of *Hyal2* KO mouse hearts revealed atrial dilation and 50 % of *Hyal2* KO mice exhibited a triatrial heart (cor triatriatum). Two separate mutations- K148R and P250L in *HYAL2* were found to be associated with syndromic cleft palate. Recently, whole exome sequencing revealed seven new *HYAL2* variants and we hypothesized that these gene variants interfere with the cellular role of HYAL2 by affecting its stability and cell-surface localization. Very low or a complete absence of expression were observed from the variants and the cell-surface localization of HYAL2 were severely compromised. Our biochemical analysis confirms that these seven variants are novel HYAL2 mutations.

Levels of HA during different stages of embryonic development are finely regulated. The action of HYAL2 towards HA removal can be explained by the excessive accumulation of HA in *Hyal2* KO mouse tissues. But, assaying the activity of HYAL2 directly has been a challenge in the field likely due to the lack of enough information on its mechanism of action. We speculate that HYAL2's activity is regulated to allow its activation only at specific times. Searching for possible interacting protein partners of HYAL2 can provide mechanistic insight into the HYAL2 regulation. We employed proximity labeling system to report a library of possible interactors of HYAL2 that can be further validated experimentally to delineate their cellular function in the HYAL2 interactome. The results reported herein, define an extensive network of interactions of HYAL2 that may facilitate identification of HYAL2 regulators which can be pivotal to assay the activity of HYAL2 in the future.

DEDICATION

"We can judge our progress by the courage of our questions and the depth of our answers, our willingness to embrace what is true rather than what feels good."

— Carl Sagan

Dedicated to my loving parents, Shrabani Ghosh and Manimay Ghosh, my little brother, Sumalya Ghosh for their invaluable support, sacrifice and love throughout my academic journey

&

the love of my life, Amitava Banerjee, for inspiring me every day to be the best version of myself.

ACKNOWLEDGEMENTS

I made a journey of over 7000 miles from my city, Kolkata to Winnipeg to pursue my dream of becoming a passionate independent researcher. After 2 years of my Master's program at this university, I am glad about the decision I took two years ago. I would like to express my heartfelt gratitude and appreciation for my supervisor, Dr. Barbara Triggs-Raine, for bringing out the best in me. I will fall short of words to express how instrumental she has been for every little success I had here. Her wise words of advice, invaluable guidance and unfailing encouragement have truly empowered me. She has taught me how to collect my thoughts, process them critically, organize the data and work collaboratively in a team. I would deeply treasure our one to one discussions in her office regarding my research questions and academic endeavours which have helped me immensely to recognize my potentials and caveats. She is truly my idol and I am thankful to her for this wonderful opportunity which allowed me to work under her precious supervision.

I would gratefully acknowledge our research associate, Dr. Richard (Rick) Hemming. I consider myself fortunate to have had a chance to work with Rick on several projects. He has been one of the biggest strengths of the Triggs-Raine lab and definitely one of the key persons in my Master's research career. I am thankful for the countless hours he has dedicated to teach me valuable techniques, shared his knowledge and provided significant inputs for my project. I have largely benefitted from his academic experiences which have helped me to design my experiments and manage my time wisely. His thoughtful questions about my project have enriched me and built my confidence over the course of my degree.

I would like to thank my committee members, Dr. David Merz and Dr. Suresh Mishra for being the most supportive mentors one could ask for. Their in-depth analysis of my results, reflective questions regarding my project and valuable remarks have helped me to self-reflect which I believe have been significant in sharpening my research acumen.

I sincerely thank Dr. Oleg Krokhin and his team at the Manitoba Centre for Proteomics for analyzing the data which is a crucial part of my thesis. I thank them for their patience with my samples and insightful knowledge that they shared with me.

I thank Agnes Fresnoza and Dr. Wafa Kammouni (past) for helping me with everything when I started in the lab. Unwinding with Agnes over our coffees has been very refreshing for me. I also

thank our team of smart Summer/Co-op students-Emily Barker, Megan Rodriguez, Natasha Osawa, Steven Cooper and Nikolas Furletti for every little help they forwarded me in the lab and for sharing their valuable feedbacks regarding my project.

I thank the entire faculty at Dept. of Biochemistry and Medical Genetics for their valuable inputs during seminars and classes. I am thankful to BMG office staff, Lisa Zhang (past), Philip Dufresne, Chloe Lepage (past) and Annan Sher for taking care of my personal requests and for reminding me of the important deadlines I tended to forget. I must acknowledge the wonderful friends I have made in this journey. I thank Tasnim Beacon, NuwanthikaGimhani, Manisha Bungsy, Samira Seif and Chloe Lepage for making this 2 year journey so memorable for me.

I thank University of Manitoba, NSERC and my supervisor for taking care of my financial aids. It has been a pleasure being a part of UofM student community and a member at the Triggs-Raine lab. These unforgettable 2.5 years of my academic career is the best I could have asked for.

TABLE OF CONTENTS

List of Tables

List of Figures

List of Abbreviations

‘~ ‘ Approximately

Ala [A]- Alanine

Amp^{r}- ampicillin resistance

ApE- A Plasmid Editor software

Arg [R]- Arginine

Ab- Antibody

AP- Anchored protein

AV- Atrioventricular

bp- base pair

BSA- Bovine Serum Albumin

BioID/BioID2- Biotin Identification

C- Control

Cys [C]- Cysteine

cDNA- complementary DNA

CD44- cluster of differentiation antigen 44

CD- cluster of differentiation

CMV- Cytomegalovirus

CL/P- cleft lip and palate

CP- cleft palate

Da – Dalton

1D- one dimensional

del- Deletion

DMEM- Dulbecco's modified Eagle’s medium

DNA- Deoxyribonucleic acid

DTT- Dithiothreitol

E- embryonic day

ECM- extracellular matrix

ELISA- enzyme linked immunosorbent assay

EMT- epithelial to mesenchymal transition

ER- Endoplasmic Reticulum

F [Phe]- phenylalanine

F425V- Phenylalanine at position 425 changed to Valine (V)

FBS- Fetal Bovine Serum

Fig- Figure

GAG- glycosaminoglycans

GFP- green fluorescent protein

Gly[G]- Glycine

G204A- Glycine (G) at position 204 changed to Alanine (A)

GlcA- glucuronic acid

GlcNAc- N-acetylgucosamine

GPI- glycosylphosphatidylinositol

GPM- Global proteome machine

GO- Gene Ontology

HA- hyaluronan/hyaluronic acid

HAS-hyaluronan synthase

HARE- HA receptor for endocytosis

HEK293 cells- Human Embryonic Kidney 293 cells

HEPES- 4-2-hydroxyethyl-1-piperazineethanesulfonic acid

HMM- high molecular mass

HRP- Horseradish peroxidase

HYAL- Hyaluronidase

Hyal2$^{-/-}$/Hyal2 KO- HYAL2 knockout

Hyal2$^{+/+}$/HYAL2 WT- Hyal2 wild type

HYAL2- human HYAL2

HYALP1- Hyaluronidase pseudogene 1

IF- Immunofluorescence

K- Lysine

KO- knockout

kDa-kilodalton

L- Leu/leucine

L238R- Leucine at position 238 changed to Arginine (R)

LB- Luria broth

LC- liquid chromatography

LMM- low molecular mass

log (I)- the base-10 log of the sum of the fragment ion intensities in the tandem mass spectra

LYVE-l- Lymphatic vessel endothelial receptor-1

M- Molar

M-CSF- macrophage colony-stimulating factor

MCS- Multiple cloning site

MEF- mouse embryonic fibroblast

$MgCl_2$- Magnesium chloride

$MgSO_4$- Magnesium Sulphate

mM- Milli Molar

mg- milligram

min- minutes

mm- millimeter

MPS-mucopolysaccharidosis

MS- mass spectrometry

MS/MS- Tandem Mass spectrometry

m/z- mass-to-charge ratio

Na_2HPO_4- sodium hydrogen phosphate

NaCl- Sodium chloride

NH_4HCO_3- Ammonium bicarbonate

NHE1- Na+/H+ exchanger 1

ng-nanogram

nm-nanometers

o-HA- Hyaluronic acid oligosaccharides

OD- optical density

OFC- Occipital Frontal Circumference

P- Pro/proline

PBS- phosphate buffered saline

PCR- polymerase chain reaction

PG- proteoglycan

PH20- sperm surface protein 20

PI-PLC- Phosphoinositide phospholipase C

PPI- Protein-protein interaction

R- Arginine/Arg

R295X- Arginine at position 295 changed to a stop codon (X)

R277C- Arginine at position 277 changed to Cysteine (C)

Rep- Replicate

RHAMM- receptor for HA-mediated cell motility

S- Serine/Ser

S65X- Serine at position 65 is changed to a stop codon (X)

SEM- standard error mean

SDS- sodium dodecyl sulfate

SDS-PAGE- SDS-polyacrylamide gel electrophoresis

SOC- super optimal broth with catabolite repression

SPAM1- sperm adhesion molecule 1

TBST- Tris-buffered saline with 1% Tween-20

TEMED- tetramethylethylenediamine

TLR- Toll-like receptors

U- Unit

UDP- uridine diphosphate

V- valine

VEGF- vascular endothelial growth factor

v/v- Volume by volume

w/v- weight by volume

WT- Wild type

X- Termination or stop codon

µM- micro molar

µg- microgram

µl- microliter

CHAPTER 1: INTRODUCTION AND BACKGROUND

1.1. Hyaluronic acid (HA) - an overview

The extracellular matrix (ECM) serves as the non-cellular backbone of all tissues and is widely involved in development and differentiation [1]. Constant remodeling and turnover make ECM a dynamic entity. Hyaluronan/hyaluronic acid (HA) is one of the most abundant and unique components of the ECM. In 1934, Karl Meyer identified HA as a component of the vitreous humor[2]. The term 'hyaluronic' was derived from the Greek word 'hyalos' meaning glass. In contrast to other glycosaminoglycans (GAGs), it is not sulfated nor protein-bound and is composed of repeating polymeric disaccharides of D-glucuronic acid and N-acetyl-D-glucosamine[3]. HA is synthesized in the cell membrane instead of the Golgi and ultimately released into the extracellular space. It is particularly abundant in loose connective tissues such as the skin and synovial fluid [4-5]. Based on previous studies in rat and other species, it is estimated that skin contains 50% of the total HA, 25% is found in the skeleton and joints, and the rest is present in brain, kidney, lung and muscle[4]. High levels of HA are also present in visceral organs and the developing embryo[6].

Physico-chemical properties including viscoelasticity, high moisture retention capacity, high biocompatibility, and hygroscopic properties make HA an excellent lubricant, shock absorber, joint structure stabilizer, and water balance and flow resistance-regulator [7]. Available data suggest physiological roles of HA in cell-differentiation, tissue injury and wound-healing. HA also provides the backbone for vessel formation or angiogenesis and fibroblast migration [3, 7]. A HA-enriched matrix promotes cell migration and proliferation crucial during early developmental processes and regeneration stages in tissue remodeling [4].

Data suggest that the functional role of HA depends on its size. HA of high molecular mass (HMM-HA), that is a mass of greater than 1000 kDa, promotes epithelial-to-mesenchymal transition (EMT) and is antiangiogenic and immunosuppressive. Low molecular mass HA (LMM-HA) inhibits EMT and exerts inflammatory and angiogenic properties [3, 8].

Figure 1. 1 Chemical structures of HA

Disaccharide unit (A) and HA tetrasaccharide (B)- The hydrophilic functional groups and the hydrophobic moieties are shown in blue and yellow respectively, while the hydrogen bonds are represented by green dashed lines [Figure from Polymers 2018, 10, 701; doi:10.3390] (Open access enabled)

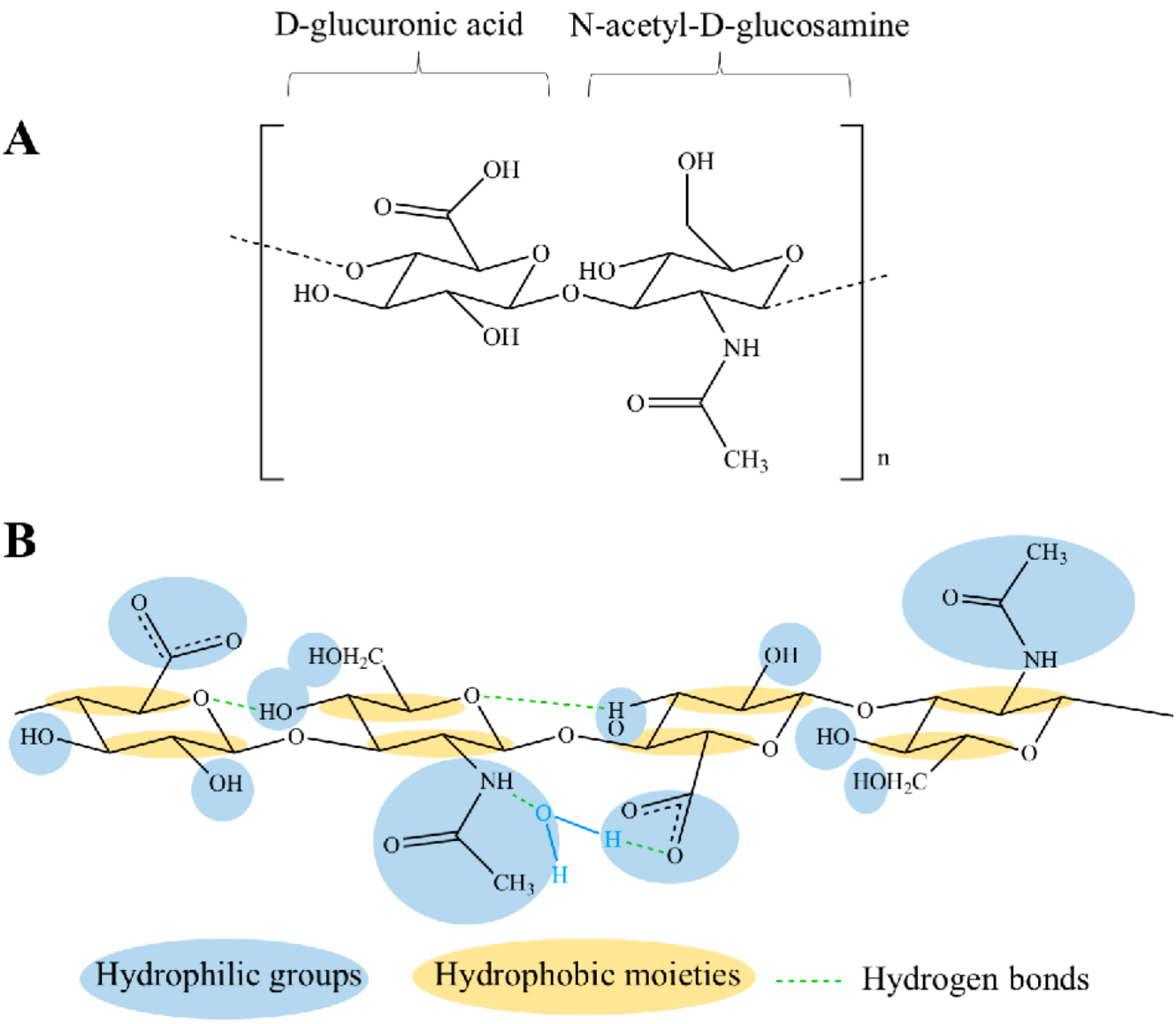

1.2. HA turnover

Among all ECM components, HA undergoes the fastest turnover with orchestrated synthesis and degradation. HA has a rapid constitutive turnover with 5 g of the total 15 g of HA present in a 70 kg individual, turned over daily [8,9]. The half-life of HA is tissue-specific. HA has a half-life of about 2-5 min in blood[10], 2.5 days in the skin[11], and up to 18 days in cartilage when it is aggrecan-bound [12]. About 30 % of daily HA is degraded locally where it is synthesized, followed by 70 % of HA entering the lymphatics[4]. HA levels increase during vertebrate development and wound-healing and decrease during differentiation which points to a regulated HA anabolism and catabolism. Though there are speculative models regarding the internalization of HA by receptor-mediated uptake and breakdown that have been proposed, identifying the players has been challenging[4]. Identification of only two genetic disorders of HA metabolism gives the impression that a defect in the turnover pathway may be embryonic-lethal.

1.2.1. Synthesis of HA by HA synthases (HASs)

HA is synthesized in the plasma membrane instead of the Golgi apparatus where other GAGs are synthesized. HA is synthesized by the HA synthases (HASs) which are glycosyltransferases embedded in the plasma membrane. HASs function by catalyzing the addition of UDP-D-glucuronic acid (GlcA) and UDP-N-acetyl-D-glucosamine (GlcNAc) monomers in an alternate fashion to make linear HA polymers [13]. In mammals, three HASs- HAS1, HAS2 and HAS3 which are isoenzymes, produce HA of different molar masses and at different rates [14]. Genes encoding HAS1, HAS2, an HAS3, are located on 19q13.3, 8q24.12, and 16q22.1 regions of the human genome respectively [15]. HAS1 is the least active of the three and produces HMM-HA from 2 X 10^5 to 2 X 10^6 Da and HAS2 is catalytically more active compared to HAS1 and synthesizes HA chains >2 X 10^6 Da. HAS3 appears to have the highest rate of synthesis but produces HA molecules with MW lower than 3 X 10^5 Da [9].

Variation in the sizes of HA may be required to regulate its diverse biological roles within an organism. The three HAS enzymes are expressed throughout the mammalian lifespan, but HAS2

is broadly expressed during early development while HAS3 expression is more evident in adult tissues [16]. The differences in HAS expression at different stages in various tissues suggested an important role during mammalian development, and subsequent knockout studies of different HASs showed the importance of these genes in normal physiology and disease development [17, 18].

HAS gene expression and HA synthesis rely on growth factors, cytokines and kinases which may be cell or tissue-specific. The responses of HAS genes toward a specific stimuli are not constant as exemplified by the dose-dependent downregulation of HAS3 but upregulation of HAS1 expression, observed in human fibroblast-like synoviocytes[9, 13]. Among three HAS enzymes, HAS2 is recognized as a major contributor to HA production during embryogenesis [19]. HAS2 deficiency in the mouse is embryonic lethal at E (embryonic day) 9.5 due to the failure of endocardial cushion development and EMT for valve and septa formation [17, 20]**.** This defect was shown to be corrected by addition of exogenous HA in *ex vivo* explant cultures of cardiac cushions from HAS2 KO embryos [20]. This suggested that HA regulated a cellular signal to control development during embryogenesis. Studies aiming to determine if HAS2 is involved in other abnormalities included a tissue-specific inactivation of *Has2* in the mouse skeleton and suggested that HA is an essential component of limb development [21].

HAS1 expression in mice is highest during early gastrulation [22] and initial studies from targeted disruption of *Has1*appeared to be normal [23]. Although alterations in the mRNA and mutations in *Has1* have been found to be associated with multiple myeloma and B-cell malignancies, the relationship between the phenotypes and role of HAS1 remains unknown [24, 25]. Although, HAS3 is the most active of the HASs, its expression was found only in ectoderm-derived organs. Studies from *Has3* KO as well as *Has1/Has3* double KO mice showed minor phenotypic changes, including altered neuronal activity and increased resistance to ventilator-induced lung injury[26].

HASs are critical mediators of physiology and tissue-maintenance. The aberrant expression of HAS leads to thickened skin and folding [4] and is associated with the increased risk of serious pathological events including tumorigenesis and several malignancies [9, 13].

1.2.2. Degradation of HA by hyaluronidases (HYALs)

Complete degradation of HA to monosaccharides requires the catalytic functions of both the endoglycosidase- hyaluronidase, and the exoglycosidases β-N-acetyl-D-hexosaminidase and β-D-glucuronidase[27]. The hyaluronidase enzyme was discovered in 1928 and has since been described to have catalytic activity against HA, a repeating polymer composed of glucuronic acid (GlcA) and N-acetylglucosamine (GlcNAc). The HA polymer is first hydrolyzed at the β1-4 linkage between GlcA and GlcNAc. The resulting fragments then act as a substrate for the β-D-glucuronidase, revealing GlcNAc, which is the substrate for β-N-acetyl-D-hexosaminidase[28] and hyaluronidases. Hyaluronidases are members of the glycosidase family 56 group of hydrolases[29]. Based on mechanisms of enzyme catalysis, HYALs were grouped into three classes- mammalian, leech and microbial hyaluronidases. The first two classes of mammalian and leech HYALs degrade HA by hydrolyzing the glycosidic bond whereas the microbial HYAL degrades HA by a β-elimination reaction to form a double bond in the product.

1.3. Mammalian hyaluronidases

In humans, hyaluronidase-related genes are found as a cluster of two groups of three. On chromosome 3p21.3, three hyaluronidase-related genes, *HYAL1, HYAL2* and *HYAL3* have been localized and an additional cluster of three genes, *HYALP4, HYALP1* and *PH20/SPAM1* are found on chromosome 7q31.3[30]. *HYALP1* is not translated into a protein-product because of an internal stop codon. The remaining five human hyaluronidases share a 22-42% identity in their amino acid sequences, which suggests a gene duplication event that formed a cluster of three genes that was subsequently duplicated on a second chromosome[29]. In mouse, the orthologous hyaluronidase genes are clustered in two groups of three on chromosome 9 (*Hyal2, Hyal1, Hyal3*) and chromosome 6 A2 (*Hyal4, Spam1* and *Hyalp1*), respectively. The numbering of these genes is a product of genetic studies that identified several candidate lung cancer tumor suppressor genes in humans, including *LuCa2, LuCa1* and *LuCa3* which were later identified as

hyaluronidases[31, 32]. Apart from these six hyaluronidase-like genes another hyaluronidase gene, *Hyal5*, is found on chromosome 6[33].

Figure 1. 2 Model for HA Turnover

HAS1 synthesizes low levels of HMM-HA (2 x 10^6), HAS2 produces significantly more HMM-HA (2 x 10^6) and HAS3 is the most active of the HAS enzymes but produces LMM-HA(2 x 10^5). HYAL2 resident on the cell-surface, in coordination with CD44, degrades HMM HA into intermediate sized fragments which are internalized and transported through the endosome into the lysosomes to be degraded by HYAL1 into tetrasaccharides or LMM HA. [Figure from doi: 10.1152/ajpregu.00332.2011] (Open access enabled)

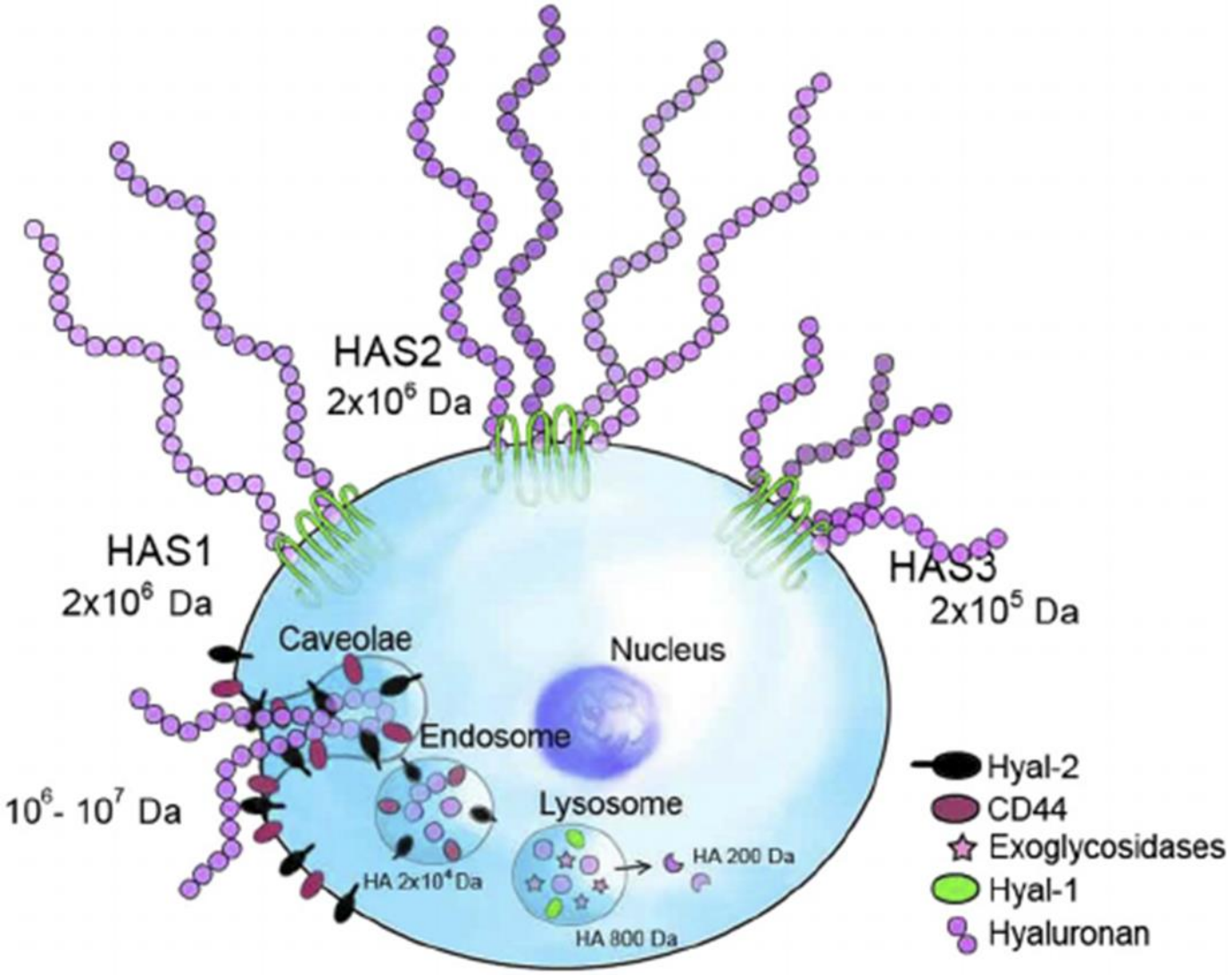
HAS2
2x10⁶ Da
HAS1
2x10⁶ Da
HAS3
2x10⁵ Da
Caveolae
Nucleus
Endosome
Lysosome
10⁶- 10⁷ Da
HA 2x10⁴ Da
HA 200 Da
HA 800 Da
Hyal-2
CD44
Exoglycosidases
Hyal-1
Hyaluronan

1.4. Distribution and characterization of mammalian hyaluronidases

Gene expression studies showed that only the human and mouse genes encoding HYAL2, HYAL1 and HYAL3 are broadly expressed in somatic tissues. The HYAL4-encoding gene is primarily expressed in placenta[30] and expression of the SPAM1-encoding gene is restricted to the male reproductive tract[34]. HYAL4 is thought to be a chondroitinase[35] and no activity has been associated with HYAL3[36]. Only HYAL1 and HYAL2 are thought to play a significant role in HA degradation in somatic tissues.

1.4.1. Activity of mammalian hyaluronidases

Most biochemical characterization of the hyaluronidases has been done on HYAL1 because it was the first to be isolated and was readily assayed. Although HYAL1 was present in very low concentrations in human serum, it showed high specificity towards HA[32]. HYAL1 had an acid pH optimum and could degrade HA of all sizes[37]. Several assays have been developed to determine the activity of hyaluronidases including the Reissig assay[38], a microtiter-based ELISA[39], and HA-substrate gel zymography. In HA-substrate gel zymography, a native gel is prepared containing HA and hyaluronidase activity is measured semi-quantitatively by analyzing the size and completeness of clearing the gel[40]. Measuring the HYAL2 activity using these approaches has been challenging. Several studies failed to show any activity associated with HYAL2, possibly because of weak activity or a requirement for other cellular partners for its activity[41-45]**.** The optimum pH for HYAL2 activity has been reported as both acidic and near neutral[44, 45], possibly reflecting the differences in the structure of the enzyme or possibly the presence of HYAL1. The model proposed for HA degradation suggested HYAL2 required a Na^+/H^+ exchanger NHE1 for the acidification of its local environment and this exchanger could be one of the additional components HYAL2 needs for its activity[42]. Moreover, some other studies also reported HYAL2 and HYAL1 activity required concomitant expression of cell surface receptor, CD44[45] possibly another important candidate required for the quantification of activity. Characteristics of the substrate HA also differs between HYAL1 and HYAL2. While

HYAL1 appears to be active against the lysosomal pool of HA, HYAL2 appears to be active towards extracellular HA. Considering the nature of HYAL2's function, additional studies are required to develop a robust assay to measure its activity.

1.4.2 Hyaluronidase 1 (HYAL1)

The *HYAL1/Hyal1*gene is comprised of 7 exons which encode several alternatively spliced mRNA species that can be translated into a 435 amino acid protein[32]. HYAL1 is an acid-active enzyme that can cleave HA to fragments as small as tetrasaccharides by hydrolyzing the β1-4 glycosidic bond between GlcA and GlcNAc[32]. Almost all human tissues express HYAL1 mRNA, but it is most highly expressed in tissues where HA degradation is highest like the liver, kidney, spleen and bone marrow[46]. Studies of HYAL1 from murine macrophage showed that it is synthesized as a 52 kDa protein that is primarily secreted out of the cell and re-internalized by endocytosis where it undergoes proteolytic cleavage and transforms into a 48 kDa mature protein[47]. Further analysis suggested that serum HYAL1 gets endocytosed by liver sinusoidal cells[48]. Studies from HEK 293 cells suggested HYAL1 function depends on the presence of the CD44 receptor, supporting previous studies showing the requirement for a receptor for HA internalization to the lysosome[45]. The crystal structure of HYAL1 showed it was an α/β barrel with the active site residing in the center of the barrel[49]. Structure/function studies have indicated that residues identified to be critical for catalysis in the bee venom hyaluronidase are conserved in HYAL1[37].

HYAL1 deficiency caused abundant HA accumulation in the lysosomes of macrophage and fibroblasts of joint tissues, resulting in mucopolysaccharidosis (MPS) IX, which is primarily characterized by an arthritis-like phenotype involving multiple joints[50]. A mouse model of HYAL1 deficiency also exhibited a similar phenotype, with pathology limited to the joints[51].

1.4.3 Hyaluronidase 2 (HYAL2)

The *HYAL2/Hyal2* genes are comprised of six exons which encode a 1.9 kbp mRNA that can be translated into a 473 amino acid protein[46, 52]. It is predicted to have a 20 amino acid signal sequence that directs the protein to the ER where it is modified by glycosylation and addition of a glycophosphatidylinositol (GPI) anchor[53]. The GPI anchor aids in HYAL2's association with lipid rafts at the cell-surface[54].

Ubiquitous expression of *HYAL2/Hyal2* mRNA was reported in expression studies from adult and embryonic human[52] and mouse[55] tissues. Histologically, HYAL2 was found to be detectable but at variable levels in the endothelial cells of most mouse tissues, and in specialized epithelial cells of lung, kidney, brain, intestine and oviduct[5].

Localization of HYAL2 has been controversial[56]. The first study of HYAL2 localized it in the lysosome by following the expression of a HYAL2 fusion with green fluorescent protein (GFP) [41]. In this experiment, the GFP was attached to the C-terminus which was later found to prevent the addition of a GPI anchor to HYAL2 or lead to cleavage of the GFP-tag. Whatever the case, the normal processing of HYAL2 failed to occur and subsequent studies by this group[57] and others[53, 58], clearly indicated the presence of HYAL2 on the cell-surface. Moreover, the characteristics of GPI-anchored proteins support their localization at the cell-surface rather than in the lysosome. However, in some cell-types HYAL2 appeared to have an intracellular localization[59]. Later, different studies suggested HYAL2 localized to the cell-surface[60], mitochondria[61] and nucleus[62] leaving the localization of HYAL2 unclear. The most recent studies of endogenous mouse HYAL2 from our own laboratory, and using control tissues from HYAL2 deficient mice, indicate that HYAL2 is expressed on the surface of many cells, but can be found intracellularly in come cell types[8].

Studies of HYAL2 activity have also been controversial. The earliest studies suggested HYAL2 functioned as a weakly-active hyaluronidase that had specificity towards HMM HA and activity at both neutral and acidic pH[41]. However, subsequent studies did not detect activity for HYAL2 at either acidic or neutral pH[53]. A Na^+/H^+ exchanger was proposed to maintain the acidic environment required for HYAL2 activity[42]. Platelet HYAL2 appeared to be active when it was translocated from α-granules to the platelet surface[63]. Convincing evidence that HYAL2 played a

role in HA metabolism came from expression of HYAL2 in HEK293 cells where there was increased turnover of HA, however in this case the activity was found to require the presence of the HA receptor, CD44[45].

1.5. HA cell-surface receptors and signaling

HA stimulates three biological processes in concert with cell-surface receptors - signal transduction, pericellular coat formation and receptor-mediated internalization[64]. The integral receptor for HA, CD44, interacts not only with HA but also with growth factors, cytokines and ECM proteins [65]. HA-CD44 interaction mediates intracellular signaling pathways like- receptor-mediated HA degradation, angiogenesis, cell migration, proliferation and cell adhesion to ECM components[13, 64, 66]. CD44 is thought to internalize HA during inflammation and wound-healing[4, 65].

The receptor for HA-mediated cell motility (RHAMM), also referred to as CD168 is alternatively spliced and is distributed over multiple cellular compartments including cell-surface, cytoskeleton, mitochondria and nucleus[66]. Cell-surface RHAMM is important for migration[69] and is essential for activation of protein tyrosine kinase cascades by endothelial cells in response to HA[70]. Though, RHAMM and CD44 operate differently in cell-signaling regulatory pathways, knocking out of either does not result in embryonic or developmental lethality possibly because of overlapping functions with other receptors or cellular function compensation of one by the other[66].

Hyaluronan receptor for endocytosis (HARE), alternatively known as stabilin-2 (STAB2) was initially isolated from endothelial cells in the organs that internalize circulating HA including liver, lymph nodes, spleen, eye and kidney[65]. *Hare*$^{-/-}$ mice show elevated levels of circulating HA, demonstrating it's importance in the uptake of HA[71]. Lymphatic Vessel Endothelial Hyaluronan Receptor 1 (LYVE-1) is abundant in lymph vessel endothelium, in activated tissue macrophages and in liver and spleen sinusoidal endothelium, the sites where maximal HA turnover is known to occur [64]. Though, it has been associated with HA removal, the abrogation of LYVE-1 was not lethal to the normal development of mice, suggesting that its function is

compensated by other receptors. The involvement of LYVE-1 is intracellular signal transduction largely remains unknown[65].

HA interaction with toll-like receptors (TLRs) mediates both innate immune responses and tissue metabolism. HMM HA facilitates the expression of IL-1R-associated kinase-M, which negatively regulates TLR signaling [72]. HMM HA negatively regulates osteoclast differentiation through TLR4 signaling [73]. Due to its active involvement in innate immunity, HA may be an important target in diseases which root from immunological processes.

Figure 1. 3 HA cell surface receptors and their involvement in cell and tissue functions

[Figure from Biochem Biophys Acta;1840(8):2452-9. doi: 10.1016] (Open access enabled)

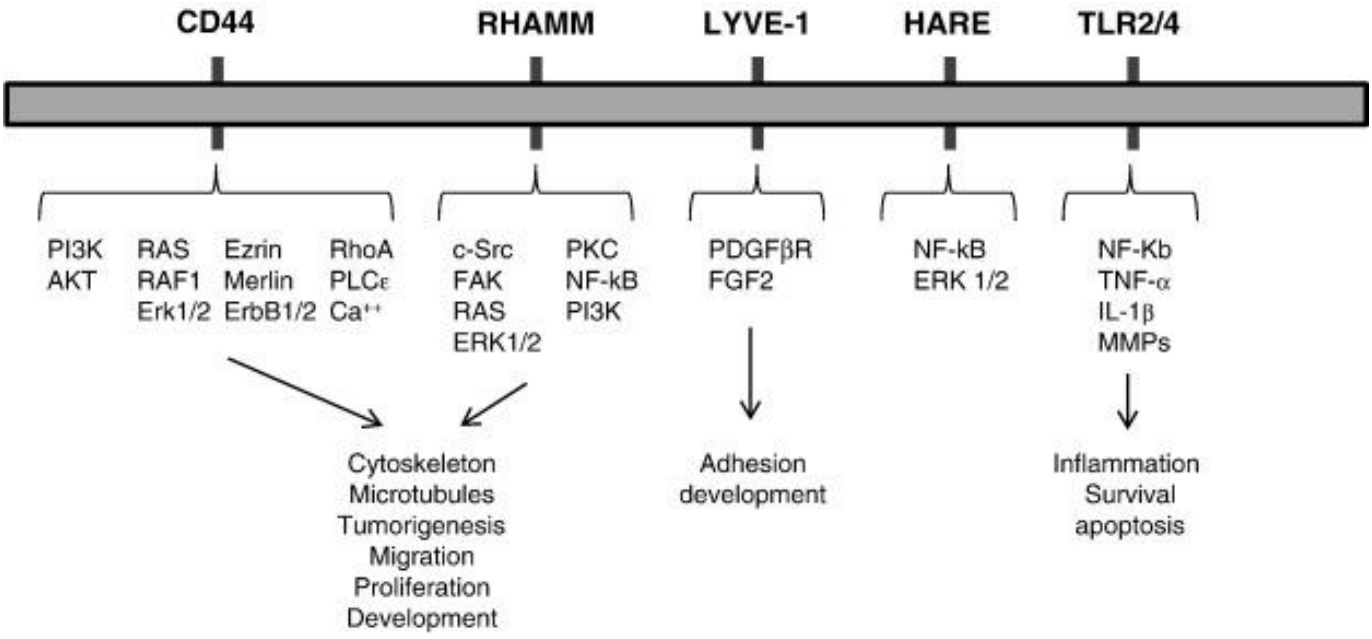

1.6. Hyaluronidase model of HA degradation

HYALs play a significant role in HA metabolism by cleaving HA for further degradation by exoglycosidases. Hydrolysis of the internal N-acetyl-D-glucosaminidic linkages (β-1,4 glycosidic bonds) of HA polymers makes the HYALs 'endoglycosidases'[9]. HYAL1 works in coordination with HYAL2 to degrade HA, the mechanism of which is still unclear. A model was proposed for HA catabolism suggesting cell-surface receptors like CD44, LYVE-1 and HARE bind with HMM HA and on binding with Na^+/H^+ exchanger, NHE1[42], HYAL2 hydrolyzes HA into oligosaccharides of approximately 20 kDa. These intermediate 20 kDa fragments are internalized into endosomes and the resulting fragments are then endocytosed into the lysosome[9, 13]. Inside the acidic lysosomal environment, acid-active HYAL1 degraded the residual HA fragments to smaller fragments which in later stages are acted upon by exoglycosidases, β-N-acetyl-D-hexosaminidase and β-D-glucuronidase[4, 27] demonstrated in **Fig 1.4.** Experimental validation and confirmation of this model has not been established yet.

Figure 1. 4 HA removal by HYALs.

HA is bound by the receptor (R), and internalized into an endosome which then matures into a lysosome (enlarged) where HYAL1 and the exoglycosidases are proposed to function [A]. HA associated with *Hyal2* WT and KO MEFs was isolated and separated by pulse field gel electrophoresis and then stained with Coomassie blue. The WT lane with intact HYAL2 shows less HA accumulation compared to the KO lane where HMM HA accumulates. To confirm that the staining material was HA, one sample from each line was treated (+) before separation with *Streptomyces* hyaluronidase to degrade the HA. The varied sizes of HA in a sample make it appear as a smear. [Hemming and Triggs-Raine, unpublished data]

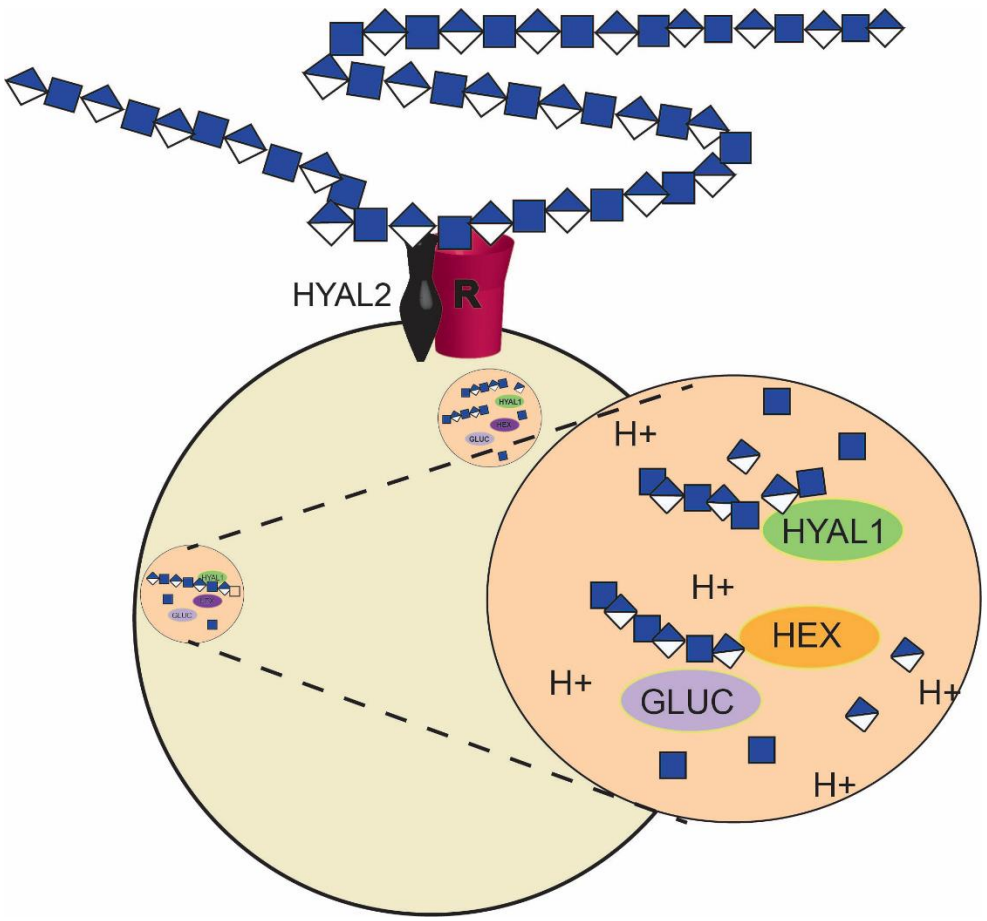

(A)

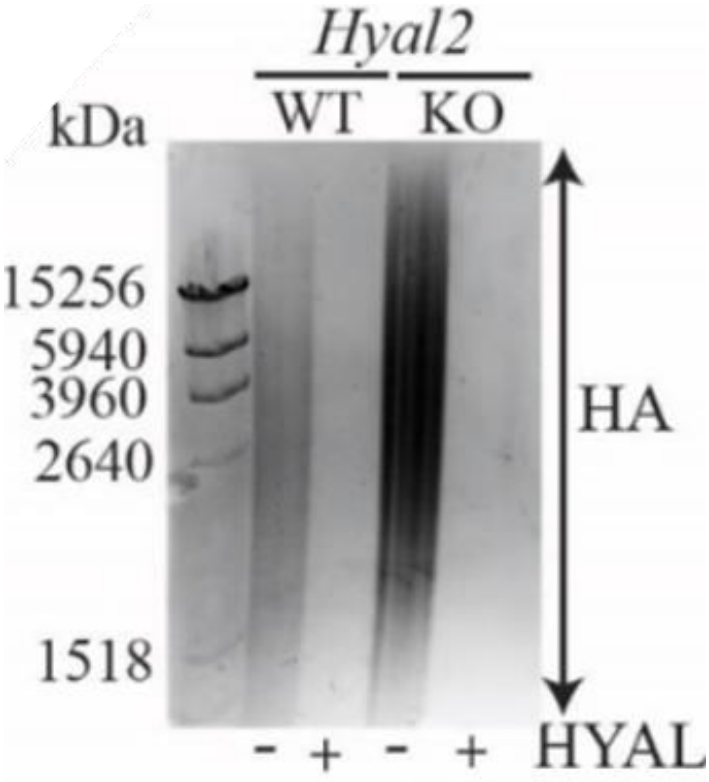

(B)

1.7. HA and development

Studies showing HA distribution during early development suggested HA levels are rapidly decreased upon implantation of the blastocyst onto the uterine wall but increased later during appearance of the primitive ectoderm and endoderm. Mapping of HA distribution during mouse embryogenesis demonstrated that by E11.5-E13, there was abundant HA present in the craniofacial mesenchyme and connective tissue throughout the body.[6]

1.7.1 HA function during development

HA has been demonstrated to be a critical component during vertebrate development and reported to play a role during tissue/organ morphogenesis by influencing several molecular functions. HA was shown to regulate embryonic cell behavior by creating a hydrated low-resistant matrix which provided cells mechanical support and gave contact inhibition characteristics that stimulated cell proliferation and migration [74]. HA has been reported to modulate the hydration of the environment by forming an HA-dependent pericellular matrix during mitosis that promoted partial separation and rounding of the ongoing dividing cells[75]. Apart from providing mechanical support to the ECM that contributed to maintaining tissue homeostasis, HA also acted as a key component to assemble the ECM by interacting with proteoglycans (PGs) through link modules, cell surface receptors and possibly through interaction with the HASs [76, 77]. HA also served as a binding partner for other proteins and provided ligands for cell attachment and motility which might shape embryonic development[78-80]. In the developing matrix, HA influenced the level of intercellular signals affecting cell growth and differentiation by interacting with growth factors [81].

1.7.2. HA in EMT

Several avenues of study have shown a role for HA in the regulation of EMT. EMT is a multi-step process which involves a series of biochemical changes in the epithelial cells as they transform into mesenchymal cells. This change is characterized by a loss of the intercellular adhesion complex, promoting the tightly linked epithelium to become motile mesenchyme. The transformed cells have increased invasiveness as well as migratory and proliferative capacity[82]. The composition and state of pericellular matrix microenvironment are very important in determining the state of cells. Elevated secretion of EMT components including HA has been reported in cells undergoing EMT[92].

HA accumulation and degradation play a role in EMT, particularly in the early stages of embryogenesis, where it is critical for tissue formation through the differentiation of the embryonic to mesenchymal stem cells[83]. Elevated HA in normal epithelial cells has been shown to influence anchorage-independent growth and change the characteristics of the cytoskeletal proteins between cell boundaries[84, 85]. Studies of the influence of HAS3 and HAS2 overexpression in human pancreatic cells showed decreased E-cadherin but increased β-catenin which promoted EMT in cells. Earlier reports have shown increased HA levels during several embryonic EMT processes including cardiac cushion formation[86], palatal shelf fusion[87], and neural crest transition[88]. At embryonic day (E) 9.5 in mice, soon after looping of the heart tube, HA synthesized by HAS2 forms a thick jelly between the endothelial and myocardial layers. These thickenings are the endocardial cushions, and cells of the endothelial layer (specialized epithelial cells) undergo EMT to form mesenchymal cells that migrate into these cushions to form the AV septum, as well as mitral and AV valves. EMT is integral to development, but also to wound healing and tumor metastasis. During EMT, epithelial cells lose their polarity and adhesive properties but gain mesenchymal features, including the capacity to proliferate, migrate, invade, and differentiate[89].

The requirement for HA in EMT was demonstrated in HAS2 null *(Has2-/-)* mouse embryos, which died at E9.5 due to a failure to form HA-rich endocardial cushions and initiate EMT[90]. During the endocardial cushion morphogenesis, the regulation of EMT depended on HA of specific sizes. Experimental evidence showed HMM HA facilitated cell migration to promote EMT. With the reduction in cardiac cushion volume during valve remodeling, HA was degraded into oligosaccharides (o-HA) which promoted VEGF expression, limiting EMT[91] (**Figure 1.5**). During development, mesenchymal cells undergo condensation after EMT for differentiation and CD44 is often localized to the condensation sites which play a role in many EMT interactions. Removal of HA during the condensation process changes the ECM characteristics of the mesenchyme leaving the residual HA to crosslink with the cell surface receptors of the adjacent cells and promote differentiation[93, 94]. Any conditions altering the interaction of HA with its receptor or affecting the removal of it might interfere with normal development resulting in cardiac[95] or craniofacial abnormalities, which involves one-third of all congenital birth defects in humans[96, 97].

Figure 1. 5 HA and VEGF activity during endocardial cushion-valve formation.

HMM (HMW) HA provides a hydrated matrix to initiate cellular migration during EMT after which it depolymerizes into oligosaccharide fragments (o-HA) during valve development. o-HA promotes VEGF attenuates EMT and induces cell-differentiation. [Figure from Circ Res;99(6):583-9. doi: 10.1161/01.RES.0000242561.95978.43.] (Open access enabled)

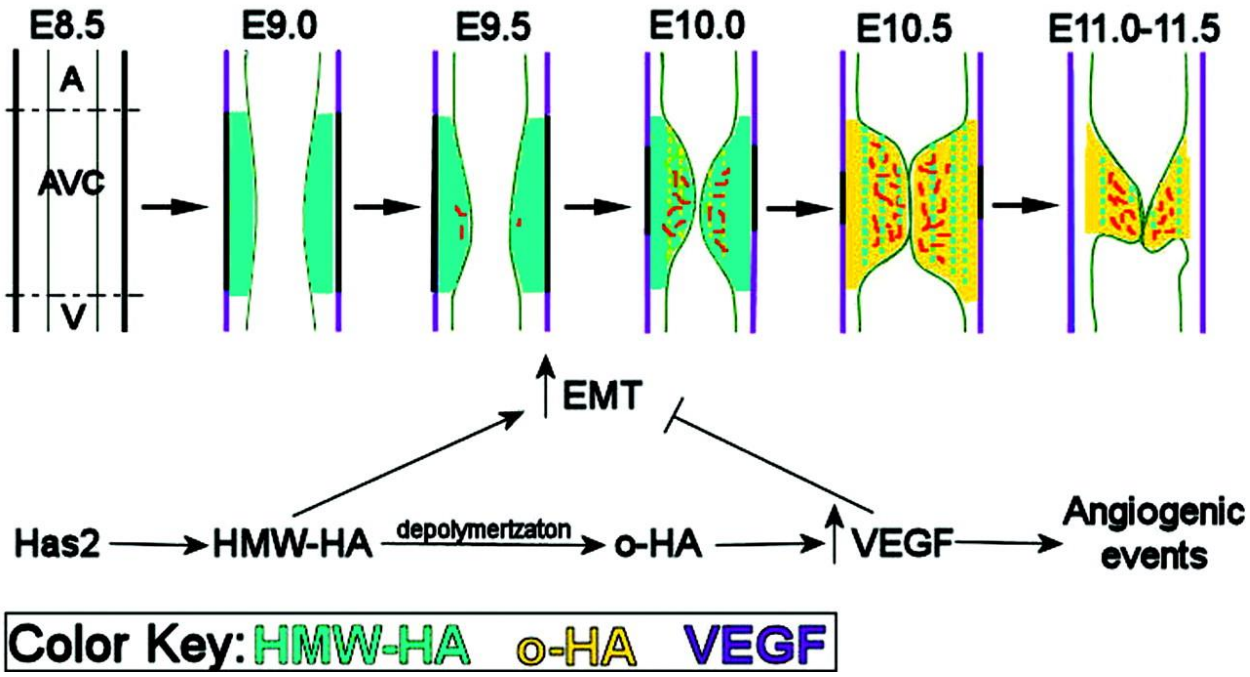

1.8. HYALs in EMT and development

Studies in the developing chick heart showed that the transition from epithelial to differentiating mesenchymal cells was accompanied by a decrease in HA[98], presumably due to the action of a HYAL. The balance between the synthesis and abundance of HA by HAS2 in the provisional matrix of the developing embryo and its degradation by HYALs, is important to support formation of the normal heart. The impact of HYAL2 deficiency on normal cardiac development was reported in both *Hyal2-/-* mice and HYAL2-deficient humans[99, 100]. Absence of HYAL2 resulted in increased HA in all murine tissues and an excess of mesenchymal cells was also observed in several tissues[99]. In vivo evidence of fibrosis in the heart, atrial dilation, hypertrophic valves, and excess tissue formation is supported by increased number of mesenchymal cells due to the presumable upregulation of EMT which leads to diastolic dysfunction in the acutely affected mice[95]. Decreased levels of VEGF expression in E14.5 *Hyal2-/-* embryos consistent with the increase in mesenchymal cell population[95] indicated loss of mesenchymal cell differentiation as a possible cause of the congenital defects associated with HYAL2 deficiency[100]. The role of HYAL2 in signaling remains unknown, but because the size and abundance of HA is increased in *Hyal2-/-* tissues, we hypothesize that HYAL2 regulates HA size and/or abundance to regulate key signaling pathways.

Besides its role in cardiac tissue development, elevated HA levels can have profound impact in the formation of other tissues including formation of the nasal folds [101], elevation of the secondary palate [102,103], differentiation of the cornea [104], formation of the semicircular canals of the ear[105] and development of the kidney[106], as reported in independent studies. Both humans and mice with HYAL2-deficiency exhibited craniofacial dysmorphism, complete or partial cleft lip and/or palate, variably penetrant cor triatriatum, valve thickening, atrial enlargement, and hearing loss [99, 100, 107]. In addition, severe myopia is present in humans and a kidney is missing in 40 % of mice[99]. Beyond the similarity to the human disease, studies published by our lab on *Hyal2-/-* mice revealed a severe central ossification defect affecting the viscerocranial bones, providing additional evidence for decreased differentiation in *Hyal2-/-* embryonic tissues. Structural and functional cardiac changes were evaluated using high resolution ultrasound and

histopathology. Cor triatriatum was identified in 50% of mice[108] and additional valve-like tissue was observed in the ventricles and atria[95], suggesting there are aberrantly localized mesenchymal cells in the *Hyal2-/-* hearts. Although HYAL2 is constitutively expressed in mouse tissues, we predict that its activity is regulated post-translationally to decrease HA only at specific times to regulate cellular phenotype.

Figure 1. 6 Model of HA and EMT.

Model shows the known outcome of HAS2 deficiency and expected outcome of HYAL2 deficiency. **[**Figure courtesy of Triggs-Raine, unpublished]

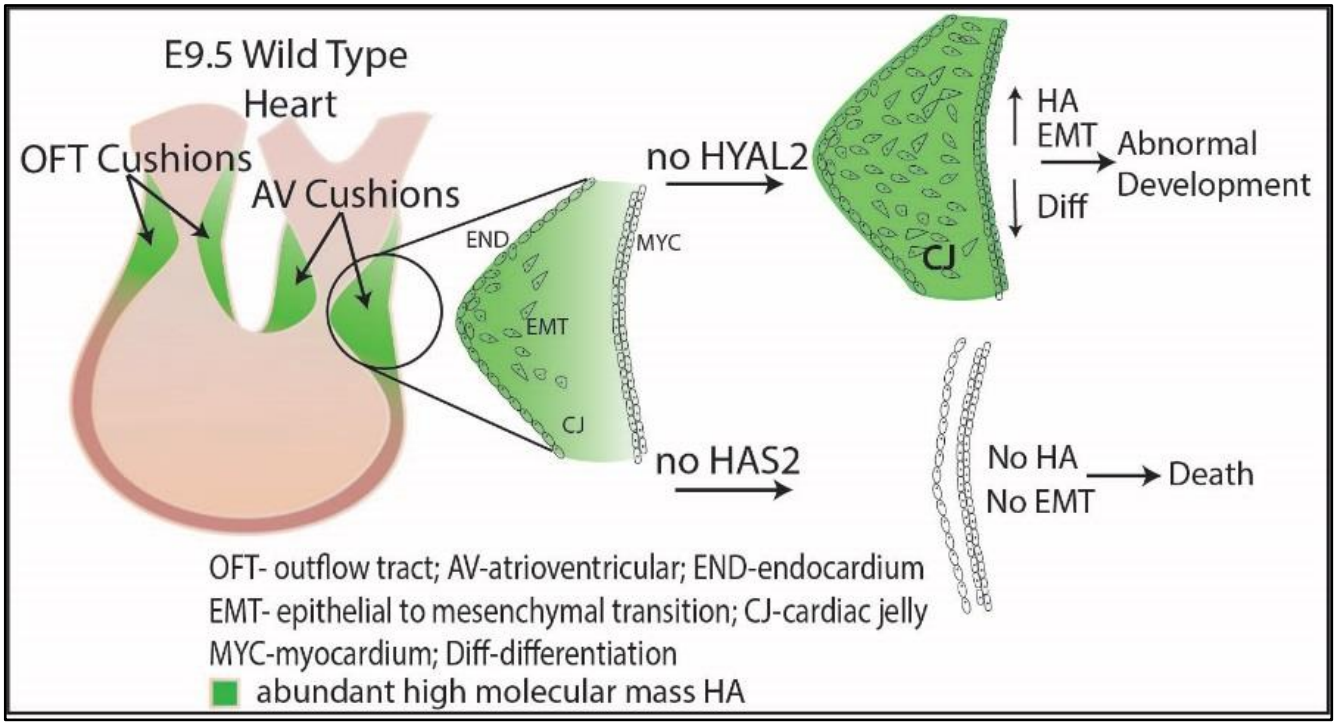

1.9. *Hyal2-/-* mouse model

The inability to definitively demonstrate HYAL2's activity made the generation of a mouse model deficient in HYAL2, an important step towards understanding its role in HA catabolism and maintaining ECM homeostasis. An initial attempt to generate a HYAL2-deficient mouse was unsuccessful, presumably due to embryonic lethality[57]. Later, a HYAL2 KO (*Hyal2-/-*) mouse was successfully generated from our group with collaborators and characterized[107]. An outbred background (129/Ola/CD1/C57BL/6) was used for the initial generation of the HYAL2 KO mouse, which were backcrossed for 6 generations on the C57BL/6 background. The initial characterization revealed elevated serum HA, but only minor hematological and skeletal abnormalities including an increased interorbital space and a shortened snout. There was also some evidence of reduced survival[107]. Subsequent characterization of the *Hyal2-/-* mouse on the outbred background showed heart abnormalities in surviving *Hyal2-/-* that were characterized by expansion of the atrium and valves[99]. Ultrasound studies revealed the presence in 40% of surviving animals of cor triatriatum sinister[108]. Beyond the craniofacial and heart abnormalities, comparison with subsequently identified human patients revealed that two-thirds of *Hyal2-/-* embryos died postnatally but before day 7 of age. Some of these mice had evidence of submucosal cleft palate and poor mineralization of the central facial bones, as well as hearing loss[100]. Accumulation of HA was evident in most tissues of the *Hyal2-/-* mice, suggesting an important role for HYAL2 in the removal of extracellular HA[5].

1.10. Novel genetic aberrations/variations in human HYAL2 (*HYAL2*)

The first two mutations in *HYAL2* - c.443A>G (p.K148R) and c.749C>T (p.P250L) were reported in families from the Amish community and Northern Saudi Arabia of (Arabic ethnicity). The study identified deficiency of HYAL2 as a novel cause for syndromic CLP and a first cause for cor triatriatum sinister in humans. Myopia and other ocular abnormalities, pectus excavatum, single palmar creases, a consistent left superior vena cava and other cardiac malformations were presented variably. The study emphasized the similarities between the phenotypes of patients with the HYAL2 mutations and *Hyal2-/-* mice, with the developmental complications being lethal to the *Hyal2-/-* mice. Immunoblot analysis of transiently expressed HYAL2 demonstrated that the p.K148R and p.P250L mutations result in 11 and 20 fold reductions respectively compared to the expression of wild type HYAL2 (**Fig 1.7**). It was speculated that residual HYAL2 produced in the individuals with the mutations- K148R and P250L allowed constitutive HA clearance but was inadequate during development [100].

Recently, whole-exome sequencing of genomic DNA from seven patients of variable ethnicities identified **seven novel variations *HYAL2*- c.713T>G p.L238R , c.611G>C p.G204A, c.1271_1272delAC p.H424Lfs*12, c.194C>G p.S65X, c.1273T>G p.F425V, c.829C>T p.R277C and c.883C>T p.R295X**. The genotype, ethnicity, gender, age, height, occipital frontal circumference (OFC) and other phenotypic features of these patients are described in **Table I** .

Figure 1. 7 Pedigrees, clinical features of individuals and expression of WT HYAL2, and mutations -K148R and P250L

Pedigree and facial pictures of individuals with HYAL2 deficiency [A].Electropherograms of mutations and sequence conservation across species [B] Expression of mutated protein in *Hyal2*-/- MEFs [C] (figure from PLoS Genet 13(1): e1006470doi:10.1371/journal.pgen.1006470, permitted use)

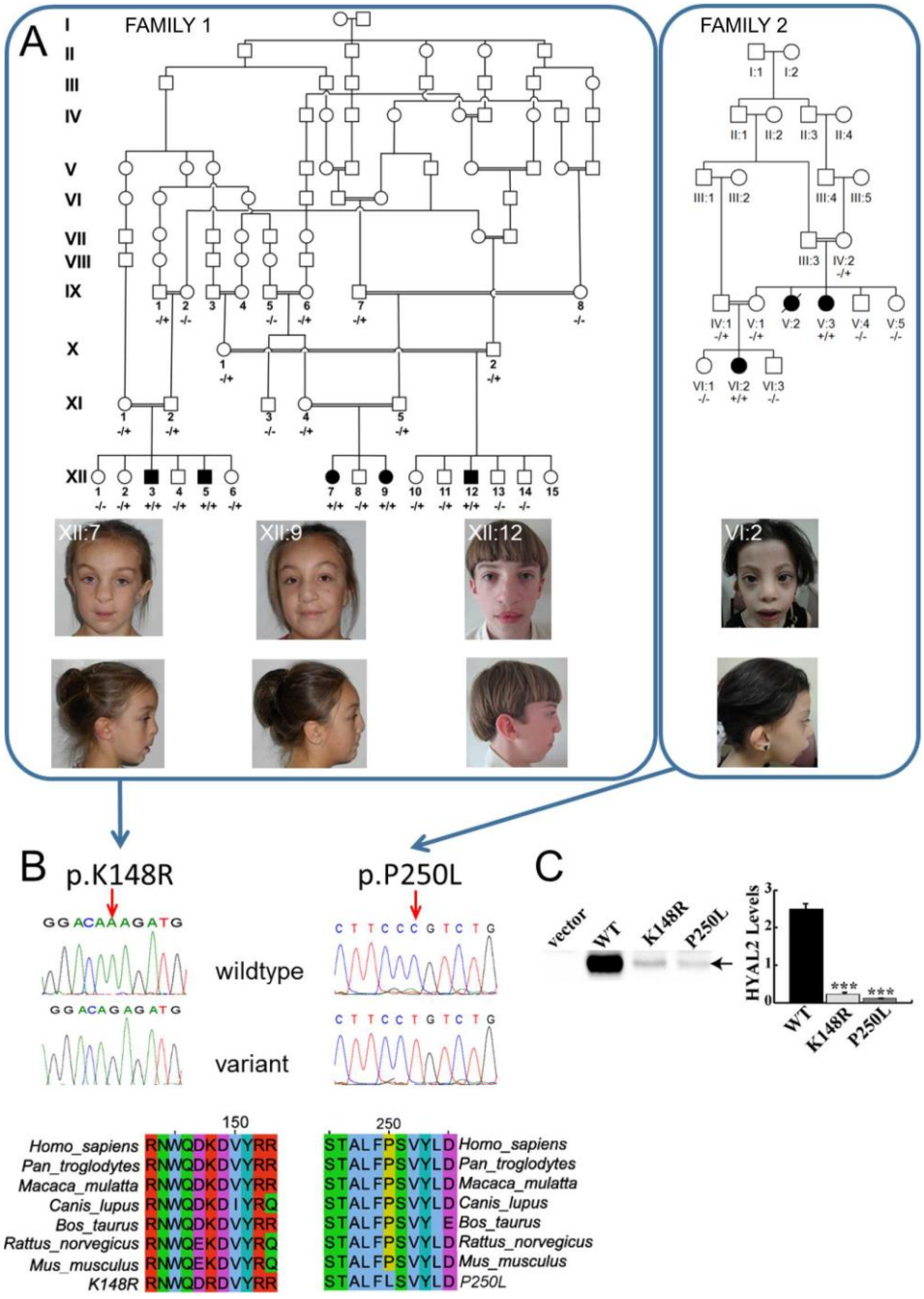

Table I. Clinical findings of individuals with novel HYAL2 variants

Abbreviations: ADHD, attention deficit hyperactivity disorder; AR, aortic regurgitation; AS, aortic stenosis; ASD, atrial septal defect; AV, aortic valve, CoA, coarctation of aorta; CLP, cleft lip and palate; D, dioptres; DD, developmental delay; DPRV, double outlet right ventricle; DV, ductus venosus; F, female; ID; intellectual disability; LSVC, left superior vena cava; LT, left; LV, left ventricle; M, male; MV, mitral valve; NA, not available; OFC, occipitofrontal circumference; PDA, patent ductus arteriosus; PHTN, pulmonary hypertension; PSC, posterior subcapsular; PV, pulmonary valve; RD, retinal detachment; RT, right; SDS, standard deviation scores; TOF, tetralogy of Fallot; TR, tricuspid regurgitation; VSD, ventricular septal defect; (√) and (**x**) indicates presence or absence of a feature in an affected subject respectively

Table by Baple et al. *(unpublished)*

	This study; 1	This study; 2	This study; 3	This study; 4	This study; 5	This study; 6	This study; 7
Genotype	p.(Lys148Arg)/ p.(Lys148Arg)	p.(Lys148Arg)/ p.(Lys148Arg)	p.(Arg277Cys)/ p.(Arg295*)	p.(Phe425Val)/ p.(Ser65*)	p.(Phe425Val)/ p.(Ser65*)	p.(Gly204Ala)/ p.(Gly204Ala)	p.(His424Leufs*12)/ p.(Leu238Arg)
Ethnicity	Amish	Amish	Italian	German	German	Turkish (Romania)	German
Gender	M	F	M	F	M	F	M
Age (years)[†]	9.4	13.8	19	1 day (deceased 10 months)	Prenatal (21 weeks gestation)	20	4
Height (cm, SDS)	124.5	152.5	163.5 (-1.75)	53 (+1.42)	NA	151 (-2.09)	NA
OFC (cm, SDS)	NA	NA	53.7 (+0.51)	33.5 (-1.32)	NA	51 (-3.26)	NA
Cleft lip and palate	✗	✗	✗	✓ Unilateral CLP	✓ RT CLP	✓ Bilateral CLP	✓ CLP
Frontal bossing	✓	✓	✗	✗	NA	✗	✗
Hypertelorism/ telecanthus	✓	✓	✓	✓	NA	✓	✓
Ptosis	✗	✗	✓	✗	NA	✗	✗
Broad depressed nasal bridge	✓	✓	✓	✓	NA	✓	✓
Micrognathia	✓	✓	✗	✓	NA	✗	✗
Ear abnormalities	✓ Small ears, overfolded thickened helices	✓ Small ears, overfolded thickened helices	✓ Small ears, overfolded thickened helices, forward facing lobes	✓ Small low set ears, small lobules, RT ear pit	NA	✓ Small ear lobes, chronic otitis media	✓ Small low set ears with small lobules, overfolded thickened helices

Cardiac anomalies	✗	✓ Mild AS and AR	✓ CoA and VSD	✓ VSD, ASD, PDA, PHTN	✓ MV atresia, hypoplastic LV, DORV with PV atresia, hypoplastic pulmonary & aortopulmonary arteries, agenesis of DV	✗	✓ TOF
Pectus excavatum	✓	✗	✓	✗	NA	✓	✗
Single palmar crease	✓	✓	✗	✗	NA	✗	✓
Myopia (refraction)	NA	✓ Mild	✓ Severe	✓ Mild	NA	✓ High	✓ High
Cataract	NA	NA	✓ Bilateral	NA	✓ RT		✗
Other ocular features			Myopic maculopathy and RD	Persistent pupillary membrane, vitreous haemorrhage RT		LT RD with enucleation, RT macular anomaly	Myopic maculopathy & suspected rod dystrophy
Hearing loss	✗	✗	✗	✗	NA	✓ RT: mild to severe sensorineural LT: mild to profound mixed	✗
Duodenal web	NA	NA	NA	✓	NA	NA	NA
Other clinical findings	Mild/moderate DD, broad halluxes and broad thumbs	Broad halluxes, broad and distally placed thumbs	Accessory oral frenulum, low posterior hairline, short webbed neck	Hypoplastic nails, bilateral extrarenal pelvises, LT congenital diaphragmatic hernia, glabellar capillary naevus, cystic hygroma 1st trimester	Cystic hygroma at 11 weeks, hydrops	No speech until age 3, ID, suspected autism spectrum disorder, ADHD, fingertip whorls, finger webbing, webbed neck	Cryptorchidism, short neck, broad halluces, 5th finger clinodactyly

CHAPTER 2: RATIONALE, RESEARCH AIMS AND HYPOTHESIS

2.1. Rationale and research aims

During embryonic development HA is broadly distributed, with its highest levels in the cardiac-cushion, the neural crest-derived craniofacial mesenchyme, the ventriculus communis, sternum and vertebral column[10, 9]. Analyzing two novel variants in HYAL2, our lab has previously reported mutations in *HYAL2* as a novel cause of syndromic CLP in humans, with other features including facial dysmorphism, septal defects, hearing loss and atrial dilations as common clinical phenotypes both in mice and humans[100] . Recently, seven novel *HYAL2* variants in patients with syndromic CLP were identified to us by clinicians around the world. Performing a biochemical analysis of these mutations is important to confirm HYAL2 as a primary cause of the clinical manifestations and to further expand our understanding of the phenotypic expression of HYAL2 deficiency. Expression and localization studies for each mutation would also help to delineate if the presence of residual HYAL2 is required to allow patient survival.

HYAL2 deficiency leads to HA accumulation and congenital defects in humans and mice[95, 100, 108]. However, detecting HYAL2's activity has been challenging with several labs, including our own, detecting weak [44, 57] or no activity associated with HYAL2[53, 60]. Most proteins tend to function in the cell as a part of a large complex and an important way to assess function of the protein is by looking at possible binding partners of the protein. Though previous studies showed the interaction of HYAL2 with CD44[60], Na+/H+ exchanger NHE1[42] and the tyrosine kinase RON1[110], very little is known about their roles in HYAL2 mediated HA degradation. Establishing and validating a method to look for possible and real partners of HYAL2 will lay the foundation of understanding the HYAL2 network which will aid in designing an enzyme assay to understand the activity of HYAL2.

2.2. Research Aims

Towards this end, I propose two research aims:

(I) To biochemically analyze the effect that patient-reported HYAL2 variants may have on HYAL2 expression and localization

(II) To establish a method for identifying and screening HYAL2 interacting partners using the novel Biotin Identification (BioID) proximity labeling system

2.3. Hypothesis:

Novel variants have been identified in *HYAL2* of individuals with phenotypes similar to those previously associated with HYAL2 deficiency. We hypothesize that these variants interfere with HYAL2 expression and/or abundance on the cell surface and therefore HYAL2 function. We also hypothesize that HYAL2 mediated HA turnover might involve additional binding proteins which control its temporal regulation, and as a first step to reveal these HYAL2 binding partners we are designing an approach to identify and sort these molecules.

CHAPTER 3: MATERIALS AND METHODS

3.1. Fusion PCR to introduce variants (mutations)

A commercial mammalian expression vector pCMV6-XL5 containing the full-length HYAL2 cDNA (NM_003773.4) was purchased from Origene (Cat #SC117754). The varinats c.713T>G p.L238R, c.611G>C p.G204A, c.1271_1272delAC p.H424Lfs*12, c.194C>G p.S65X, c.1273T>G p.F425V, c.829C>T p.R277C and c.883C>T p.R295X were introduced into the WT-HYAL2 cDNA by fusion-PCR following the PCR protocol for Phusion® High-Fidelity DNA Polymerase (M0530). The primers for each variant were designed such that they contain extra bases flanking the desired single-nucleotide change. Each primer was at least 23 nucleotides long. Outer primers for WT-HYAL2 – 5'-atgcgggcaggcccaggccccacc-3' (forward) and 5'-gctacaaggtccaggtaaaggcca-3' (reverse) were used in combination with variant-specific forward and reverse primers (**Table II**) to generate two PCR products for each variant. These PCR products were separated on 1% agarose gels, and identified by comparison to the GeneRulerTM 1 kb or 1 kb plus DNA Ladder (SM 0313 and SM1334), excised with a sterile razor and purified using the QIAquick PCR Purification Kit (Cat #28704). The two isolated fragments for each variant served as templates for PCR amplification with the outer primers of WT HYAL2 cDNA to make a region of HYAL2 cDNA containing a specific nucleotide change. The concentration (ng/µl) and purity of the resulting fused PCR products were determined by measuring the absorbance at 260 and 280 nm using a Nanodrop 2000 Spectrophotometer.

3.2. Restriction enzyme digestion

The fused-PCR product of HYAL2 containing the variants were then checked for restriction enzyme sites using ApE- A plasmid Editor software. The same was done for the pCMV6-XL5 vector containing the WT-HYAL2 cDNA sequence which would serve as the vector for the variant-containing HYAL2 sequences. The mutations and the pCMV6-XL5 containing WT-HYAL2 were digested with a specific pair of restriction endonucleases as provided in **Table II**). Restriction enzymes Fast Digest EcoRI (ThermoFisher) and ApaI or FseI or PpuMI (New England Biolabs) were used to digest both PCR product and vector DNA following a standard restriction digestion protocol. For restriction enzyme digestion, 0.1-0.5 µg of vector DNA or 0.1-0.3 µg of PCR product, 5 µl of 10X Buffer (Cut Smart or NEB Buffer) and 1-2 U of restriction enzyme were used to make the reaction volume of 50 µl for both PCR product and vector DNA. 1 hour (EcoRI/ApaI/FseI) or overnight incubations (PpuMI) at 37°C (PpuMI/EcoRI/FseI) or 25°C (ApaI) were followed. Following restriction digestion, dephosphorylation of the plasmid DNA was done to inhibit recircularization of linear plasmid. For dephosphorylation, 2ul of 10X Antarctic Phosphatase Reaction Buffer and 5 U of Antarctic Phosphatase (New England Biolabs) were added to the digest. This reaction was incubated at 37°C for 30 mins and heat-inactivated at 80°C for 2 mins. The digested reaction mixes of both vector and insert (HYAL2 variants) were then separated on 1 % agarose gels, and the fragments were identified, isolated and quantified as described in **3.1** for fusion PCR.

Table II. List of primers and cloning sites used to generate mutations in HYAL2 cDNA.

The nucleotides introducing mutations are capitalized in the primers, except for primers generating the 2 bp deletion, where the nucleotides are italicized after the position of the deletion

Mutation	Forward/Reverse Primers	Cloning enzymes
c.713T>G p.L238R	WPG1210 5' gcaatgaccagcGggcctggctgtgg 3' WPG1211 5' ccacagccaggccCgctggtcattgc 3'	EcoRI / ApaI
c.611G>C p.G204A	WPG1185 5'ggcacctctgggCcttctacctctt 3' WPG1186 5'aagaggtagaagGcccagaggtgcc 3'	EcoRI / ApaI
c.1271_1272delAC p.H424Lfs*12	WPG1208 5'cacctgcagacac*ttccgctgccag* 3' WPG1209 5'ctggcagcggaa*gtgtctgcaggtg* 3'	EcoRI / PpuMI
c.194C>G p.S65X	WPG1305 5'tgtgcaggcctGacctaatgagg 3' WPG1306 5'cctcattaggtCaggcctgcaca 3'	EcoRI / ApaI
c.1273T>G p.F425V	WPG1303 5' tgcagacacacGtccgctgccag 3' WPG1304 5'ctggcagcggaCgtgtgtctgca 3'	EcoRI / PpuMI
c.829C>T p.R277C	WPG1299 5'caggaggcccttTgtgtggctcgca 3' WPG1300 5'tgcgagccacacAaagggcctcctg 3'	EcoRI / ApaI
c.883C>T p.R295X	WPG1301 5'acgtcttcacaTgacccacctac 3' WPG1302 5'gtaggtgggtcAtgtgaagacgt 3'	EcoRI / ApaI

3.3. Ligation of vector and insert

Ligation of vector and insert was done with three different vector to insert ratios for each mutation. Each ligation reaction contained 2 µl of 10X T4 DNA Ligase Buffer (Thermo Scientific), different concentrations of vector and insert DNA (~ 30-50 ng vector DNA, 30-40 ng insert DNA), 2 µl T_4 DNA Ligase (Invitrogen™) making a total reaction volume of 20 µl. The ligation reactions were incubated overnight at room temperature and their ligation efficiency was checked by separation on a 1 % agarose gel the next day. The reaction demonstrating the most ligation, and its non-ligated control were transformed into *E. coli* following 3.4 the following day.

3.4. Transformation of HYAL2 mutants into *Escherichia coli* by electroporation

Electo-competent *Escherichia coli* DH5α cells were prepared following a standard protocol (see **Supplementary Methods I**). One µl of the ligation mixture was mixed with 40 µl of electrocompetent *E. coli*, and was transferred to a cold sterile 0.1 mm electroporation cuvette (BTX ™). Electroporation was performed in a BTX Electroporation Electro Cell Manipulator ECM-600 using the settings- 1.3 kV, 129 Ω, 50 µF and the cuvette was immediately flooded with 960 µl of pre-warmed SOC media (0.5 % yeast extract, 2 % tryptone, 10 mM NaCl, 2.5 mM KCl, 10 mM $MgCl_2$, 10 mM $MgSO_4$ and 20 mM glucose). After 1 hr incubation at 37°C, 50 and 100 µl volumes of the bacterial cultures were spread on Miller's Luria agar (Gibco-BRL Life Technologies) plates containing 100 µg/ml ampicillin. Plates were inverted and incubated overnight at 37°C. The following day, single colonies were sub-cultured into 3 ml LB Broth (Gibco-BRL Life Technologies) containing 100 µg/ml ampicillin and grown overnight at 37°C with shaking.

3.5. Plasmid isolation

Plasmids were isolated from 1 ml of *E. coli* culture using a NucleoSpin® Plasmid Kit (Macherey-Nagel) and following the manufacturer's instructions. Briefly, bacterial cells were pelleted in a microcentrifuge tube and the supernatant was discarded. After resuspension of the pellet in the supplied buffer, cells were lysed using sodium dodecyl sulphate (SDS)-alkaline lysis buffer and neutralized with an acetate buffer that precipitated all proteins and chromosomal DNA. The neutralized lysate was cleared and spun through a silica membrane of a NucleoSpin® Plasmid/Plasmid (NoLid) Column in a supplied collection tube. The silica membrane was washed with a kit-supplied buffer and pure plasmid was eluted with water.

3.6. Sequencing of plasmid DNA

To confirm error-free construction of the mutated HYAL2 constructs, the isolated plasmids were sequenced at the Toronto Centre for Applied Genomics (TCAG) to verify the presence of the desired but no other mutations in the PCR-amplified region of the cDNA. At least 3 samples of independent clones were analyzed for each mutation using Sanger sequencing. Outer primers specific to WT-HYAL2 5'-atgcgggcaggcccaggccccacc-3' (forward) and 5'-gctacaaggtccaggtaaaggcca-3' (reverse) were sent along with the inner forward and reverse primers specific to each mutation provided in **Table III**. The sequencing data were analyzed and the mutated bases were verified from the chromatograms on FinchTV 1.4.

3.7. Secondary culture of plasmid DNA and maxiprep

Once verified by sequencing, one clone was selected to prepare a larger scale plasmid preparation. The remaining 2 ml of bacterial cultures was used to inoculate 200 ml of LB Broth supplemented with 100 µg/ml of ampicillin. After overnight incubation at 37°C with vigorous shaking, the cultures were checked for their OD_{600}~4-6 and verified. The bacterial cells were

pelleted and pure plasmid DNA was isolated using the NucleoBond® Xtra Endotoxin-free plasmid purification kit (Macherey-Nagel). After the elution of pure endotoxin-free DNA for each mutation, their concentrations (ng/µl) and purity (A260/280 ratio) were measured using the Nanodrop 2000 Spectrophotometer.

3.8. Culture of mouse embryonic fibroblasts (MEFs)

Mouse embryonic fibroblasts (MEFs) deficient in HYAL2 were derived from *Hyal2-/-* embryos as a part of previous studies. These cells were transfected with a vector expressing the large T antigen to immortalize the cells. MEFs were grown in 6-well culture dishes with Dulbecco's Modified Eagle Medium (DMEM) containing 10 % fetal bovine serum (FBS) supplemented with glutamine and 1 % penicillin/streptomycin (1 % P/S). Cells were incubated in 5 % CO_2 at 37°C until they reached ~ 85-90 % confluency.

3.9. Transfection of MEFs with HYAL2 variants

DNA for transfection was prepared by equalizing the concentrations of all plasmids by comparing their intensities to a DNA mass ladder after separation on an agarose gel. A transfection reaction mix was prepared by combining 4 µg of plasmid DNA and 8 µl of Turbofect Transfection Reagent (Thermo Scientific) to serum-free DMEM to make a final volume of 400 µl of transfection mix per well in a 6-well plate. The transfection reaction mix was kept at room temperature for 20 mins and then added dropwise to the appropriate well. The plates were incubated at 37°C in 5 % CO_2 for 24 hrs. The following day the media containing the transfection reagent was removed and replaced with fresh DMEM.

3.10. Cell harvest

After 48 hrs of transfection, the media on the 6-well plates containing the transfected MEFs was discarded and washed three times with 2 ml of 1X Phosphate Buffer Saline or PBS (1.1 mM KH_2PO_4, 8.1 mM Na_2HPO_4, 2.7 mM KCl, 137 mM NaCl, pH 7.6). The plate was held on ice while the cells were scraped from each plate into 250 µl of PBS containing a 1:500 dilution of a protease inhibitor cocktail (Sigma). Cell lysates were sonicated using a Sonic Dismembrator 100 (Fisher Scientific) at 15 amplitudes and giving 2 bursts of 5 secs each on ice with a 30 secs interval between the bursts.

3.11. Protein quantification

The protein concentration of the transfected cell lysates was determined using the Bradford assay. In this assay, 1 µg/µl of bovine gamma globulin was used to prepare a standard curve for the interpretation of protein concentration in the experimental samples. For each sample, 2 µl of the sonicated cell extract was added to a 1.5 ml tube containing 798 µl of sterile water and 200 µl of Bradford reagent (BioRad). The tubes were then incubated at room temperature for 5 mins and the absorbance was read using an Ultrospec 1000 spectrophotometer at 595 nm. As a control, 2 µl of lysis buffer (in this case 1X PBS containing the protease inhibitors) was added to a 1.5 ml tube containing 798 µl of sterile water and 200 µl of Bradford reagent (BioRad) to assay the background. Each of the experimental samples were analyzed in triplicate and compared to the absorbance of samples of known protein concentration.

3.12. Western Blot analysis of the expressed proteins

For western blot analysis, the cell lysates with their protein quantified were subjected to sodium dodecyl sulphate-polyacrylamide gel electrophoresis (SDS-PAGE) for separation based on size. Polyacrylamide gels were cast using 7.5 % acrylamide as the resolving gel (40 mM Tris pH 8.8,

0.1 % SDS, 7.5 % polyacrylamide [29:1 acrylamide:bisacrylamide], 0.1 % tetramethylethylenediamine (TEMED), 0.075 % ammonium persulfate). Following polymerization of the resolving gel, a 4 % stacking gel (60 mM Tris pH 6.8, 0.1 % SDS, 4 % polyacrylamide, 0.1 % TEMED, 0.01 % ammonium persulfate) was poured between 1.5 mm ethanol-sterilized glass plates fixed to a casting stand and a 10 well 1.5 mm comb was inserted and was left to polymerize. The polymerized gel was placed in a gel tank with running buffer containing 0.1 % SDS, 25 mM Tris and 192 mM glycine. Based on the protein quantification by Bradford assay 20 µg of protein was mixed with sample prep buffer (8 % SDS, 250 mM Tris pH 6.8, 40 % glycerol, 0.01 % bromophenol blue, 400 mM dithiothreitol [DTT]), and boiled for 5 mins at 95°C followed by cooling and a short centrifugation. The boiled samples were loaded into their respective wells next to the control (WT HYAL2) and 5 µl of PageRuler Prestained Protein Ladder (Thermo Scientific). The gel was run at 160 V for 1-1.5 hrs or until the bromphenol blue marker in the sample prep buffer reached the bottom of the gel. Following the separation of proteins by SDS-PAGE gel, the gel was equilibrated in ice-cold transfer buffer (80 % running buffer and 20 % methanol) for 15 mins. The gel was stacked between pre-equilibrated filter papers, sponges and 0.45 µm nitrocellulose membranes (GE Healthcare) and the sandwich was assembled in the transfer cassette. The cassette was placed into the transfer tank filled with ice-cold transfer buffer and ice pack and the transfer was run at 100 V for 1 hr at 4°C. After the transfer, the nitrocellulose membrane was checked for protein transfer on the membrane by staining the membrane with Ponceau S (0.1 % Ponceau S in 5 % acetic acid). Once the bands were visualized and the Ponceau S was washed off with Tris-buffered Saline Tween or TBST (20 mM Tris pH 7.4, 0.15 M NaCl, 0.1 % Tween-20), the membrane was blocked in 5 % skim milk in TBST for 1 hr. Following blocking, the membrane was incubated overnight with anti-HYAL2 primary antibody (Proteintech, Cat #15115-1-AP) diluted 1:500 in blocking solution. The following day, the membrane was washed 3 times for 10 mins each with TBST to remove any unbound primary antibody and was reincubated with horseradish-peroxidase (HRP) conjugated secondary donkey anti-rabbit antibody for 1 hr, washed 3 times with TBST for 10 mins each and visualized using Immobilon Western Chemiluminescent HRP Substrate (Millipore). The chemiluminescent signals from the expressed proteins were captured and quantified by using the Image Lab™ Software for PC Version 6.0.1 (BioRad). For quantification of the signal, the lane frame was resized manually for each lane area, and the band was detected

using the automatic band detection tool. Next, the quantification tool was used to determine the light emitted (light units) from each band. Equal loading was verified by detecting β-actin using anti-β-actin (1:5000) on the same blot. Each sample was calculated as a proportion of the wild type level which was set at 1.

3.13 Immunofluorescence analysis of MEFs expressing HYAL2 mutant constructs

The subcellular localization of mutant HYAL2 proteins compared to WT-HYAL2 was monitored using immunofluorescence. HYAL2-deficient MEFs were transfected with WT and mutant HYAL2 constructs as described in **UNITS 2.2.8** and **2.2.9**. Post-transfection, cells were counted and culture media containing approximately 2000 cells were added to sterile coverslips in 6-well plates. DMEM was added to each well and growth was allowed for 24 hrs. The next day, the media was aspirated and each well was washed three times for 5 min in 2 ml of cold PBS for 5 mins each. The cells were fixed in 2 ml of 4 % paraformaldehyde in PBS pH 7.4 for 10 mins at room temperature. The paraformaldehyde was removed and cells were washed three times with ice-cold PBS for 5 mins. For each construct one permeabilized (0.1-0.5 % Triton X-100 for 10 min) and one non-permeabilized well was blocked with 1 % BSA in 1X PBS for 1 hr and incubated with diluted primary antibody, anti-HYAL2 primary antibody in 1:500 dilution (Proteintech, Cat #15115-1-AP) in a humidified chamber for 2 hrs at room temperature. The primary antibody solution was removed and the coverslips were washed with 1X PBS three times for 5 mins each and re-incubated in the dark with donkey anti-rabbit IgG (H+L) Highly Cross-Adsorbed Secondary Antibody, Alexa Fluor 568 (ThermoFisher Scientific, Cat # A10042) diluted 1:1000 in 1 % BSA for 45 mins. After incubation with secondary antibody, the cells were incubated with Hoechst dye 33342 (diluted to 1:100 from stock) for 1 min in the dark and washed three times with 2 ml of 1X PBS. Coverslips were mounted onto slides using 20 µl of ProLong Gold antifade reagent (P36930; Life Technologies) and sealed with clear nail polish. Images were captured using Axio Imager.Z2 with a 63x/1.4NA oil objective using the 465 nm and 555 nm channels to pseudo color the nuclei and HYAL2 in the cells respectively. Images were cropped and figures assembled using Adobe Photoshop and Illustrator CS6.

3.14. Release of Cell Surface HYAL2 by PI-PLC

To detect GPI-anchored cell surface HYAL2, MEF cells were transfected with WT or mutant HYAL2 in six well plates as described earlier. At 48 h post-transfection, cells in each well were washed twice with PBS and incubated at 37^{o}C for 2 h with 0.5 U/ml PI-PLC (Sigma P-5542) in serum-free DMEM supplemented with 25 mM HEPES pH 7.4 (0.5 ml/well with gentle rocking). The media from each well was collected, concentrated (using Bio Max 0.5 ml spin concentrators) and used as single samples. Sample proteins were separated by SDS-PAGE and PI-PLC released cell surface HYAL2 was detected by western blotting with anti-HYAL2 antibody.

3.15. Construction of Flag-tagged human HYAL2 (Flag-HYAL2)

To fuse Flag-tag with *HYAL2* cDNA, we used a construct where *HYAL2* cDNA starting at second methionine was inserted into pFLAG-CMV1 expression vector. The vector was a generous gift from Dr. Dusty Miller[53]. The Flag-tag sequence along with a stretch of *HYAL2* cDNA was used to replace a region of the commercial mammalian expression vector pCMV6-XL5 containing the full-length *HYAL2* cDNA (Origene Cat #SC117754) employing the restriction digestion-ligation method of cloning. The DNA concentrations of donor vector [pCMV1-Flag-Hyal2] and the recipient vector [pCMV6-Hyal2] were measured by Nanodrop 2000 Spectrophotometer and 0.1-0.5 µg DNA for both donor [insert] and recipient vector [vector] were mixed with 5 µl of 10X Buffer (Cut Smart) and 1-2 U of restriction enzymes ApaI and SnaBI (New England Biolabs) to make a total reaction volume of 50 µl. The reaction mix incubated at 25°C for 1hr to enable restriction digestion by ApaI and then moved to a 37°C water bath for 1 hr to enable restriction digestion by SnaBI. The restriction digested samples were then loaded on a 0.8 % agarose gel and after separation the fragments to be cloned were identified by comparing their position of migration to that of fragments in GeneRulerTM 1 kb or 1 kb plus DNA Ladder (SM 0313 and SM1334). The appropriate fragments were excised with a sterile razor and the DNA was purified using the QIAquick PCR Purification Kit (Cat #28704). The

purified digested vector and insert were then subjected to ligation following the same protocol as described in **3.3**. After verifying successful ligation, 1 µl of ligated pCMV6-Flag-Hyal2 plasmid or 1µl of control (no ligase) were added to tubes containing 40 µl of electrocompetent *E. coli*. Transformation followed the protocol described in **3.4**. The transformed plates (both the pCMV6-Flag-Hyal2 plasmid and control) were checked for colonies, sub-cultured and verified by sequencing. The sub-culture was used to inoculate larger culture volumes for preparation of larger quantities of DNA.

3.16. Flag-HYAL2 protein expression and localization

The newly constructed pCMV6-Flag-Hyal2 plasmid was checked for its concentration (ng/µl) and purity by A260/280 ratio using the Nanodrop 2000 Spectrophotometer (Thermo Scientific). The DNA was then ready for transfection into pre-made *Hyal2-/-*MEFs. The transfection of pCMV6-Flag-Hyal2 into *Hyal2-/-* MEFs was performed into 6-well plates following the method described in **3.9**. Post-transfections, the cells were harvested in 250 µl of PBS containing a 1:500 dilution of a protease inhibitor cocktail (Sigma) and sonicated as described in **3.10**. Protein was quantified following the same protocol as described in **3.11**. After the protein quantification, the cell lysates were separated by SDS-PAGE and HYAL2 was detected as described in **3.12**. The Flag-HYAL2 protein was assessed for glycosylation with PNGase F treatment **(Supplementary Methods II)**

To confirm the cell-surface localization of Flag-HYAL2 and to compare that with WT-HYAL2, immunofluorescence was employed. The *Hyal2-/-* MEFs were transfected with both pCMV6-Flag-HYAL2 and WT HYAL2 and grown on coverslips inside a 6-well plate. The cells were subjected to both permeabilized and non-permeabilized conditions. The immunofluorescence protocol followed as described in **3.13.**

3.17. Cloning of signal sequence-BioID2-Hyal2 (SS-BioID2-Hyal2) by fusion PCR

The Flag tag on the pCMV6-Flag-Hyal2 cDNA was replaced by BioID2[136] by fusion PCR. The mammalian expression vector myc-BioID2-MCS was a gift from Kyle Roux (Addgene plasmid # 74223 ; http://n2t.net/addgene:74223 ; RRID:Addgene_74223). Constructing the SS-BioID2-HYAL2 plasmid was achieved in parts. The first round of fusion PCR enabled the fusion of BioID2 to HYAL2 generating BioID2-HYAL2 cDNA of 7490 bp. After the generation of BioID2-HYAL2, the ER signal sequence was introduced upstream to the BioID2 at the N-terminus. The complementary primer sequences containing restriction enzyme sites or the sequences of HYAL2, BioID2 and SS are outlined in **Table III**.

Table III. Primers required to construct SS-BioID2-HYAL2 fusion protein

Primer specification	Primer sequence
WPG 1287 Forward primer with XhoI site (underlined)	5’ -agctcctcgagatggagctcaagcccacagcacca-3’
WPG 1289 Reverse primer to PCMV1-Flag Hyal2	5’-cttggttcccgaatagaccc-3’
WPG 1290 Forward primer with an EcoRI site (underlined) and ER signal sequence (italicized)	5’- cgaattc*atgtctgcacttctgatcctagctcttgttggagctgcagttgct*ttcaagaacctgatctggctgaagga-3’
WPG 1294 Reverse primer extending from Hyal2 into BioID2	5’-cttgagctccatgcttcttctcaggctgaa-3’
WPG 1293 Forward primer extending from BioID into Hyal2	5’-ttcagcctgagaagaagcatggagctcaag-3’
WPG 1295 Reverse primer downstream to ApaI site	5’-cactggcattgctcaccactc-3’

3.18. Validation of expression, biotinylation and localization of SS-BioID2-Hyal2

3.18.1. Transfection of SS-BioID2-Hyal2 fusion protein into *Hyal2-/-* MEFs

The newly generated SS-BioID2-Hyal2 fusion construct was first checked for the DNA concentration (ng/µl) using the Nanodrop 2000 Spectrophotometer. For expression verification, 4 µg DNA of each of SS-BioID2-HYAL2, BioID2-only and WT HYAL2 were used to transfect 3 wells in a 6 well-plate. 2 wells in the same plate were transfected with SS-BioID2-HYAL2 and myc-BioID2 for biotinylation efficiency assessment. 24 hrs post-transfection the wells reserved for biotinylation assessment were supplemented with fresh media containing 50 µM of biotin [**Supplementary methods III**] (Sigma, Cat #B-4501) and incubated at 37°C in 5 % CO_2 incubator for another 18-22 hrs for optimal biotin labelling.

3.18.2. Harvesting cells for expression and biotinylation validation

The cells from all the wells were briefly rinsed in room temperature fresh 1X PBS to remove serum proteins prior to lysis. The cells were lysed with SDS-PAGE lysis buffer (50 mM Tris-Cl pH 6.8, 12 % sucrose, 2 % SDS, 20mM DTT] supplemented with protease inhibitor cocktail (Sigma). Cells were scraped with 150-200 µl of lysis buffer per well (1 X 10^6 cells), sonicated (2 bursts of 5 secs) each to shear DNA and heated in SDS-PAGE sample buffer (8 % SDS, 250 mM Tris pH 6.8, 40 % glycerol, 0.01 % bromophenol blue, 400 mM DTT) and boiled for 5 mins at 95°C to denature proteins.

3.18.3. Protein expression analysis of SS-BioID2-HYAL2

To analyze the protein expression of SS-BioID2-HYAL2 and to determine if it's at the right size, the lysed cell-lysates were run on a 7.5 % SDS-PAGE gel and a 10 % SDS-PAGE gel and were probed by anti-HYAL2 primary antibody (Proteintech, Cat #15115-1-AP) in 1:500 dilution and

anti- BioID2 antibody [SS 3A5-E2] (ab232733) in 1:500 dilution respectively. After primary antibody incubations, the blots were incubated with anti-rabbit (1:5000) and anti-mouse secondary (1:5000) antibodies and the chemiluminescent signals from the expressed proteins were captured using the Image Lab™ Software. The protocol followed for immunoblotting is same as described in **3.12**

3.18.4. Validation of biotinylation of SS-BioID2-HYAL2

Following the whole-cell lysis, the cell lysates were separated by a 7.5 % SDS-PAGE, proteins were transferred to an equilibrated nitrocellulose membrane and the membrane was agitated in Bovine serum albumin (BSA) blocking buffer (1 % BSA, fraction V, 0.2 % [w/v] Triton X-100 in 1XPBS) for 30 mins at room temperature. The membrane was next agitated in streptavidin-peroxidase polymer, (Ultrasensitive/ Streptavidin-HRP Sigma, Cat #S2438-250UG) at 1:20,000 in BSA blocking buffer for 1 hr at room temperature. The membrane was rinsed twice in 1X PBS to wash away unbound Streptavidin-HRP followed by agitation in Fetal Bovine Serum or FBS blocking buffer (10 % [v/v] FBS, 1 % [w/v] Triton X-100 in 1X PBS) for 5 mins. This was followed by three 5 mins washes in PBS and a final incubation in Immobilon Western Chemiluminescent HRP Substrate (Millipore) for 5 mins to observe biotinylated proteins. After the biotinylation image was captured, the HRP signal was quenched by agitating the membrane in 30 % H_2O_2 (Fisher Scientific) for 20 mins followed by washing the membrane in PBS for two or three times to remove residual H_2O_2 before re-probing the membrane with other antibodies if required.

3.18.5. Validation of localization of SS-BioID2-HYAL2 by immunofluorescence

For localization experiments, *Hyal2*$^{-/-}$ MEF cells were plated onto glass coverslips in a 6-well plate and transfected in duplicate with 4 µg of SS-BioID2-HYAL2, BioID2-only or WT-HYAL2. The cells on coverslips were processed for immunofluorescence 24 hrs after transfection. Briefly, the cells were washed in PBS and fixed with 2 ml of 4 % PFA for 10 mins.

Cells were then incubated with (permeabilized) or without (non-permeabilized) Triton X-100 for 15 mins followed by a 2 hrs incubation with 1:500 dilution of anti-HYAL2 antibody (Proteintech, Cat #15115-1-AP) in a humidified chamber at room temperature. The coverslips were then washed and incubated for 45 mins in the dark with Alexa fluor 568 conjugated donkey anti-Rabbit IgG (H+L) Highly Cross-Adsorbed Secondary Antibody (ThermoFisher Scientific, Cat # A10042) diluted 1:1000 in 1 % BSA. DNA was labelled with Hoechst dye 33342 (1:100000) for 2 mins in the dark, washed, mounted and imaged as described in **3.13**.

3.19. BioID2 pull-down of proteins in proximity to HYAL2

To generate biotinylated proteins in proximity to, *Hyal2*$^{-/-}$MEFs were transfected in eight 10 cm tissue-culture dishes (4 experimental and 4 control) as described in **3.9**. SS-BioID2-HYAL2 and BioID2 control plasmid were scaled up to 32 µg/dish in a 2 ml volume of transfection reaction mix for each confluent plate containing about 1 X 10^7 cells. The cells in each plate were supplemented with 50 µM biotin and incubated for 24 hrs.

3.19.1. Cell lysis and affinity purification of biotinylated proteins

The media was aspirated from the biotin-treated cells and the dishes were rinsed twice with sterile PBS at room-temperature. The cells from each 10 cm plate were then scraped using 540 µl of lysis buffer (50 mM Tris-Cl, pH 7.4, 500 mM NaCl, 0.1 % SDS, 1 mM DTT) supplemented with protease inhibitor cocktail (Sigma). The four plates from the lysed experimental or control transfections were combined into a DNase/RNase free 15 ml tubes and 120 µl of 20 % Triton X-100 were added to each tube and mixed by trituration. The lysed cells were next sonicated using a Sonic Dismembrator 100 (Fisher Scientific) at 15 amplitudes and giving 2 bursts of 5 sec each on ice with a 30 sec interval between the bursts. The sonicated samples were then diluted with 2.52 ml of prechilled lysis buffer, mixed well and sonicated a second time as described above. The samples were divided into three prechilled 2 ml tubes and spun at 16,500 X g for 10 mins at 4°C.

For the affinity capture, 80 µl Streptavidin Sepharose™ High Performance beads (GE Healthcare Cat # 17-5113-01) were added to two tubes containing 1 ml of room temperature lysis buffer and centrifuged at 1000 X g for 2 mins to preclear and equilibrate the beads. The supernatant was discarded and the centrifuged experimental and control samples were added to these tubes containing the beads, mixed well and left on a rotator at 4°C overnight.

3.19.2. Bead washing

After the affinity capture, the two tubes containing experimental and control samples were spun at 1000 X g for 5 mins to collect the streptavidin beads. The supernatant was gently removed without disturbing the beads and the beads were suspended in wash buffer (8 M urea in 50 mM Tris-Cl, pH 7.4) and rotated for 8 mins. The process was repeated a second time followed by two additional washes with 50 mM TrisCl pH 7.4 without urea. The samples were resuspended in 1 ml of 50 mM TrisCl pH 7.4. From those samples, 900 µl were set aside for mass spectrometric analysis and 100 µl were saved for western blot analysis. In preparation for mass spectrometric analysis, the beads were pelleted by centrifugation at 1000 g for 2 mins and the supernatant was removed. The beads were resuspended in 50 µl of 1 mM biotin in 50 mM ammonium bicarbonate. These samples were sent for mass spectrometry at the Manitoba Centre for Proteomics and Systems Biology (Winnipeg, MB, Canada). To verify that proteins were recovered in the pull-down, the beads in 100 µl sample were resuspended in 100 µl of 1X SDS-PAGE buffer and heated at 98°C for 5 mins. A 15-20 µl aliquot of this sample was analysed by western blot following the procedure outline in **3.12**.

3.20. Mass spectrometry (MS) analysis

Samples isolated by BioID2 pulldown were subjected to tryptic digestion in 50 mM NH_4HCO_3 on the beads for 16 hours. After separation by 1D liquid chromatography (LC) with a 90-minute nonlinear gradient, digested peptide solutions for each biological replicate were subjected to a Q Exactive™ ¬¬HF-X Orbitrap mass spectrometer (Thermo Scientific, Waltham, MA) in standard

tandem MS/MS with data-dependent acquisition. The protein identification parameters were as follows: minimum fragment M/Z of 100; precursor mass tolerance of ± 10 ppm; fragment mass error of 0.02 Da, and a maximum E-value of 0.01. Fixed modifications for oxidation of methionine and tryptophan, deamination of asparagine and glutamine, and carboxyamidomethylation of cysteine were also included in the analytical parameters. Peptides were compared against the SwissProt mouse protein database and were identified and quantified using X!Tandem (Alanine, 2017.02.01). Total proteins quantified (including protein homologs, unique peptides) by X! Tandem search from two biological replicates have been provided in **Table V**. The Global proteome machine (GPM) links to the experimental (SS-BioID2-HYAL2) and control (BioID2 only) results are also attached (**Supplementary Table I**).

3.21. MS data analysis

3.21.1. Unique protein sorting

Peptides identified by MS were first compared between control (BioID2-only) and experimental samples (BioID2-HYAL2) for two biological replicates to find the peptides unique to only the experimental sample, that is proteins specific to the HYAL2 pull-down. The unique peptides from both replicates were then compared across each other to sort only those peptides appearing in both replicates. The final list of proteins specific to HYAL2 and present in both biological replicates was then analyzed based on label-free quantification by considering the values of their ion intensities (log I). Log (I) values ≥5.8 were only considered for further analysis. After their sorting based on log I values, they were compared to an online contaminant repository, the CRAPome[112], to eliminate non-specific proteins (histones, keratins, heat-shock proteins, elongation factors, ribosomal proteins) often reported in control purifications and thus considered background. The final list of proteins unique to HYAL2 pull-down are provided in **Supplementary Table II**

3.21.2. Gene Ontology (GO) analysis of enriched proteins

To further define the proteins (genes), the three categories on which GO analysis is based (molecular function, the biological process and the cellular location) were assessed by GOTermMapper[120]. The unique protein list was entered in the input box followed by independent category selection and '*Homo sapiens*' was selected for annotation (organism). The 'Generic Slim' Ontology was selected for analysis. The charts for each category with GO terms and their frequency of occurrence are provided in **Results 5.10.**

3.21.3. Functional annotation clustering of unique proteins

To identify the GO terms which are enriched in Biological Process (BP) category of the unique proteins, DAVID Bioinformatics Resources 6.8[121] was used. In order to search for the most common GO terms annotated in a cluster, the unique proteins list was submitted to the Gene list panel, the gene identifier 'Official_Gene_Symbol' and 'Gene List' option were selected. To limit random and large annotations from multiple species, *Homo sapiens* was selected. The Human repository was used as a comparator for calculations. From the options in the Functional Annotation, only Biological process category was chosen and the stringency was set to 'High'. From the Display options, Fold change (FC) and False Discovery Rate (FDR) were selected. The results are tabulated in **Table VI.**

3.22.Network map of unique proteins

3.22.1. Network construction and visualization

Proteins uniquely identified from HYAL2 pull-down were mapped onto a network of interactions using NetworkAnalyst version 3.0 [122]. The putative proteins identified through our proximity-labeling approach were submitted. The Generic PPI option with the IMEx Interactome database was set to build the network. After the network construction, Polyubiquitin-C (UBC) node which is known to be involved in many nonspecific interactions was removed as suggested by Xia et al.[122]. The proteins with node degrees ≥ 15 were only selected to create the protein network. The 'Force Atlas' layout was selected to enable the visualization of closely connected hubs. (**Figure 5.11**).

3.22.2. Extraction of functional modules

To enable the identification of enriched functions in the key hubs (nodes), the key nodes from the network were selected and extracted to form modules which are subnetworks with more internal connections inferred by the algorithm (**Figure 5.12**). Gene-disease association networks were analyzed to correlate disease manifestations (if present) with a gene and to assess if the phenotypes related to a certain gene relates to a few phenotypes or the phenotypic spectrum associated with HYAL2 deficiency (**Supplementary Figures 2 and 3**).

CHAPTER 4: RESULTS-I

Biochemical analysis of novel *HYAL2* variants- Expression and localization analysis of novel *HYAL2* disease-causing mutations

The assistance of Dr. Richard Hemming in the protein expression analysis including the PI-PLC analysis to look at cell surface HYAL2 and cooperation of summer students- Emily Barker, Natasha Osawa and Megan Christine Rodriguez in the construct preparation is gratefully acknowledged.

Supervision of Dr. Barbara Triggs-Raine is appreciated throughout the duration of the project.

4.1. Introduction

HYAL2 is a cell-surface protein that is broadly expressed both in mouse and human tissues and is thought to initiate the degradation of HMM HA[4]. Though there has been controversy regarding the role of HYAL2 in HA turnover, our previous studies have established that HYAL2 deficiency is the cause of syndromic cleft lip and palate (CLP) in two unique human populations[100]. Characterization of the two HYAL2 substitution mutations identified in these patients, and a comparison of the human phenotype to that of mice deficient in HYAL2, supported this conclusion. Facial dysmorphism, thickened cardiac valves, cor triatriatum sinister, myopia, hearing loss and pectus excavatum were found to be associated with HYAL2 deficiency. In this study we examined seven novel *HYAL2* variants identified in patients through next generation sequencing to determine if these variants cause deficiency of the cell surface HYAL2, and possibly extend our understanding of the phenotypic spectrum associated with HYAL2 deficiency.

We used a combination of cDNA mutagenesis, protein expression, immunofluorescence and enzyme-based approaches to analyze the intracellular HYAL2 levels and monitor any change in its cell-surface localization due to these reported *HYAL2* variants.

4.2. Generation of HYAL2 constructs expressing novel variants

To assess the impact of the seven novel variants that were identified in patients described in **Table I**, we used fusion PCR which enabled the construction of precisely engineered constructs containing only the desired nucleotide changes in *HYAL2* **(Fig 4.1)**. These included the HYAL2 variants- **713T>G p.L238R , c.611G>C p.G204A, c.194C>G p.S65X, c.1273T>G p.F425V, c.829C>T p.R277C, c.883C>T p.R295X** and **c.1271_1272delAC p.H424Lfs*12** which were introduced by substitution/deletion mutagenesis. Briefly, sense and anti-sense primers containing the desired nucleotide(s) changes in *HYAL2* were used in combination with upstream and downstream primers to generate two PCR products, each bearing the variant. The two PCR products containing the nucleotide variant were then isolated and used as a template for a fusion PCR using only the outermost primers. The resulting fusion PCR amplicon and the full-length HYAL2 cDNA construct were digested with compatible restriction enzymes (**Table III)** to allow replacement of a region of WT HYAL2 with a variant-containing region**.** The digested products were gel purified, ligated and transformed into electrocompetent *E. coli* DH5α by electroporation. After plating onto LB agar containing ampicillin and overnight incubation at 37^{o} C, the experiment was considered successful if the number of colonies on the experimental plate was at least twice that on the control plate. When the experiment was successful, colonies were picked and grown overnight in 3 ml of LB.

Figure 4. 1 Site-directed mutagenesis by primer extension.

Primers B and C (inner primers) contain the desired nucleotide alterations (orange lines). First round of PCR is performed using primer pairs A/B and C/D. The resulting amplicons are subjected to the second round of PCR with the outer primer pair A/D to create the final product with the desired alteration

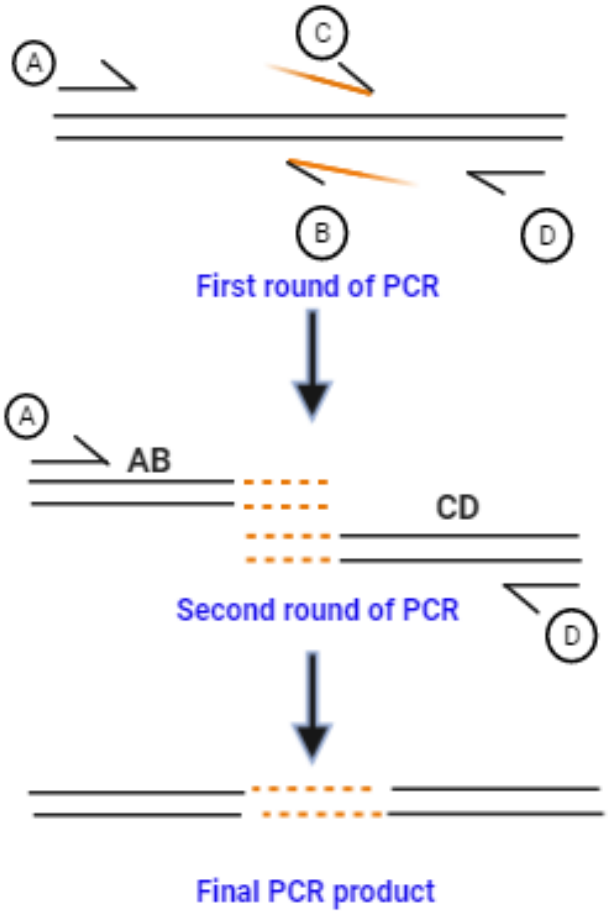

4.2.1. Restriction enzyme analysis of *HYAL2* expression constructs

To verify that each HYAL2 construct harboring a HYAL2 variant was correctly assembled the undigested and digested forms of the plasmids were analyzed by agarose gel electrophoresis **(Fig. 4.2).** The uncut constructs were expected to migrate at the same positions as the WT expression construct. Digestion of the constructs with the same restriction enzymes that were used to generate at the constructs was expected to recut the plasmid if no alterations in sequence took place during cloning and to generate the same sized fragments as that generated from WT-HYAL2. As shown in **Fig**.**4.2**, in all the cases the uncut plasmids ran at a position similar to the uncut WT plasmid. The restriction enzyme digestion resulted in the same fragments as WT. R277C, R295X, L238R, S65X and WT resulted in 1098 bp containing the desired change with EcoRI/ApaI. **(Fig 4.2. A).** In **Fig 4.2. B,** F425V and del AC when digested with EcoRI/PpuMI, resulted in 1361 bp fragment containing the desired change. G204A when digested with EcoRI/ApaI resulted in a fragment of 1098 bp similar to **Fig 4.2.A**.

Figure 4. 2 Restriction digestion analysis of the WT and variant containing constructs.

Uncut (UC) or Cut (C) DNA samples were separated on a 1.0 % agarose gel, stained with ethidium bromide and visualized. The uncut plasmids are ~ 6192 bp. The expected sizes of the restriction for R277C, R295X, L238R, S65X, G204A and WT HYAL2 digested with EcoRI/ApaI resulted in the desired fragment sizes of 1098 bp and 5094 bp [A and B]. The expected sizes for F425V and del AC when digested with EcoRI/PpuMI, resulted in 1361 bp and 4831 bp fragments. 1 kb DNA ladder is used as reference.

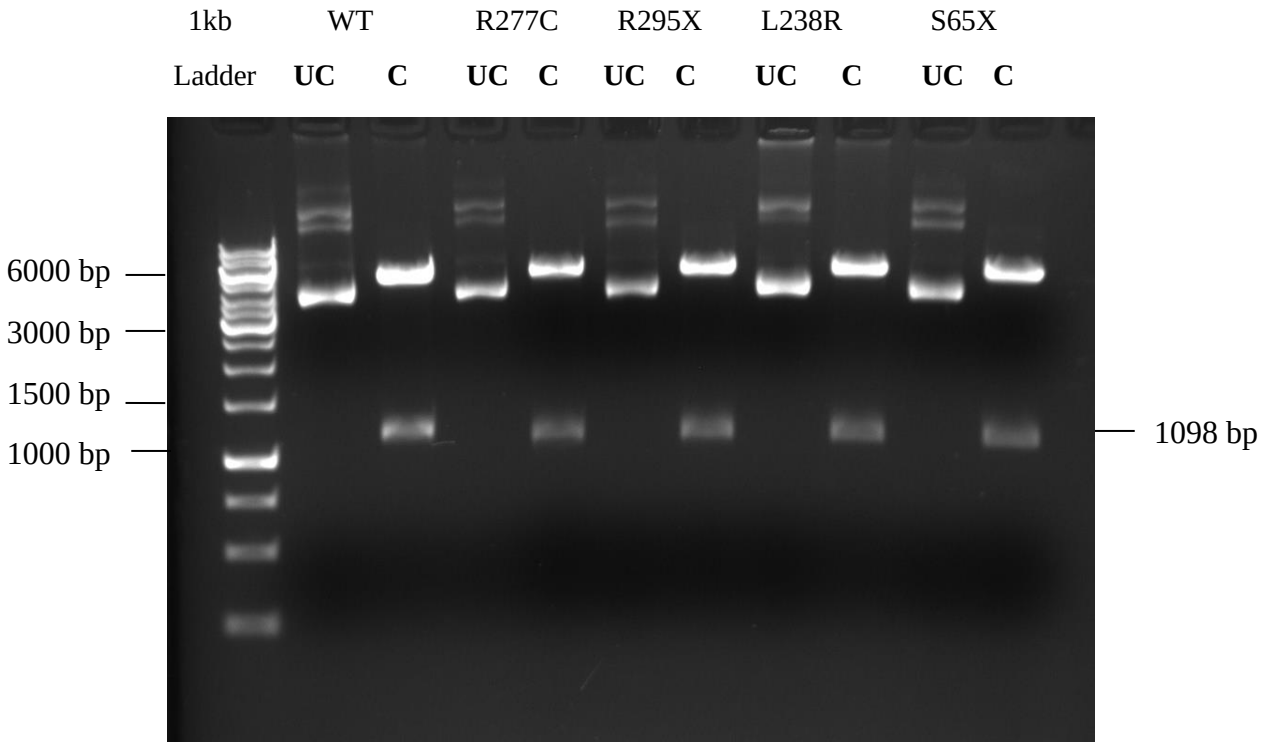

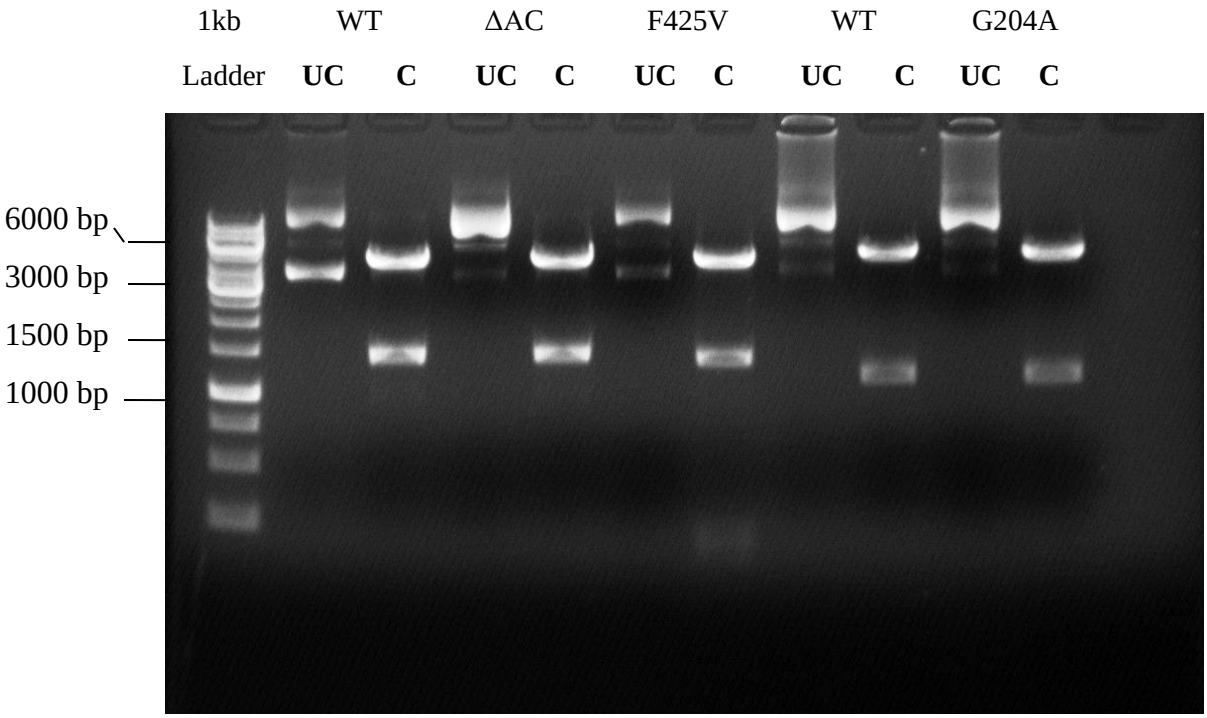

4.2.2 Verification of *HYAL2* variants by sequence analysis

The *HYAL2* variants c.713T>G p.L238R, c.611G>C p.G204A, c.1271_1272delAC p.H424Lfs*12, c.194C>G p.S65X, c.1273T>G p.F425V, c.829C>T p.R277C and c.883C>T p.R295X were introduced into the HYAL2 expression vector. After their successful restriction digestion, ligation and transformation, the newly made *HYAL2* constructs were isolated and sent for sequencing to ensure the desired base pair changes, and no others, were present. As shown in **Fig 4.3.**, the desired mutations were found to be present in the Sanger sequencing results for each construct. No other mutations were found within the coding sequencing (data not shown).

Figure 4. 3 Electropherograms of HYAL2 variants.

The altered base is highlighted with a light blue bar. For delAC, two base pairs (AC) between AC and TT (light blue bar) were deleted

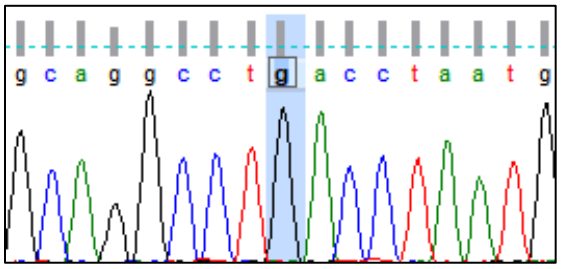

p.Ser65Ter (c.194C>G)

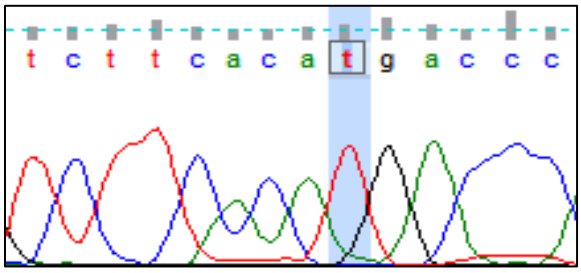

p.Arg295Ter (c.883C>T)

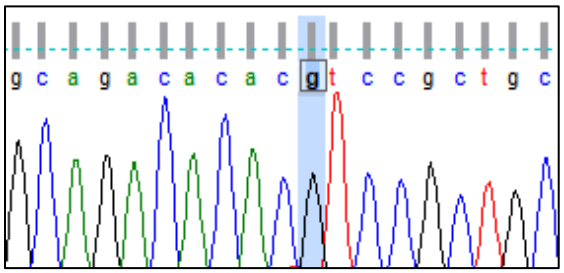

p.Phe425Val (c.1273T>G)

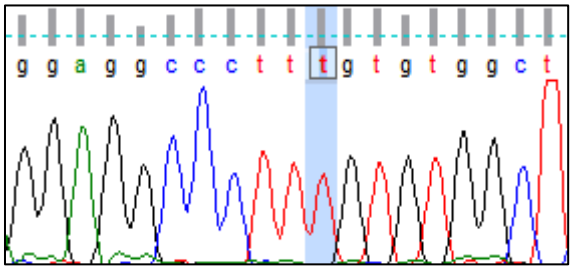

p.Arg277Cys (c.829C>T)

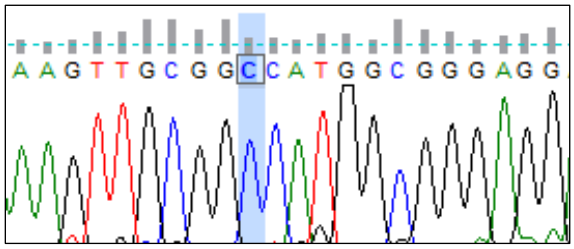

p.Gly204Ala (c.611G>C)

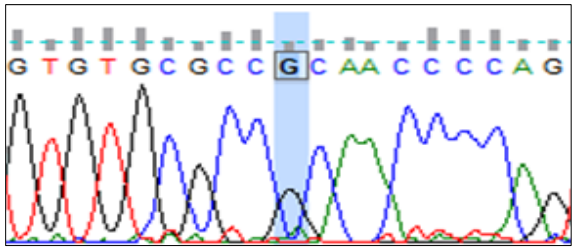

p.Leu238Arg (c.713T>G)

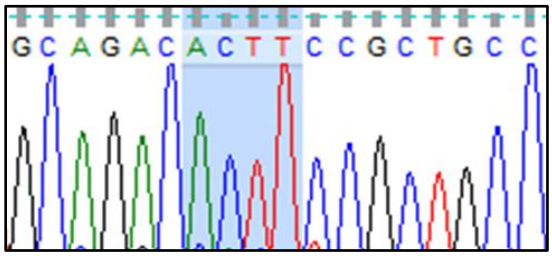

p.H424Lfs*12 (c.1271_1272delAC)

4.3. Analysis of the impact of *HYAL2* variants on protein expression

The impact of the seven novel variants on the steady-state levels of the HYAL2 protein were analyzed by transiently transfecting constructs expressing wild type and variant-containing proteins in HYAL2-deficient MEFs. A plasmid containing a deletion near the beginning of HYAL2 that included the starting methionine was included as a negative control. Each construct was transiently expressed in each well of a six well plate following the protocol that was previously optimized and described in **3.9**. Lysates were prepared from the wells after 48 hrs, the time point at which the transient expression of HYAL2 was determined in previous studies to be maximal. Equal amounts of protein lysates were separated on a western blot to visualize HYAL2 protein expression from all the variants.

The levels of expression were compared to the HYAL2 expressed from the WT cDNA. As shown in **Fig 4.4. A** S65X and R295X terminations resulted in no detectable HYAL2 protein. L238R, F425V and R277C resulted in very low levels of detectable HYAL2, suggesting that the protein is unstable. Two variants, G204A and delAC resulted in levels similar to that of the WT HYAL2. These outcomes are also illustrated in **Fig.4.4. B** which shows the average volume intensities (luminescence units) of four experiments (tabulated in **Table IV**) examining the impact of the variants on HYAL2 levels.

Figure 4. 4 Expression of HYAL2 in *Hyal2-/-* MEFs.

Immunoblot analysis of protein lysates (10 µg per lane) prepared from transfections with HYAL2 expression vectors were analyzed with anti-HYAL2 (upper panel) and anti-β-actin (lower panel). HYAL2 is indicated by an arrow and the asterisk indicates a cross reacting band that is evident even in the control. The control was transfected with a vector that does not express HYAL2 [A]. Quantification of the immunoblots. The average ± SEM of the luminescence units from four separate transfection experiments (Table IV) are shown by the bars. The significance for each mutant compared to the WT was determined using a paired t-test using the ratios from each experiment. (ns-not significant; p≤0.0001 (****); p ≤0.001 (***); p≤0.01 (**) [B]

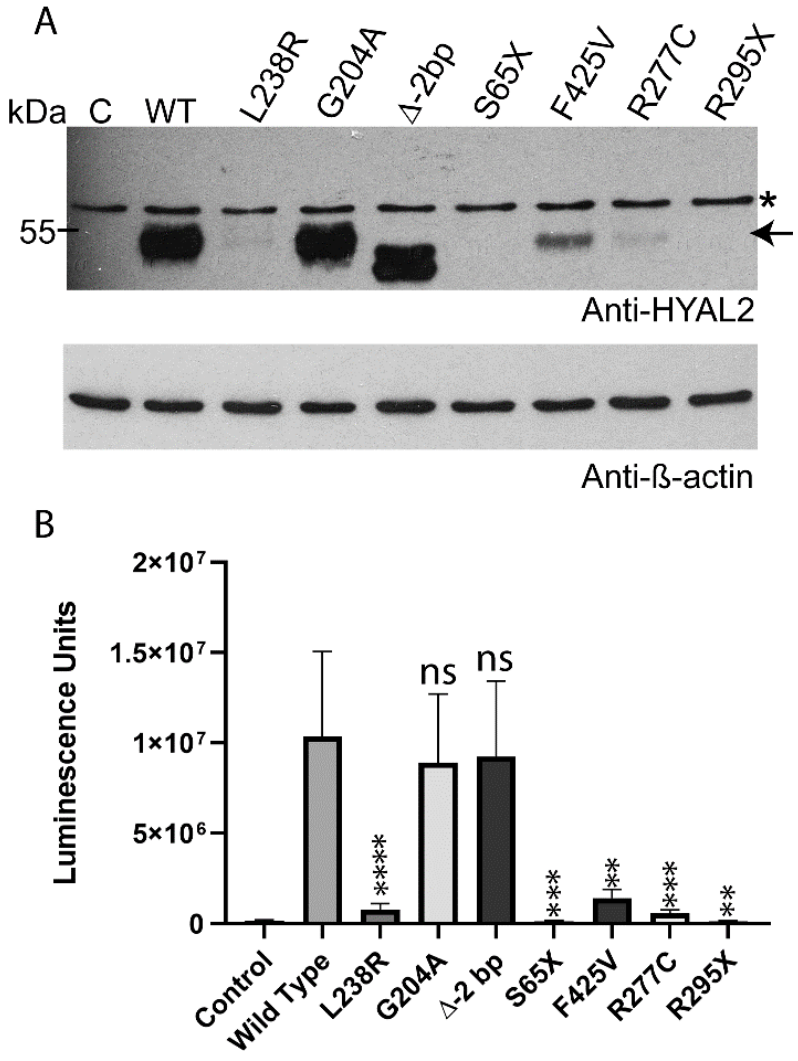

Table IV. Adjusted volume intensities of seven HYAL2 variants with WT and control (C).

The ratio (relative quantity volume) of background-adjusted volume intensity and background-adjusted reference volume intensity for each biological replicate is provided. The ratios across all four biological replicates are averaged (Avg) and standard deviation (SD) is calculated.

Sample	Ratio Rep 1	Ratio Rep 2	Ratio Rep 3	Ratio Rep 4	Avg	SD
WT	1	1	1	1	1	
L238R	0.05	0.09	0.06	0.06	0.065	0.017
G204A	0.4	0.87	0.81	1.09	0.80	0.28
AC Del (Δ2bp)	0.54	0.8	0.88	1.09	0.82	0.22
S65X	0	0	0	0.001	0.00	0.00
F425V	0.09	0.23	0.08	0.15	0.13	0.068
R277C	0.04	0.08	0.03	0.06	0.05	0.02
R295X	0	0	0	0	0	0
Con (C)	0	0	0	0	0	0

4.4. Removal of cell surface HYAL2 with phospholipase C

GPI-APs contain an ER signal sequence directing them to the ER lumen where the hydrophobic C-terminal sequence is cleaved off and replaced with a GPI anchor which further directs the protein through the secretory pathway and finally helps in its anchorage to the external leaflet of cell-membrane. PI-PLC releases the GPI-linked protein from the cell-surface to the extracellular space. To evaluate if the variants have impacted the GPI-anchor and to confirm the presence of low levels of HYAL2 at the surface of some of the mutant HYAL2-transfected cells, we released cell surface HYAL2 with phosphatidylinositol-specific phospholipase C (PI-PLC). **(Fig. 4.5.)** Media collected from cells expressing the WT form of HYAL2 was analyzed before and after treatment with PI-PLC. A low level of HYAL2 (-PLC) was detected in the medium, but this was much lower than the amount released into the medium after 2 hrs of incubation with PLC. Only two other variants, L238R and G204A resulted in a substantial level of HYAL2 released from the cell surface. No other variant showed any release of cell-surface HYAL2. This was consistent with the results of the immunolocalization **(Fig 4.6.)**. Interestingly, although HYAL2 typically has two bands visible by immunoblot that differ in glycosylation (as demonstrated in past PNGase F studies that resulted in a single band), one of each of these bands predominated in the presence of each of these mutations, resulting in a slower migrating form of HYAL2 predominating in the L238R sample.

Figure 4. 5 Immunoblot analysis of HYAL2 released by PI-PLC treatment.

Hyal2-/- MEFs that were transfected with WT HYAL2 and HYAL2 variants were incubated with (+) or without (-) PLC to release the cell surface HYAL2. HYAL2 was detected by immunoblot after the protein in the media was concentrated. The arrow indicates HYAL2. This blot is representative of three independent experiments.

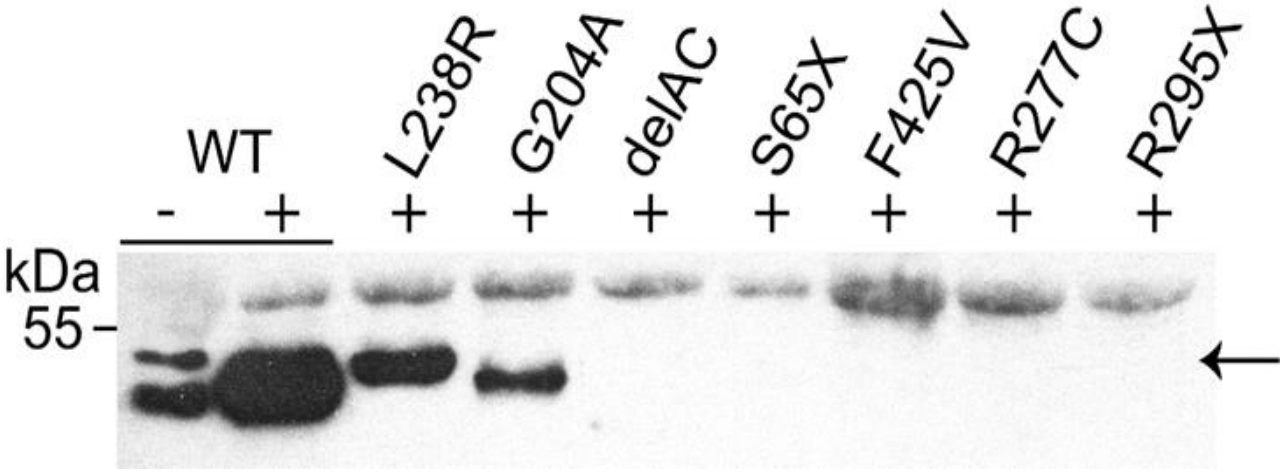

4.5. Localization analysis of HYAL2 variants by immunofluorescence

HYAL2 that is normally processed and targeted is glycosylated, has a GPI anchor added, and is localized to the cell surface. Mutations that impact folding could lead to ER-mediated degradation and/or a failure to add the GPI anchor to the C-terminus. These mutations would be expected to result in a reduced presence of HYAL2 at the cell surface. To assess this immunofluorescence was performed on transfected cells under non-permeabilized conditions to detect cell surface HYAL2 and permeabilized conditions to detect intracellular HYAL2 following the protocol described in 3.13. As shown in **Fig 4.6**., WT HYAL2 was abundantly detected at the cell surface and within the cells and no signal was detected from untransfected *Hyal2-/-* MEFs acting as the negative control. L238R and G204A mutants showed low expression of cell-surface HYAL2. None of the mutations resulted in a substantial level of HYAL2 at the cell surface although several of the mutations allowed for the expression of a substantial level of intracellular HYAL2. The only mutations that resulted in no HYAL2 intracellularly and at the surface were the two termination codons (S65X and R295X).

Figure 4. 6 Comparative immunolocalization of *HYAL2* variants expressed in *Hyal2-/-* MEFs

The transfected Hyal2-/- MEFs were fixed and incubated with anti-HYAL2 primary antibody under permeabilized (Perm) and non-permeabilized (N-Perm) conditions. HYAL2 was detected with Alexa Fluor 568-conjugated donkey anti-rabbit secondary antibody (orange-fluorescent). Nuclei are stained blue with DAPI. Scale bars, 20µm. 63X magnification. Representative microscopy images of at least three independent experiments are shown.

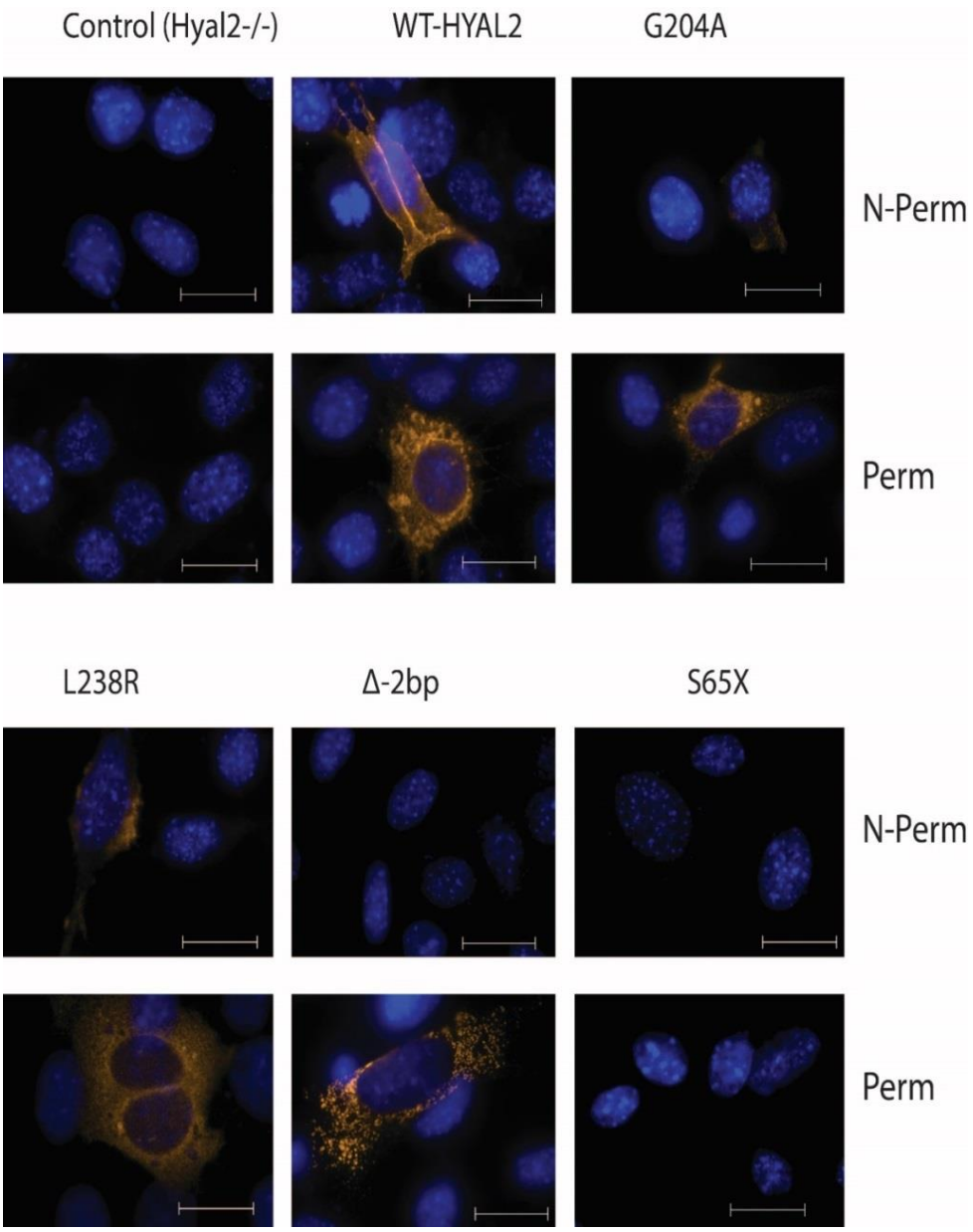

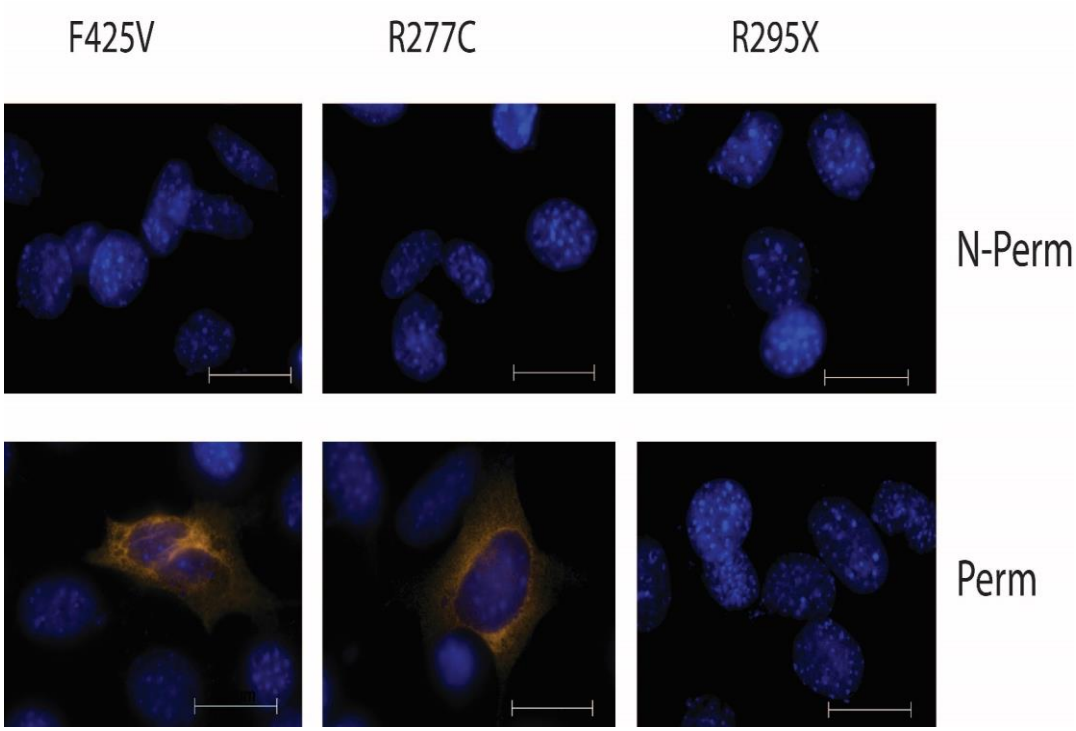
F425V
R277C
R295X
N-Perm
Perm

Chapter 5 : RESULTS- II

Establishing a method for identifying HYAL2-interacting partners using the Biotin Identification (BioID) proximity labelling system

The assistance of Dr. Carina Villacres, Ying Lao, Victor Spicer and Dr. Oleg Krokhin from Manitoba Centre for Proteomics and Systems Biology in conducting the Mass spectrometry analysis and providing insights into the data, is deeply acknowledged. Help from Co-op student, Nikolas R. Furletti in literature survey and the supervision of Dr. Barbara Triggs-Raine during construct preparation are appreciated.

5.1. Introduction

In the current model of HA degradation, HYAL2 is presumed to generate HA fragments (10-20 kDa) from large-sized extracellular HA (>200 kDa) that are bound by a receptor and internalized for lysosomal degradation[4]. However, we (unpublished) and others have found either weak[57] or no activity[60] associated with HYAL2 using exogenous HA as a substrate. Our studies show that the size and levels of HA are increased in tissues of *Hyal2-/-* mice[5], clearly indicating that HYAL2 has a role in HA degradation. The broad expression and cell surface localization of HYAL2 suggested that it functions in the daily turnover of 5 g of HA in an average human[4]. However, the extent of HA accumulation in *Hyal2-/-* mouse tissues[5] could not account for this level of turnover. We speculate that HYAL2's activity is regulated to allow the activation of signaling pathways only at specific stages/times or that the HA must be decorated with specific binding proteins in order to be recognized as a substrate by HYAL2. The identification of HYAL2-interacting partners is an important step in determining the full spectrum of molecules involved in HYAL2-mediated turnover of HA. Though there are a few cell-surface receptors that are thought to interact with HYAL2, there is still not enough evidence to call them bona fide interactors of HYAL2.

To enable the identification of protein partners of HYAL2 without excluding transient or weak interactors, we employed the novel biotin proximity labeling system called Biotin Identification or BioID. BioID takes advantage of a prokaryotic biotin protein ligase which when fused to a protein of interest or 'bait' promiscuously biotinylates vicinal 'preys' or interactors of the bait protein[128, 136]. The biotinylated proteins are then captured using an avidin or streptavidin based affinity matrix and analyzed by mass spectrometry for peptide identification. The BioID approach is represented via the schematic below (**Fig 5.1**). BioID is especially valuable for studying the PPIs of membrane proteins which are often lost due to harsh membrane disruption conditions during conventional affinity purification approaches. Besides employing BioID as the protein-capture method, we have used a combination of proteomics, functional analysis and network biology validated by statistical parameters to establish a screening method and build a library of probable HYAL2 proximal proteins which is likely to include interacting binding partners of HYAL2.

Please note: BioID2 (26 kDa)[136] which is a smaller and advanced form of BioID (35 kDa) has been used to conduct the PPI study of HYAL2. The terms BioID and BioID2 have been used interchangeably throughout the document. SS-BioID2-HYAL2 and BioID2-HYAL2 used alternatively in the document refers to the same construct- BioID2 fused to HYAL2.

Figure 5. 1 Proximity-dependent labeling of proteins by BioID

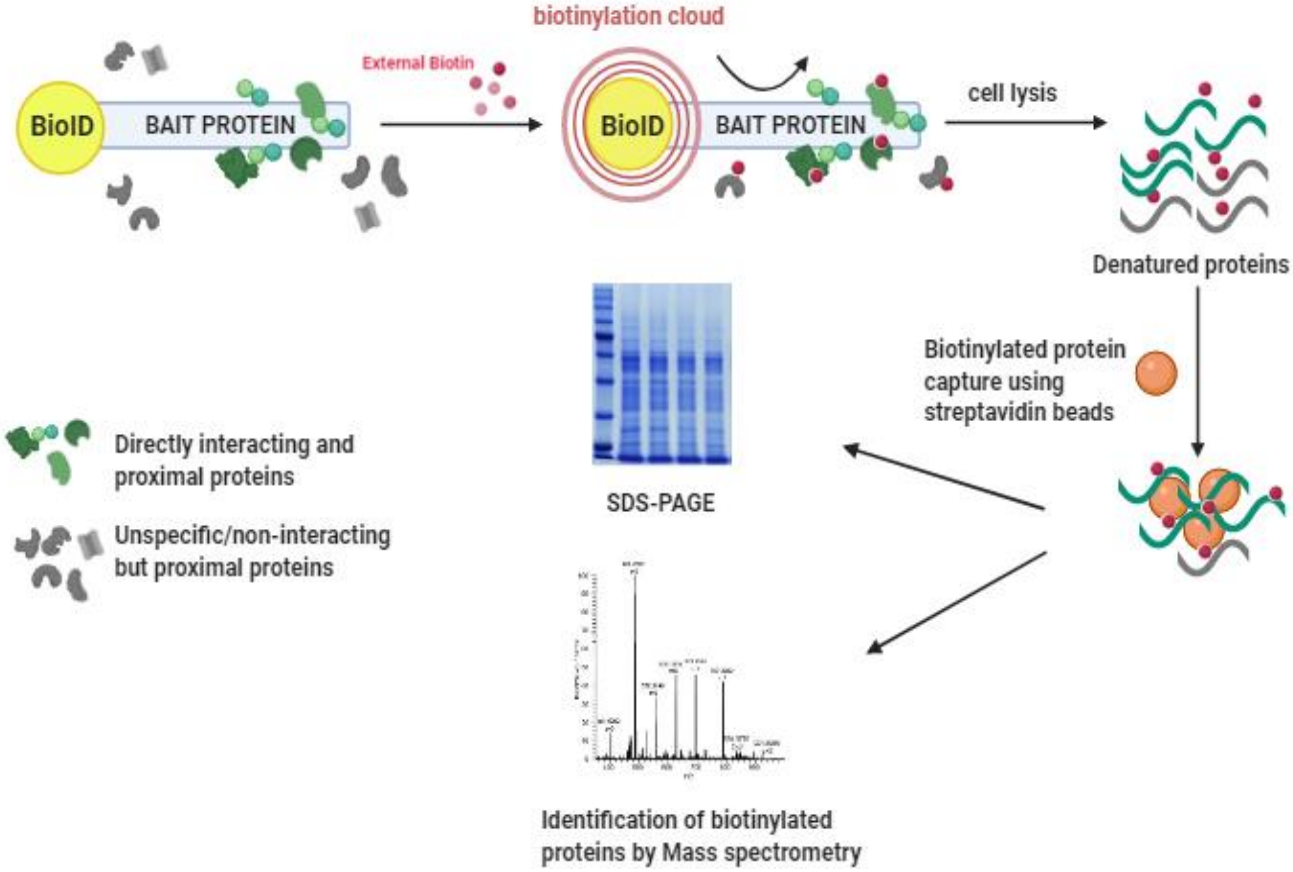

5.2. Generation of Flag-HYAL2 plasmid construct

HYAL2 is a cell-surface protein with an ER signal sequence (SS) at the N-terminus and a GPI anchor at the C-terminus. Therefore, finding a position to fuse the biotin ligase (BioID2) within HYAL2 to ensure its function remained unchanged after the fusion was an important first step. In an attempt to the find an ideal site within HYAL2, we analyzed a previously reported fusion between the Flag tag and HYAL2 to verify it did not interfere with the localization or stabilization of HYAL2. If we found no change in the expression or cell-surface localization of HYAL2, we intended to use the same site for BioID fusion. We received Flag-tagged Hyal2 cloned into the pCMV1 vector (Sigma) as a kind gift from Dr. Dusty Miller (**Rai et al. 2001, PNAS 98:4443-8**).This construct had the Hyal2 cDNA starting at the second Met (M2) cloned into the pFLAG-CMV1 vector (sequences attached), resulting in the CMV promoter driving expression of the protein: SS (ER signal sequence) - Flag tag - Hyal2.The SS with Flag epitope and a portion of *HYAL2* cDNA was cloned from the pCMV1-Flag-HYAL2 construct (6088 bp) into our mammalian expression vector, pCMV6-XL5 containing the full-length *HYAL2*cDNA (6192 bp) using the restriction enzymes ApaI and SnaBI and following the protocol described in **3.15**.

Figure 5. 2 Plasmid maps of donor (pFLAG-CMV1) and recipient plasmids (pCMV6-XL5 FLAG-HYAL2.

Restriction enzymes ApaI and SnaBI were used to clone SS-FLAG-HYAL2 from donor (A) plasmid to the recipient (B) generating a construct of 6216bp. SS- signal sequence, M2- second methionine, N- N-terminus, C- C-terminus

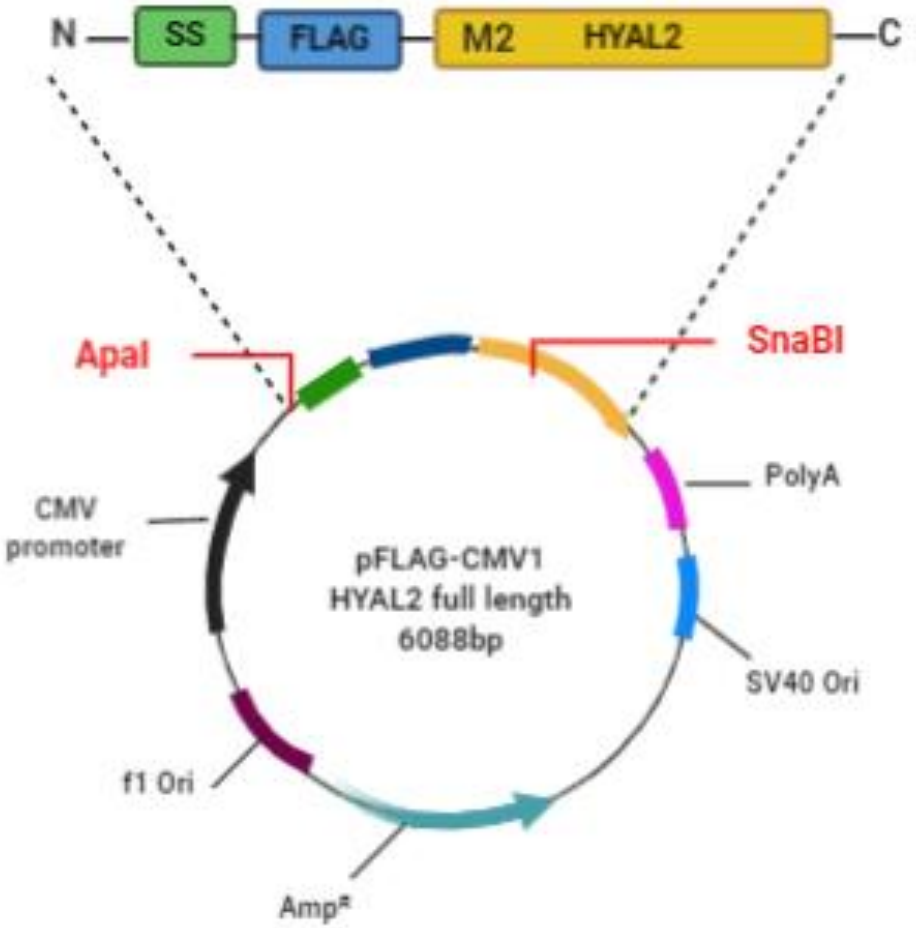

(A)

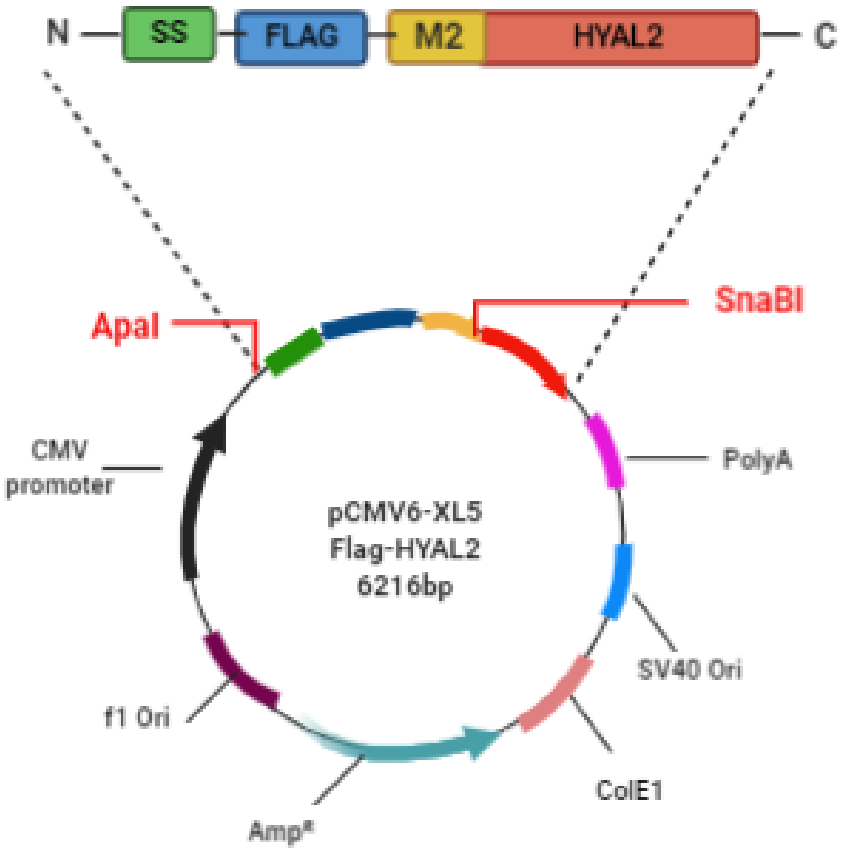

(B)

\

5.3. Protein expression analysis of Flag-HYAL2

To verify if the newly constructed Flag-HYAL2 was functional, we assessed HYAL2 protein expression and stability.To use the construct further, the level of steady-state Flag-HYAL2 should be similar to that of WT-HYAL2. Flag-HYAL2 was transfected into *Hyal2-/-* MEFs following the procedure outlined in **3.9**. Lysates were prepared from the wells after 48 hrs, the time point at which the transient expression of HYAL2 was determined in previous studies to be maximal. Equal amounts of protein were separated by SDS-PAGE.

Levels of Flag-HYAL2 were compared to that of WT-HYAL2 by western-blot using an anti-HYAL2 antibody (**Fig. 5.3.**). As shown in **Fig 5.3**., lane 1(from left) containing the cell lysate

preparation from *Hyal2-/-* MEFs showed no HYAL2 expression. Lane 2 containing the cell lysate transfected only with the vector backbone (pCMV6-XL5) also showed no expression as expected. In lane 3, Flag-HYAL2 resulted in levels similar to that of WT HYAL2 in lane 4. In lysates from Flag-HYAL2 and WT-HYAL2 –transfected cells, two bands are detected that were not present in untransfected cells. Two bands are often detected for WT-HYAL2 and because only one band is detected after PNGase F treatment (data not shown) these two bands are due to differences in N-linked glycosylation. The two bands detected in Flag-HYAL2 lysates were also found to result from differences in N-linked glycosylation (**Supplementary Figure 1**). The slightly larger size of the two Flag-HYAL2 bands is thought to be due to the presence of the added Flag tag which has a mass of 1.013 kDa and a few additional amino acids acting as a linker.

Figure 5. 3 Flag HYAL2 expression in transfected *Hyal2-/-* mouse embryonic fibroblasts (MEFs).

Immunoblot analysis of protein lysates (20 µg per lane) prepared from transfections with HYAL2 expression vectors were analyzed with anti-HYAL2. HYAL2 is indicated by an arrow and the asterisk indicates a cross reacting band that is evident even in the control.

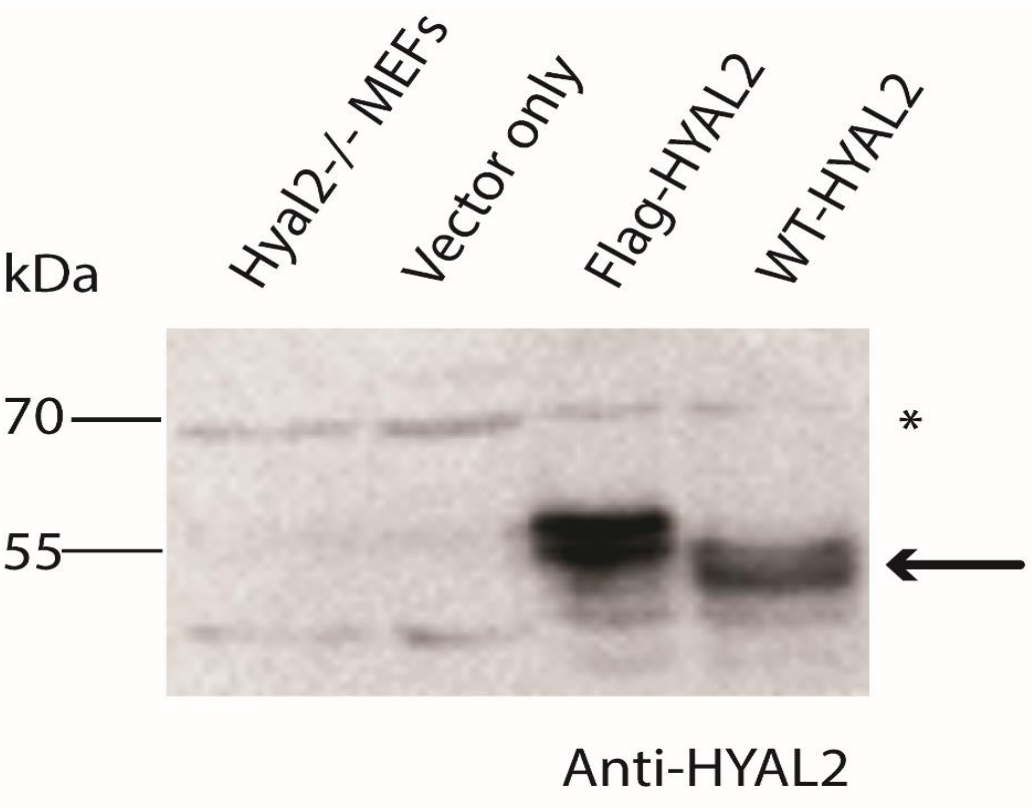

5.4. Cell-surface localization analysis of Flag-HYAL2 by IF

An important determinant of HYAL2 function is its localization. HYAL2 gets processed as a GPI-anchored protein resulting in its integration into the external leaflet of the plasma membrane. To verify if the newly made Flag-HYAL2 protein localized to the cell-surface similar to WT-HYAL2, cells transfected with both Flag-HYAL2 and WT-HYAL2 were subjected to immunolocalization following the protocol described in 3.13. The localization analysis showed that Flag-HYAL2 translocated to the cell-surface similar to that of WT-HYAL2 when examined under non-permeabilized conditions. Under non-permeabilized conditions with the cell-membrane intact, distinct orange-fluorescent signals specific to HYAL2 were detected on the surface of the *Hyal2*-/- MEFs (**Fig 5.4.)** which confirms the report of **Rai et al. (2001)** theat the Pre-protrypsin signal followed by the Flag-tag at the N-terminus of HYAL2 did not interfere with its localization to the plasma membrane. The WT-HYAL2 (**Fig 5.4.A)** and Flag-HYAL2 (**Fig 5.4. B)** were compared to negative control, *Hyal2*-/- MEFs (**Fig 5.4. C)** expressing no cell-surface HYAL2 to test for any non-specificity of the antibody or to avoid any artifacts based on autofluorescence of the cells. No background fluorescence was recorded with the negative control. The Flag-HYAL2 did appear to have a slightly reduced signal compared to the WT-HYAL2 but given that this was an overexpression system, we did not think this would be a disadvantage in the BioID system.

Figure 5. 4 Localization of Flag-HYAL2 and WT-HYAL2 by IF.

Flag-HYAL2 and WT-HYAL2 were transiently expressed in *Hyal2-/* -MEFs. HYAL2 (orange) was localized using anti-HYAL2 and Alexa Fluor 568-conjugated donkey anti-rabbit secondary antibody under permeabilized (Perm) and non-permeabilized (Non-Perm) conditions. Nuclei are stained blue with DAPI. Scale bars, 20μm. 63X magnification. Representative microscopy images from at least three independent experiments are shown.

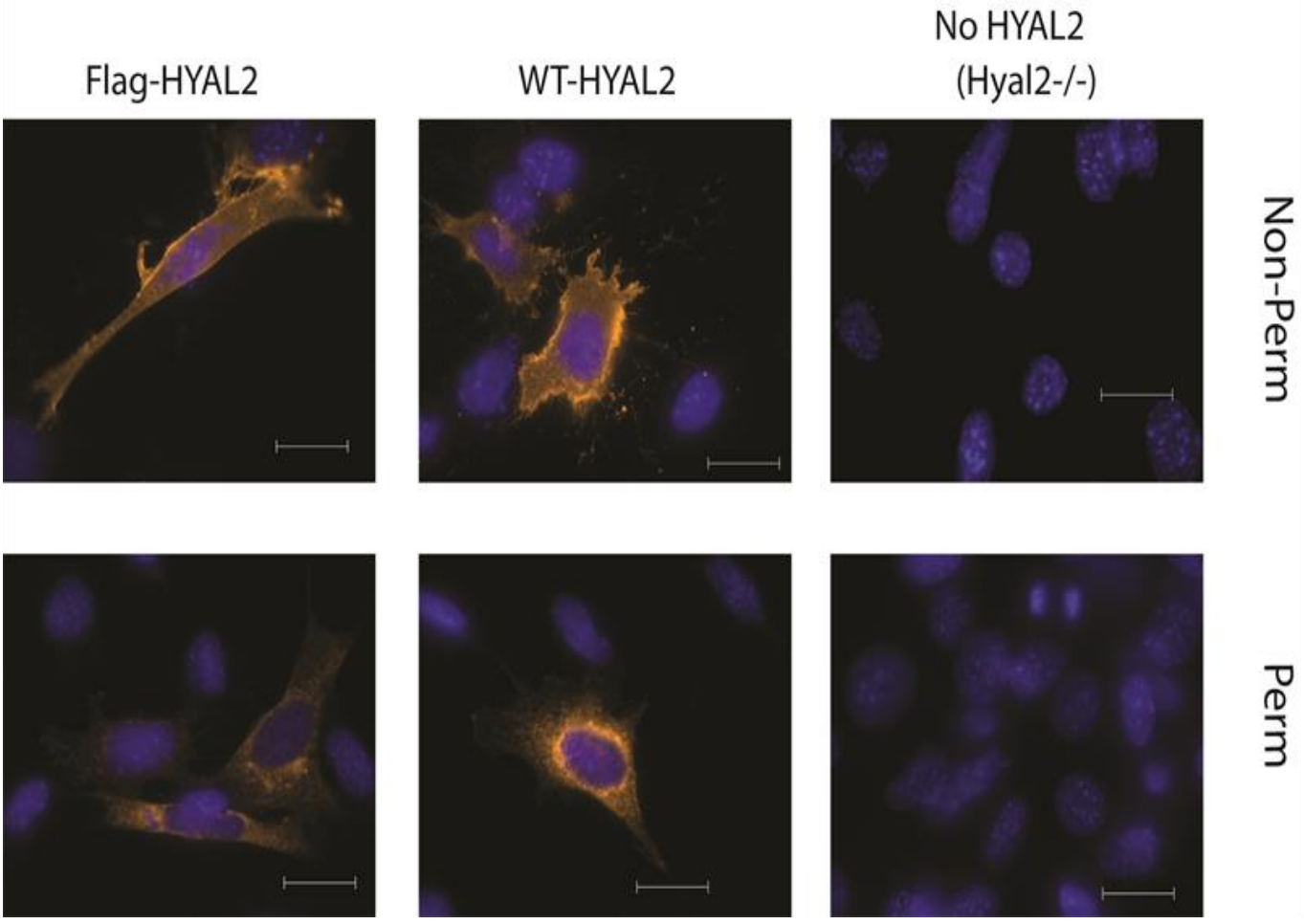

5.5. Cloning of SS-BioID2-HYAL2 and restriction digestion verification

Once the expression and appropriate localization of Flag-HYAL2 were ensured, biotin ligase, BioID2[136] required to conduct the proximity biotinylation study, was fused to HYAL2 at the exact site where Flag-tag was fused. The signal sequence (SS) which essentially guides HYAL2 to travel through the secretory pathway inside the cell to anchor itself on the cell surface, was also introduced upstream to the the BioID2-HYAL2 at the N-terminal. This was achieved through two major steps by fusion-PCR based cloning. The first step included fusing BioID2 (696 bp) to HYAL2 (~1422 bp) and the second step was to fuse SS to BioID2-HYAL2 and clone it back to our mammalian expression vector, pCMV6-XL5. After two rounds of fusion-PCRs and restriction digestions by EcoRI and ApaI, the desired SS-BioID2-HYAL2 was constructed.

5.5.1. Making the BioID2-HYAL2 construct:

Step 1: Hyal2 was amplified by fusion PCR by using forward primer (WPG 1287) 5' -AGCTCCTCGAGATGGAGCTCAAGCCCACAGCACCA-3' containing an XhoI site (underlined) and reverse primer (WPG 1289) 5'-CTTGGTTCCCGAATAGACCC-3' from the PCMV1-Flag Hyal2 (Dr. Dusty Miller's construct).

Step 2: The successful PCR product was then gel purified and restriction enzyme digested with XhoI and BamHI (downstream to the WPG 1289 primer sequence). The recipient vector which in this case was myc-BioID2-MCS (Addgene) was also digested with the same pair of restriction enzymes. The length of the PCR amplified insert after digestion was 1405 bp and length of the BioID2 containing vector post digestion was 6085 bp.

Step 3: The digested products were then gel purified and subjected to ligation. After successful ligation, colonies were picked, cultured and DNA was prepared. The ligated BioID2-Hyal2 construct was 7490 bp.

5.5.2. Making the Signal sequence (SS)-BioID2-HYAL2 construct:

With the BioID2-Hyal2 now fused together, our aim was to introduce the ER signal sequence upstream to BioID2 at the N-terminus. Therefore, the primers were designed accordingly. The primers used were:

WPG 1290 (Forward primer with an EcoRI site [underlined below], the entire signal sequence [italicized] and a short portion of BioID2):
cgaattc*atgtctgcacttctgatcctagctcttgttggagctgcagttgct*ttcaagaacctgatctggctgaagga

WPG 1294 (Reverse primer extending from Hyal2 into BioID2): cttgagctccatgcttcttctcaggctgaa

WPG 1293 (Forward primer extending from BioID into Hyal2): ttcagcctgagaagaagcatggagctcaag

WPG 1295 (Reverse primer after ApaI site): cactggcattgctcaccactc

Step 1: Two separate fusion PCRs were run using the already made BioID2-Hyal2 construct as the template. For the first PCR (to introduce the SS into BioID2-Hyal2), the forward primer WPG 1290 and reverse primer 1294 were used generating a 760 bp fragment after gel purification. The second PCR was run with the forward primer WPG 1293 and reverse primer WPG 1295 generating a 1277 bp fragment.

Step 2: The two fragments were joined by fusion PCR to generate the entire construct containing the EcoRI-SS-BioID2-Hyal2. The fragment length was 2037 bp.

Step 3: This construct was then subjected to restriction digestion by EcoRI (upstream to the SS) and by ApaI (inside the Hyal2 construct) and then gel purified. The recipient vector, PCMV6-WT Hyal2 was digested with the same. The insert length was found to be 1780 bp and the vector length was 5081bp.

Step 4: The vector and insert were subjected to ligation and after successful transformation and miniprep, the entire fragment SS-BioID2-Hyal2 was found to be 6861bp. Cloning was complete.

Step 5: Just as an additional step to verify the newly made SS-BioID2-HYAL2, it was subjected to EcoRI and ApaI digestion. As a control, WT Hyal2 was also digested by the same. It was observed that the SS-BioID2-Hyal2 has a bp length of 1780 bp (as observed before, step 3) and the WT Hyal2 without the (SS and BioID2) was found to be around 1100bp as expected.

Figure 5. 5 SS-BioID2-HYAL2 and WT-HYAL2 comparison on agarose gel.

pCMV6-XL5 expression vector containing SS-BioID2-HYAL2 (6861 bp) and pCMV6-XL5 expression vector containing WT-HYAL2 (6192 bp) were restriction enzyme digested with EcoRI and ApaI to demonstrate the change in size due to BioID2 (~ 690 bp) incorporation.

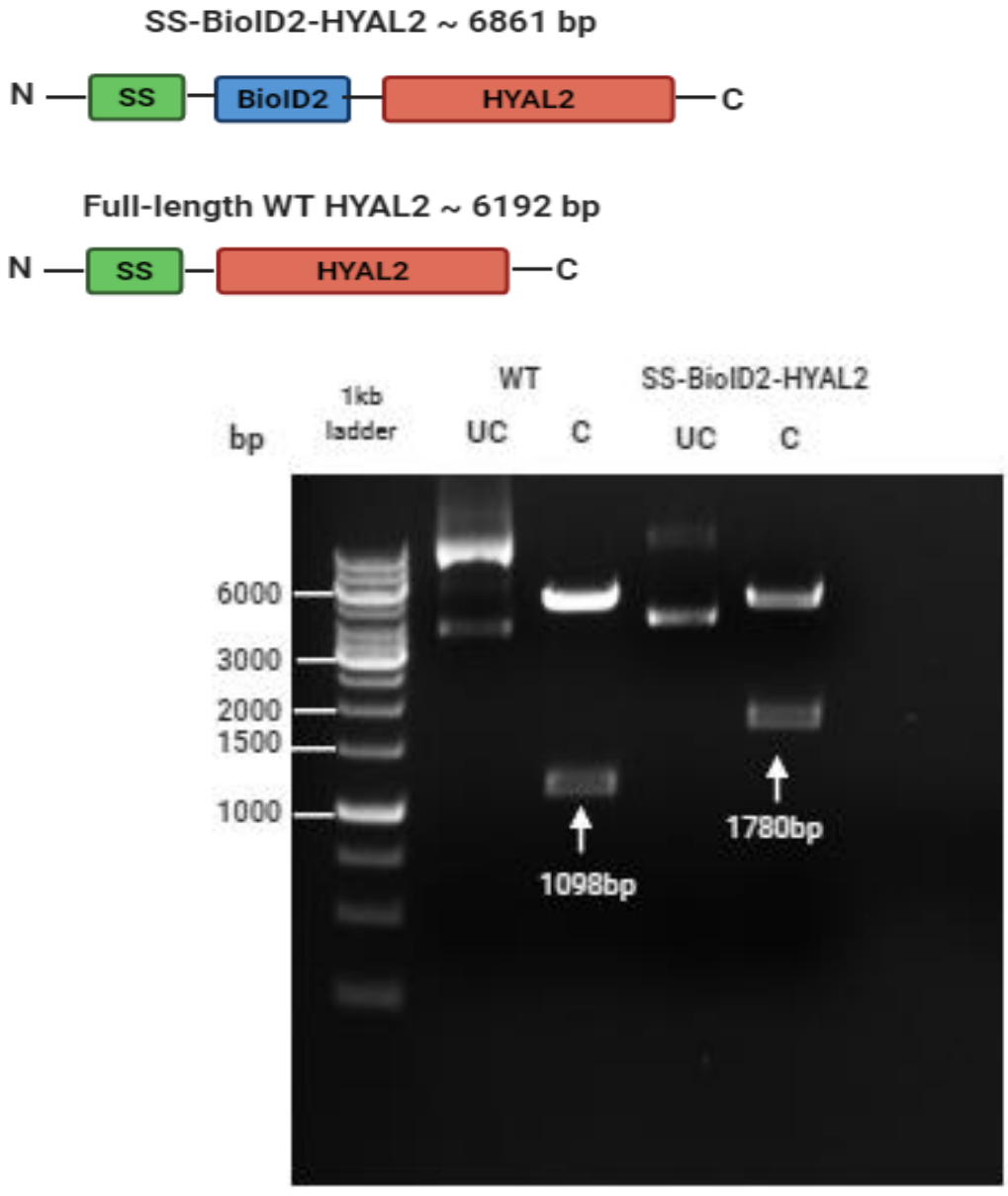

5.6. Protein expression analysis of SS-BioID2-HYAL2(BioID2-HYAL2)

The expression levels of the BioID-tagged fusion protein (BioID2-HYAL2) should ideally mimic the wild-type protein (WT-HYAL2) expression levels[137].The availability of anti-HYAL2 antibody to ensure the specific detection of HYAL2 facilitated the comparison of the expression levels. BioID2-HYAL2 after its construction and purification was expressed in *Hyal2*$^{-/-}$ MEFs alongside the WT-HYAL2 and BioID2-only (vector containing only BioID2) to assess the expression and stability of the proteins. The cDNAs were transfected into *Hyal2*$^{-/-}$ MEFs in 6-well plates following the protocol described in 3.9. The cells were scraped and sonicated and the resulting lysates were analyzed by SDS-PAGE followed by western blotting. In **Fig 5.6.A**. lane 1(from left) shows a band of WT-HYAL2 with a molecular weight of approximately 53 kDa. Lane 2 with cells transfected with BioID2-only shows no band when incubated with anti-HYAL2 antibody. Lane 3 shows a band approximately 80kDa (calculated molecular weight of SS-BioID2-HYAL2 ~ 81 kDa) which when compared to lane 1 with WT-HYAL2, is clearly larger in size. An extra band at 55 kDa similar to WT-HYAL2 can be seen in lane 3, which we speculate to be a minor degradation product of the expressed fusion protein. To further validate the fusion protein we used a 10 % SDS PAGE gel and probed with anti-BioID2 antibody. In **Fig 5.6.B,** lane 1 shows a band of ~ 80 kDa which is thought to be SS-BioID2-HYAL2 and lane 2 shows a distinct and clear 26 kDa band which is just BioID2 without SS or HYAL2 fused to it.

Figure 5. 6 Western blots of WT-HYAL2 and SS-BioID2-HYAL2

Cell lysates (20 µg of protein) from WT HYAL2, BioID2, or BioID2-HYAL2 transiently transfected MEFs were analyzed by western blot following separation by 7.5 % [A] or 10% [B] SDS-PAGE. The blots were probed with anti-HYAL2 [A] or anti-BioID2 [B] respectively.

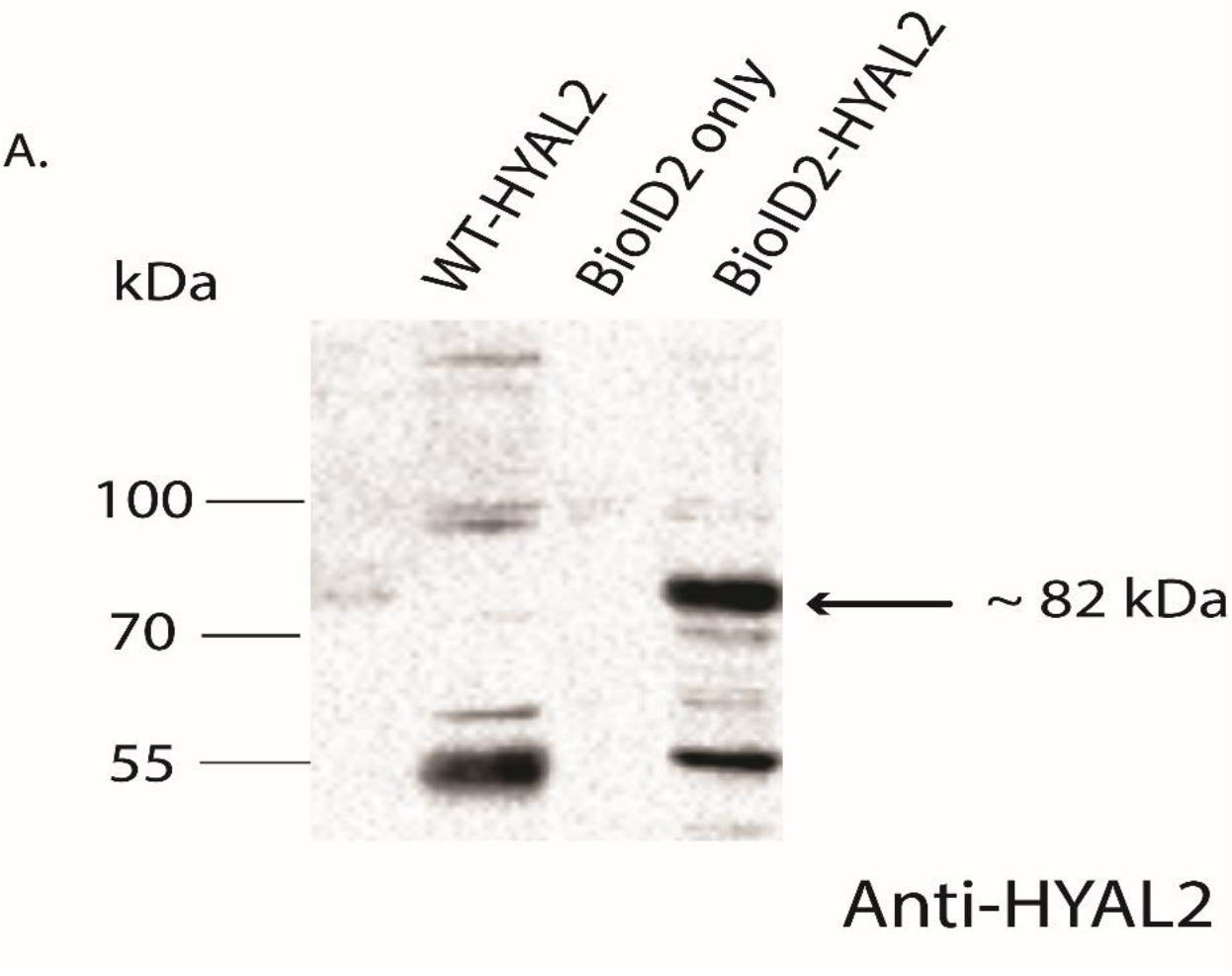

-

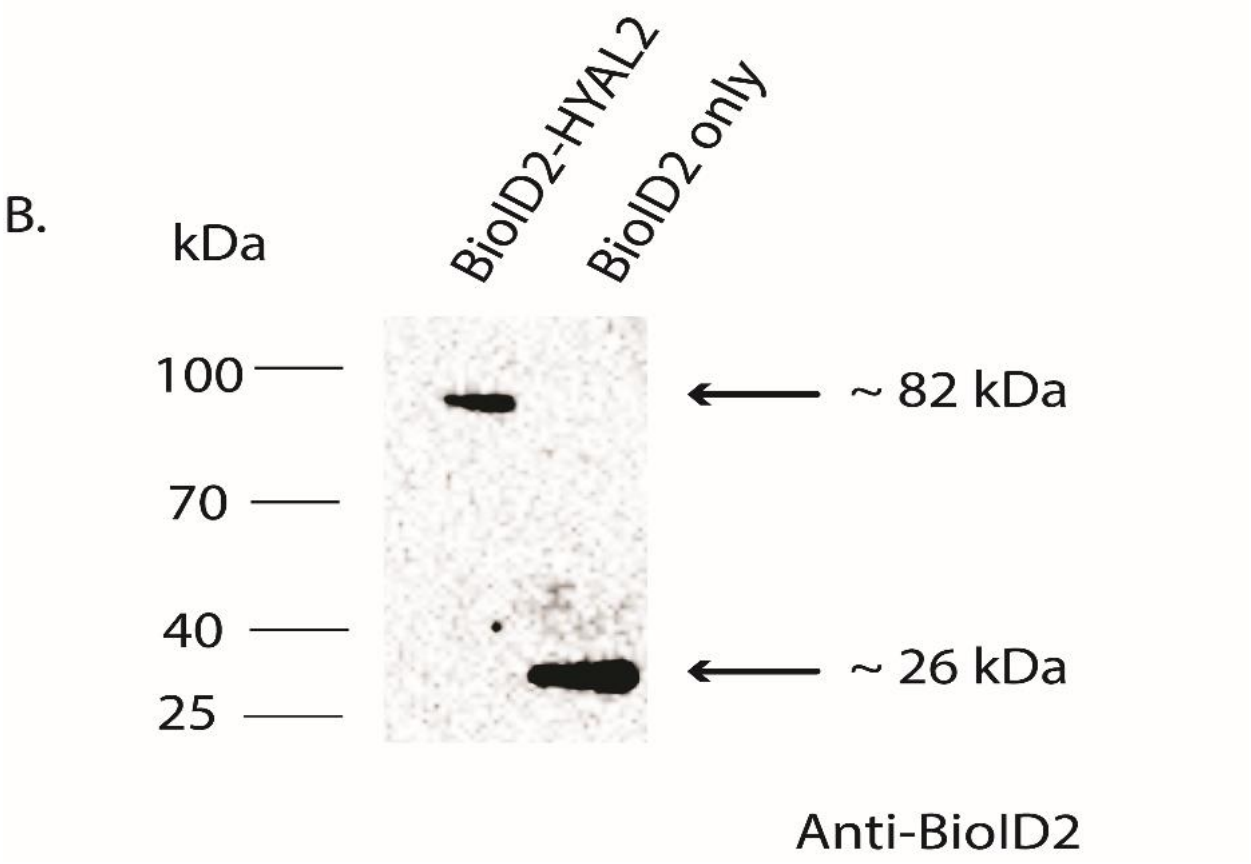

5.7. Analysis of biotinylation by BioID2-only and SS-BioID2-HYAL2 constructs

The biotin ligases are designed to enable promiscuous biotinylation of proteins in a proximity-dependent fashion. Proteins covalently marked with biotin are captured by an avidin or streptavidin-based affinity system. It was crucial to assess if the newly made constructs expressing SS-BioID2-HYAL2 and BioID2-only were capable of biotinylation of proximal proteins when supplemented with exogenous biotin. The cells expressing SS-BioID2-HYAL2 and BioID2-only were supplemented with 50 µM biotin 24 hrs post-transfection. After18 hrs of biotinylation, cells were harvested, and cell lysates were separated by 7.5 % SDS-PAGE. After transfer to nitrocellulose the blot was probed with HRP-conjugated Streptavidin for 1 hr. Streptavidin binds to biotin with a high-affinity and the conjugated HRP acts as a detection

system for biotinylated targets. Lane 1 in **Fig 5.7.**shows extensive biotinylation of endogenous proteins by cells expressing BioID2-only. Lane 2 with cells expressing SS-BioID2-HYAL2 showed comparatively less biotinylation of proteins compared to lane 1 possibly due to increased specificity of the fusion protein towards biotinylating proteins proximal to HYAL2. The BioID2-only control often identifies proteins that are randomly biotinylated based on their overabundance or due to their affinity toward biotin ligase. There are also certain proteins which tend to attach to streptavidin beads specifically or non-specifically which supposedly leads to more biotinylation in the controls than in the experimental samples where BioID is fused to a bait protein[142] .We also speculate, since BioID2-HYAL2 shows a more targeted cellular localization i.e. to the cell-surface unlike the BioID2-only control, it shows more restricted and targeted biotinylation of proteins in the cell.

Figure 5. 7 Biotinylation by BioID2 and BioID2-HYAL2.

Following SDS-PAGE separation, the protein lysates (20 µg) of BioID2 and BioID2-HYAL2 were supplemented with externall biotin and incubated with streptavidin-HRP. Increased biotinylation of the proteins in cells transfected with BioID2-only were detected compared to BioID2-HYAL2-transfected cells.

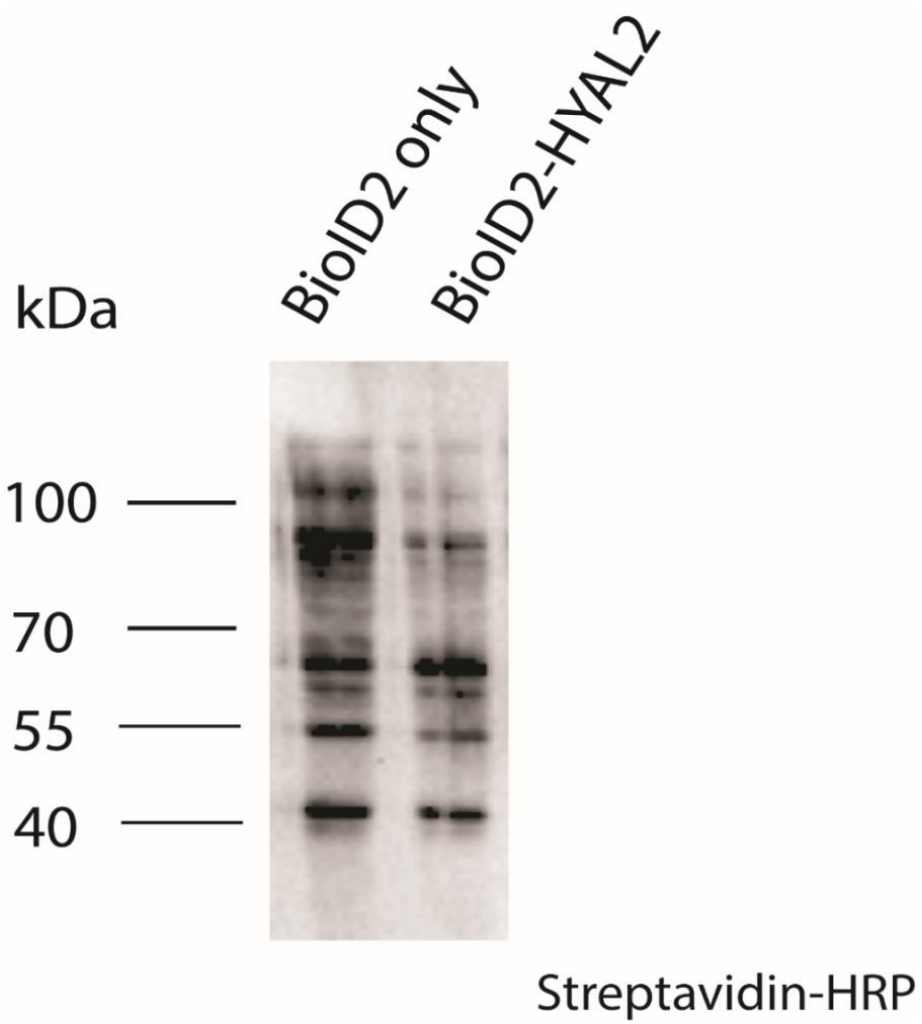

5.8. Verification of cell-surface localization of SS-BioID2-HYAL2

HYAL2 that is normally processed and targeted is glycosylated, has a GPI anchor added, and is localized to the cell surface. Any change that impact folding and structural conformation, could lead to ER-mediated degradation and/or a failure to add the GPI anchor to the C-terminus. We have verified effective cell-surface localization of the Flag-HYAL2 protein. However, it was important to ensure that SS-BioID2-HYAL2 reached the cell-surface as WT-HYAL2 or Flag-HYAL2 since confirming the subcellular localization of the BioID-tagged fusion protein is necessary to permit the biotinylation of proximal cell surface proteins. Immunofluorescence was performed on *Hyal2-/-* MEFs transfected with WT-HYAL2, SS-BioID2-HYAL2 and BioID2-only for effective comparisons. Following the protocol described in **3.13**, the cells were subjected to both non-permeabilized conditions to detect cell surface HYAL2 and permeabilized condition to detect intracellular HYAL2**.** In **Fig 5.8.** the 1st column showing SS-BioID2-HYAL2 (alternatively termed as BioID2-HYAL2) under non-permeabilized conditions shows cell-surface targeting and is comparable to the WT-HYAL2 in 2nd column when incubated with anti-HYAL2 primary antibody. Permeabilized cells expressing either SS-BioID2-HYAL2 or WT-HYAL2 show intracellular HYAL2. In the 3rd column, cells expressing BioID2-only shows no HYAL2 expression both under non-permeabilized and permeabilized conditions when probed with anti-HYAL2 antibody demonstrating no false positive detection by the antibody.

Please note: GPI-anchored proteins (GPI-APs) tend to move in homoclusters and they have high affinity for each other. They fuse into heteroclusters which are fully functional[111]. The clustering of SS-BioID2-HYAL2 observed under non-permeabilized condition might be attributed to this heteroclustering of GPI-APs.

Figure 5. 8 Cell-surface localization of BioID2-HYAL2.

The *Hyal2-/-* MEFs transfected with BioID2-HYAL2 showed cell-surface localization when incubated with anti-HYAL2 antibody similar to WT-HYAL2. Cells transfected with vector containing only BioID2 showed no expression with the anti-HYAL2 antibody. HYAL2 is detected with Alexa Fluor 568-conjugated donkey anti-rabbit secondary antibody (orange-fluorescent). Nuclei were stained blue with DAPI. Scale bars, 20 μm. 63X magnification. Representative microscopy images are from at least three independent experiments are shown. (Perm- permeabilization, Non-Perm- Non-permeabilized)

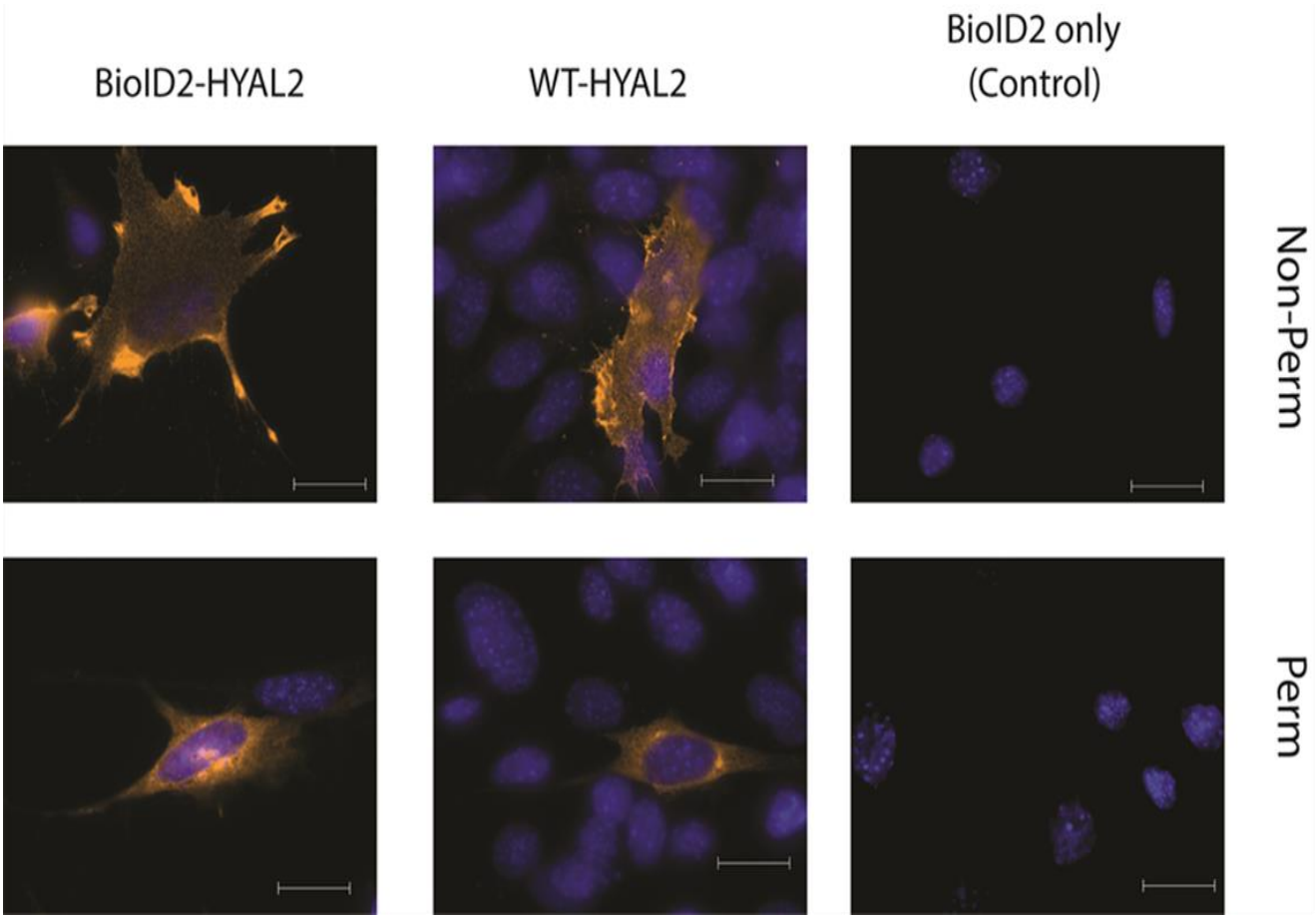

5.9. Analysis of peptides in BioID2 and BioID2-HYAL2 samples by mass spectrometry

Peptides prepared from two biological replicates as described in **3.20** were analyzed and detected masses from both SS-BioID2-HYAL2 and BioID2-only samples were identified and quantified using X!tandem [ALANINE (2017.02.01)]. X!Tandem open source is software that can match tandem mass spectra with peptide sequences. Modified peptides were not identified if a predicted mass for this modification was not included in the matching database. The total proteins detected for both replicates of control (BioID2) and experimental (SS-BioID2-HYAL2) samples can be searched using the links provided in **Supplementary Table I**. Unique peptides were identified by MS (**Table V**). Two or more unique peptides were required to identify a mouse protein or human homologue. These are referred to as "selected peptides".

Table V. Peptides detected by MS and predicted proteins.

Summary of MS data defined using X! Tandem. Control- BioID2 only sample, Exp- Experimental (SS-BioID2-HYAL2) sample, Rep- Biological replicate. Unique peptides- number of unique peptide sequences associated with a protein assignment (mouse protein or human homologue), Selected peptides- peptides selected from unique peptides which are assigned a statistical confidence.

	Control (Rep I)	Exp (Rep I)	Control (Rep II)	Exp (Rep II)
Proteins	2125	1884	2518	2338
Homologs	7795	5078	8535	6128
Total proteins	9920	6962	11053	8466
Unique peptides	15069	21158	15977	22338
Selected peptides	9733	12191	9859	14321

Proteins that were identified were further analyzed to define those that were unique to the BioID2-HYAL2 sample **(Fig.5.9).** Comparisons of the proteins identified in the BioID2 and BioID2-HYAL2 replicates revealed 456 and 819 unique protein/homologues respectively. There were 93 proteins that were consistently present in both replicates with a log (I) (the base-10 log of the sum of the fragment ion intensities in the tandem mass spectra) value ≥ 5.8 were selected for further analysis. This list of 93 proteins was further filtered using the CRAPome contaminant repository to eliminate common background contaminants, mitochondrial ribosomal and Electron transport system proteins. The final list of unique proteins/homologues was reduced to 64 after excluding common electron transport chain proteins (**Supplementary Table II**).

Figure 5. 9 Unique protein sorting pipeline

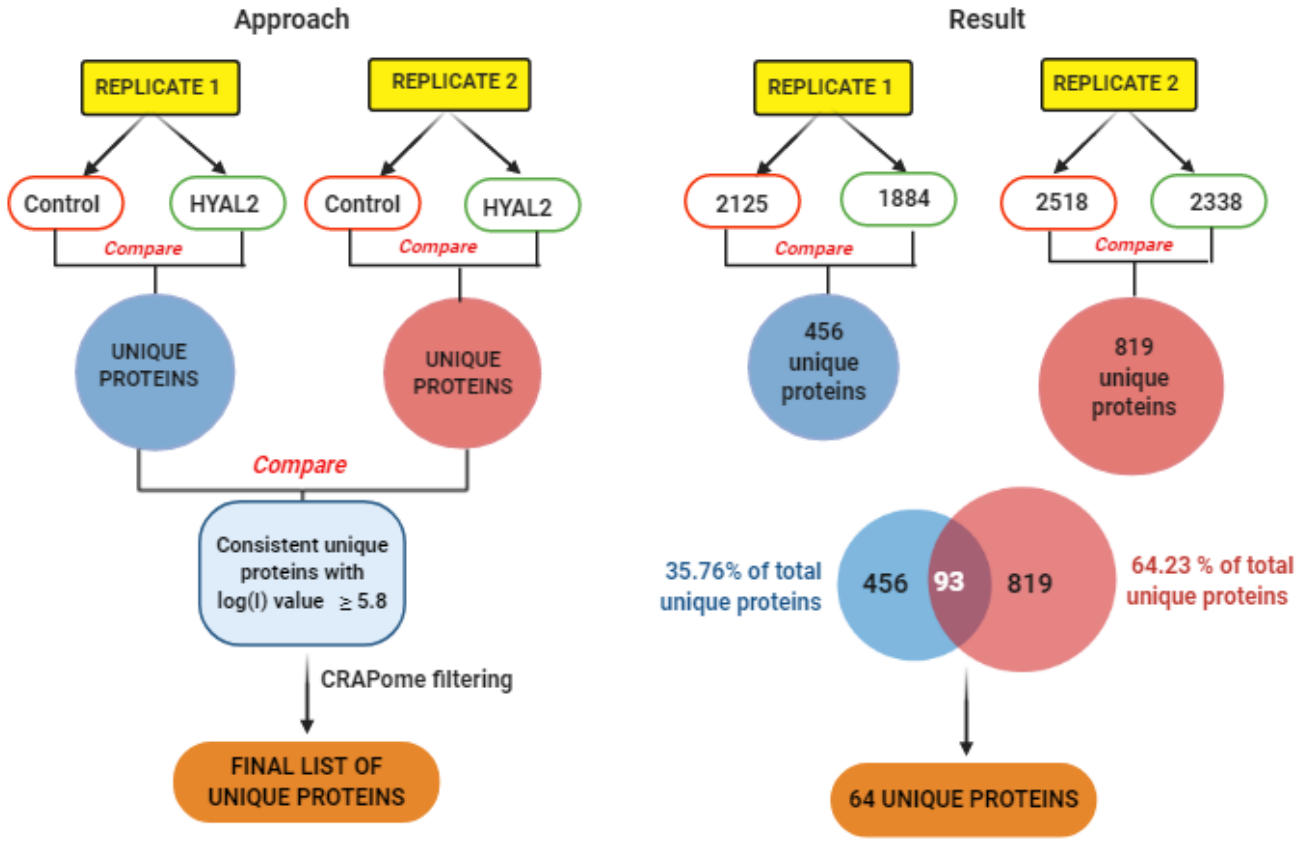

5.10. Gene Ontology (GO) analysis

Gene Ontology annotations form a comprehensive and dynamic way of describing sets of genes or proteins. GO terms are highly structured and provide a collective nomenclature containing numerical identifiers (GO ID) to delineate the functional characteristics of a gene or protein.The combined information from repositories of published research and data mining using bioinformatics and artificial intelligence makes the GO project an excellent resource to categorise the biological attributes of a gene or protein[138, 139].

Manual GO annotation was performed using the GO browser, GOTermMapper[120] with the goa_human (Generic GO slim) terms for biological process (BP), molecular function (MF) and cellular component (CC) selected. GO subsets (also known as GO slims) are trimmed versions of the GO representing the major gene ontology categories (From http://geneontology.org/docs/go-subset-guide/). Based on GO recommendations, terms that were represented by more than one gene were included from each category The numbers of proteins annotated to each term are expressed as a percentage of the total number of Uniprot identifiers submitted to this term in GO Term Mapper.

For the BP category, 63 of our final list of 64 unique proteins were annotated. The majority of these were part of the signal transduction, transport, response to stress and anatomical structure development terms (**Fig 5.10 A**). One protein, PRORP, was not annotated in this category.

There are many genes/proteins for which no molecular function is defined and therefore it is not surprising that for MF, only 43 out of 64 unique proteins were found to be annotated. In the MF category, ion binding and enzyme binding were the highest occurring terms (**Fig 5.10 B**). Eighteen proteins (NOMO1, ARL6IP1, TMED1, TMED5, CLPTM1, ERP29, IGFN1, YIPF3, TMEM97, SYNGR2, CD151, MRC2,MANBAL, HDDC2, LYST, CX3CL, GPRC5A and NIPSNAP2) were not part of any major annotated terms in GO slim.

All of the proteins were annoted in the CC category which defines the predicted localization of proteins inside the cell or its extracellular environment. The majority of the proteins were plasma-membrane proteins followed by ER and extracellular proteins (**Fig 5.10 C**).

Figure 5. 10 Gene ontology (GO) annotation of unique proteins using GOTerm Mapper.

The horizontal axis represents GO term annotation frequency in percentage. The vertical axis is the GO Terms annotated.

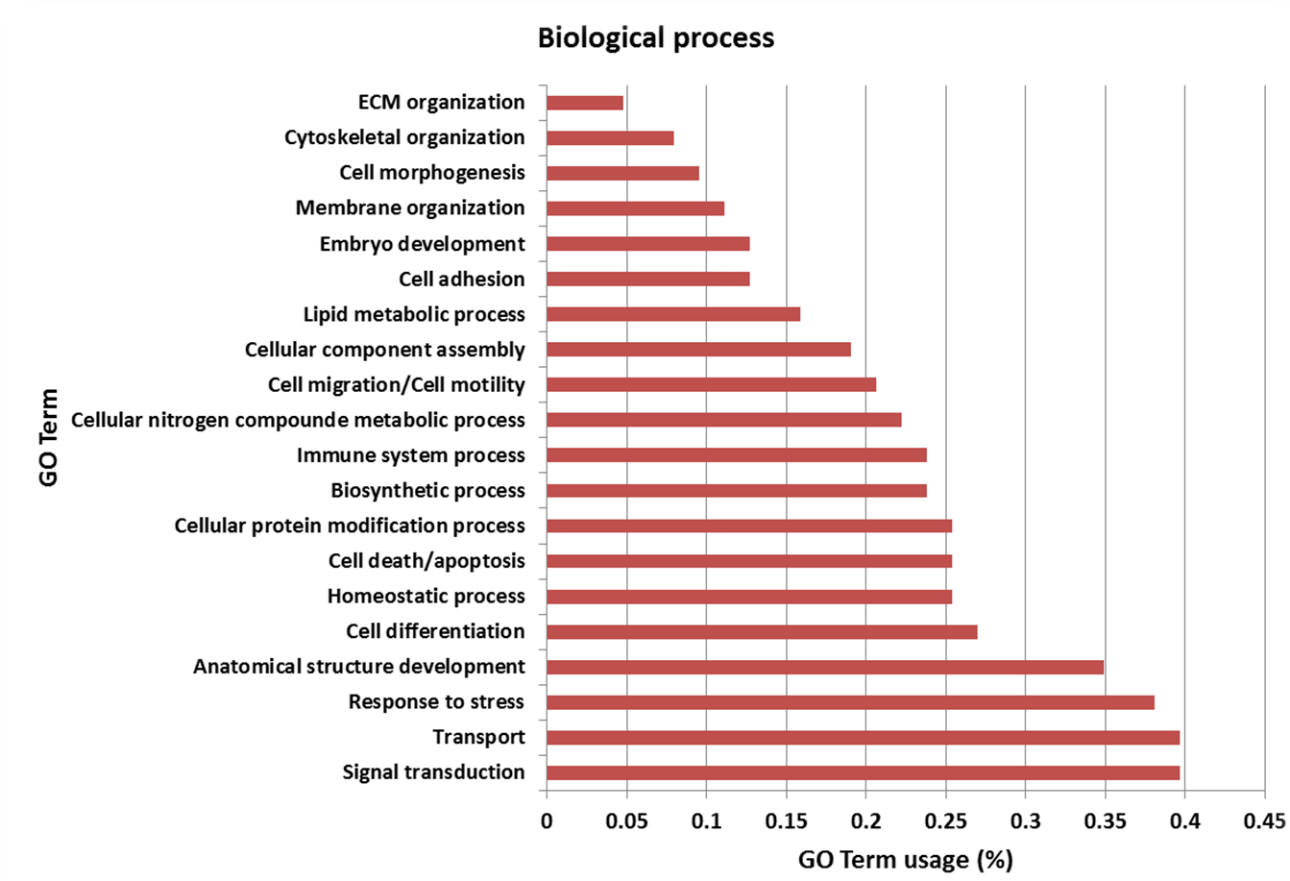

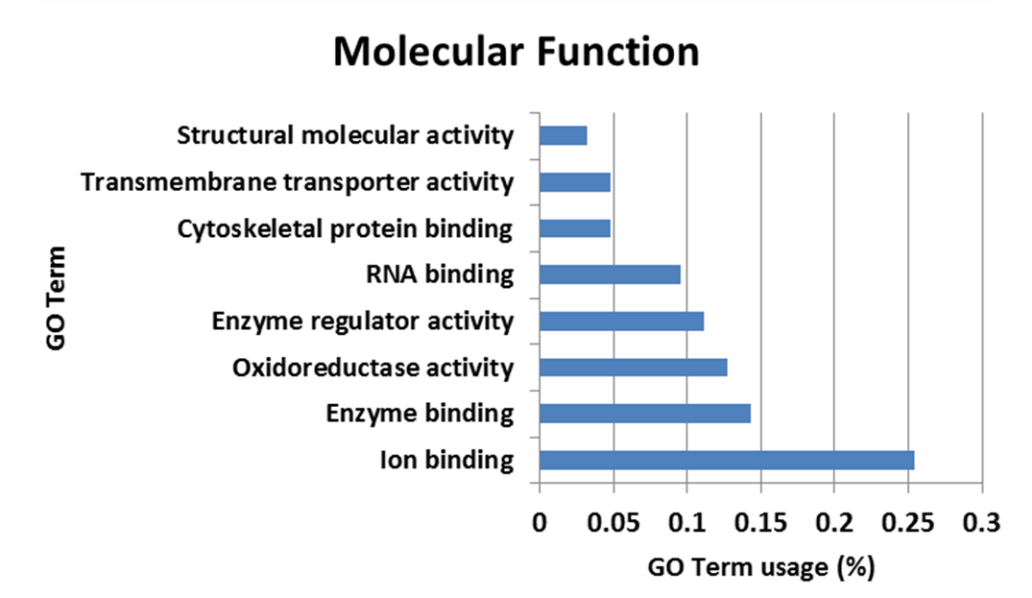
Molecular Function
Structural molecular activity
Transmembrane transporter activity
Cytoskeletal protein binding
RNA binding
Enzyme regulator activity
Oxidoreductase activity
Enzyme binding
Ion binding
GO Term
0
0.05
0.1
0.15
0.2
0.25
0.3
GO Term usage (%)

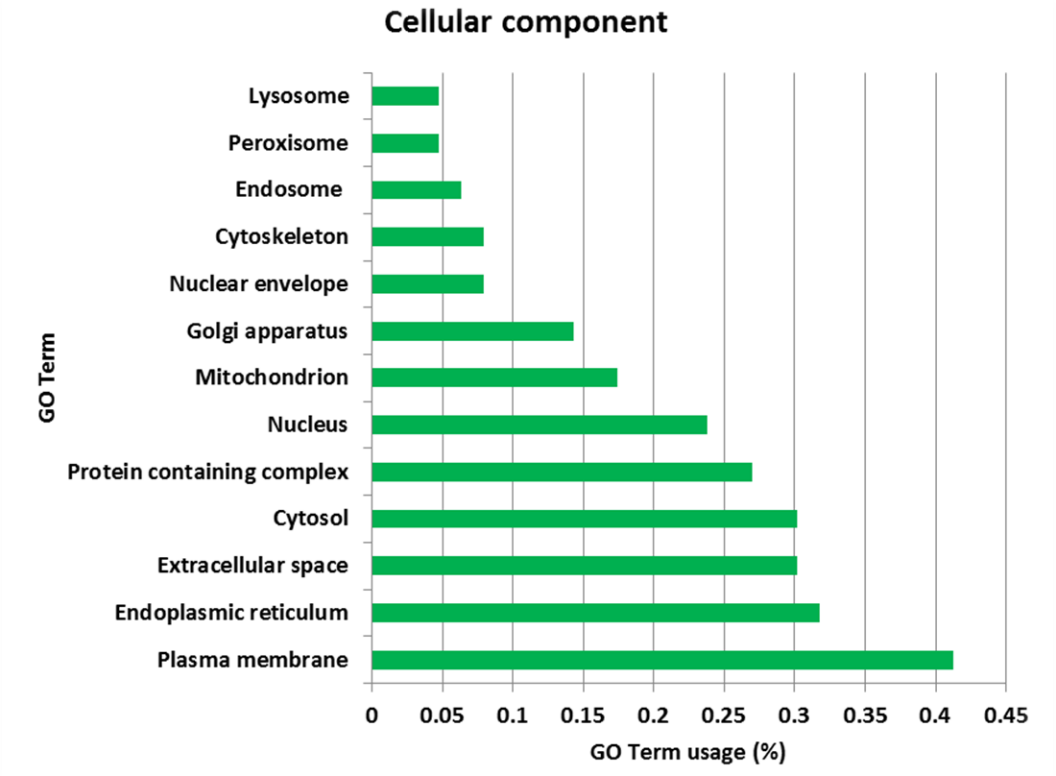
Cellular component
Lysosome
Peroxisome
Endosome
Cytoskeleton
Nuclear envelope
Golgi apparatus
Mitochondrion
Nucleus
Protein containing complex
Cytosol
Extracellular space
Endoplasmic reticulum
Plasma membrane
GO Term
0
0.05
0.1
0.15
0.2
0.25
0.3
0.35
0.4
0.45
GO Term usage (%)

5.11. Functional Annotation Clustering

Functional Annotation clustering classifies genes by measuring relationships among annotation terms on the basis of their occurrence and associations with the genes provided by the user. To conduct functional clustering on our unique protein dataset, the bioinformatics resource, DAVID (the database for annotation, visualization and integrated discovery) which incorporates biological meaning to large datasets by GO term enrichment[121].

The top 12 DAVID annotation clusters (n=64 proteins from 2 replicates) were obtained after functional clustering of the unique proteins predicted to interact with HYAL2 (**Table VI**). Six clusters derived from the dataset namely- cell migration, response to stress, apoptosis regulation, wound healing, anatomical structure morphogenesis and cardiovascular system development [all of which abide by the recommended statistical parameters of fold change (FC≥1.5), low false discovery rate (FDR) and *P*-values ≤ 0.05] are interesting because these six clusters bear significant relevance to the biological function associated with HYAL2. HA and HYAL2 are speculated to be involved in all of these biological processes (represented by these six clusters) either through direct interaction or through in association with other complexes. All the clusters obtained from DAVID analysis significantly pass the statistical threshold for selection (FC ≥1.5 and *P*-values ≤ 0.05)[121]. Redundant clusters have been merged.

Table VI. Functional annotation clustering of unique proteins by DAVID.

Fold Change (FC) referes to the magnitude of enrichment in comaprison to the whole proteome. FC values ≥1.5 are considered interesting.. **Enrichment Score** ranks the overall importance of the annotated groups. It is the geometric mean of the *P*-values of the enriched terms in a group. A higher score for a group is indicative of an important role being played by the genes in the group. **False Discovery Rate (FDR)** exist to correct the enrichment *P*-values of the terms in the cluster to control family-wide FDR . The more terms that get examined, the more conservative are the corrections.

Annotation cluster	Enrichment score	Gene count	p-value	FC	FDR	Gene names
Homeostatic process/Cell homeostasis	4.36	15	4.70E-04	2.80E+00	8.30E-02	AFG3L2, GNA13, ORMDL2, SLC9A3R1,CCDC47, CORO1A, FITM2, MCU, PRDX3, PRDX5, PTPRN2, STX4, TMX2, TMX3, TMEM97
Cell migration/Cell motility	2.84	13	7.30E-04	3.00E+00	1.60E-01	CX3CL1, CD151, GNA13, RAP2C, SLC9A3R1, CORO1A, ITGA5, ITGA9, LYST, PDCD10, PTK7, STX4, ZEB2
Regulation of cell death/Apoptosis	2.75	14	6.50E-04	2.90E+00	1.60E-01	ARL6IP1, BCL2L13, CX3CL1, DNAJC3, SLC9A3R1, AXIN2, CORO1A, ERP29, ITGA5, IFIT2, PRDX3, PRDX5, PDCD10, STX4
Regulation of lipid biosynthetic process	2.63	5	7.10E-04	1.20E+01	1.60E-01	DHCR7, ERLIN1, ORMDL2, FITM2, IDH1
Response to stress	2.32	23	1.00E-03	1.90E+00	1.80E-01	CX3CL1, DNAJC3, ERLIN1, GNA13, AXIN2, CCDC47, CORO1A, ERP29, EIF2B1, ITGA5, ITGA9, IFIT2, IDH1, LYST, PRDX3, PRDX5, PDCD10, PTK7, STX4, TMX3, TOR1B, TRA2B, UBE4B
Cardiovascular system	1.52	8	2.80E-02	2.60E+00	7.50E-01	DHCR7, CX3CL1, GNA13, AXIN2, ITGA5, PDCD10, PTK7, UBE4B
Tissue morphogenesis/Morphogenesis of epithelium	1.44	7	1.30E-02	3.50E+00	6.30E-01	GNA13, SLC9A3R1, GPC4, ITGA5, PDCD10, PTK7, UBE4B
Cell adhesion	1.42	11	3.80E-02	2.00E+00	7.80E-01	CX3CL1, CORO1A, ITGA9,STX4, CD151, CLPTM1, FBLN2, ITGA5, IDH1, PTK7, GPRC5A
Wound healing/Response to wounding	1.4	6	2.80E-02	3.40E+00	7.50E-01	CX3CL1, GNA13, ITGA5, ITGA9, PDCD10, PTK7
Blood vessel development/Vasculature development	1.4	6	3.50E-02	3.20E+00	7.70E-01	DHCR7, CX3CL1, GNA13, ITGA5, PDCD10, PTK7
Anatomical structure morphogenesis	1.28	10	5.20E-03	3.00E+00	3.90E-01	CX3CL1, GNA13, SLC9A3R1, AXIN2, CORO1A, FITM2, GPC4, ITGA5, PDCD10, PTK7
Regulation of kinase activity	1.22	7	3.70E-02	2.80E+00	7.80E-01	DNAJC3, GPRC5A, RAP2C, SLC9A3R1, ERP29, PRDX3, PDCD10

5.12. PPI network maps of unique proteins and module analysis

The unique protein dataset of 64 proteins was analyzed by NetworkAnalyst v3.0[122] to produce the network in **Fig 5.11.** The PPI network is built of proteins with a node degree ≥15 (the 'degree' of a node is the number of connections it has to other nodes) which retains the major nodes acting as 'hubs' in the network with maximum connections with other clusters. Extensive PPI was observed among these candidate proteins.

Figure 5. 11 Protein-protein interaction network of unique proteins.

Twenty-one proteins (degree ≥ 15) act as hubs in the network. Red dots (representing hubs) are the major nodes in the networks; the larger the dot, the greater the number of connecting proteins.

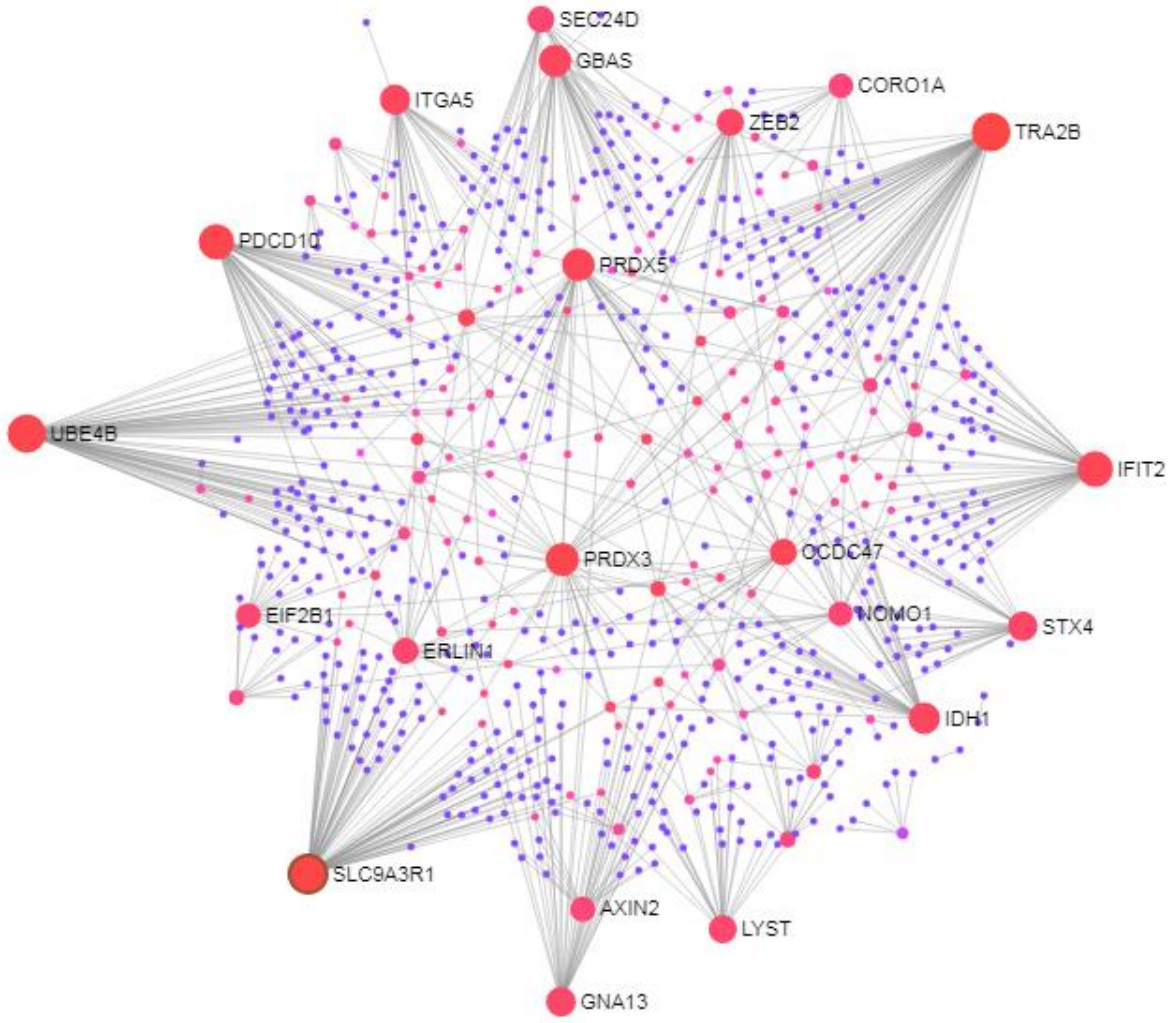

Twenty-one hubs were selected and extracted to create modules of tightly clustered subnetworks containing hub proteins and their interactors forming interacting complexes (**Fig 5.12).** Members within a module are likely to perform a specific biological function. The BPs found to be signficant with DAVID functional clustering, were also found to be statistically significant (*P*-value < 0.05) with low FDR in the network map of the unique proteins. Each module below features hub proteins and their interactors (non-hubs) associated with a specific biological pathway/process.There are a total of six modules highlighting the biological roles usually associated with HA and HYAL2 with significant *P*-values.

The first module is **(A) 'Wound healing'** which features 11 hits with 4 being hubs- STX4, ITGA5, GNA13, LYST and 7 non-hubs with a *P*-value of 0.00113 and FDR- 0.0377.

The second module is **(B)'Cell migration'** featuring 14 hits with 7 hubs- CORO1A, ZEB2, GNA13, LYST, ITGA5, RAP2C, SLC9A3R1 and 7 non-hubs proteins with *P*-value- 0.00119 and FDR value-0.0377.

The third module is **(C) 'Response to stress'** features 35 hits with 14 hubs- STX, ITGA5, PRDX3, IFIT2, GNA13, CORO1A, PRDX5, UBE4B, IDH1, AXIN2, ZEB2, CCDC47, LYST and 21 non-hubs with a *P*-value 0.00121 and FDR value-0.0377.

The fourth module is **(D) 'Apoptotic process'** which features 22 hits with 7 hub- ITGA5, PDCD10, SLC9A3R1, PRDX3, IFIT2, PRDX5, YBE4B with 15 non-hubs with a *P*-value 0.00124 and FDR- 0.0377.

The fifth module is **(E) 'Regulation of anatomical structure morphogenesis'** with 10 hits among which 3 are hubs- GNA13, CORO1A, AXIN2 and 7 non-hubs with a *P*-value of 0.00391 and FDR-0.0582.

The sixth and the final module highlights **(F) 'Regulation of kinase activity'** with a total of 10 hits- 6 being hubs- PDCD10, SLC9A3R1, PRDX3, AXIN2, ZEB2, RAP2C and 4 non-hubs with a *P*-value 0.00581 and FDR-0.0768. The hubs and non-hubs in each module are represented by blue dots.

Please note: The non-hubs are not obtained through our pull-down data but generated through NetworkAnalyst enabled algorithm.The non-hubs can be checked for their functional association with HYAL2 if a specific hub (unique protein) becomes experimentally significant to HYAL2.

Figure 5. 12 Enriched functional modules of hubs extracted from unique protein network.

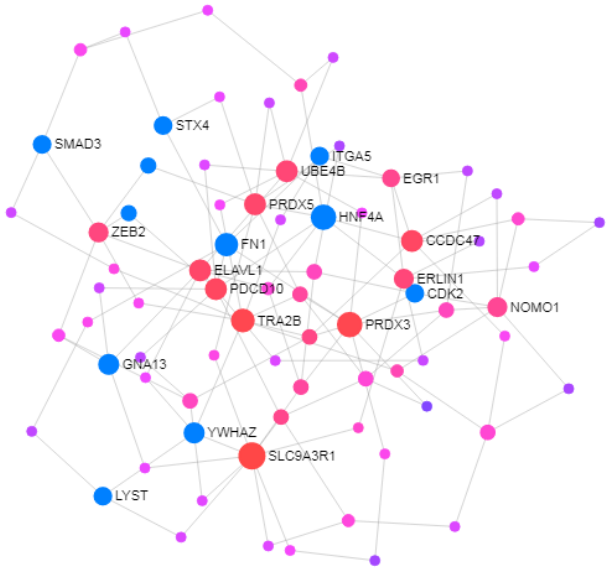

(A) Wound healing (*P*-value of 0.00113)

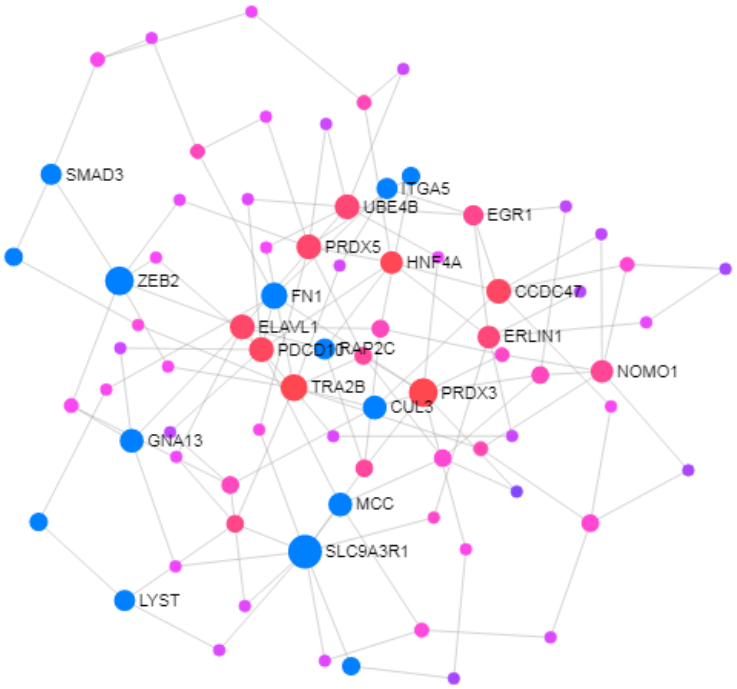

(B) Cell Migration (*P*-value- 0.00119)

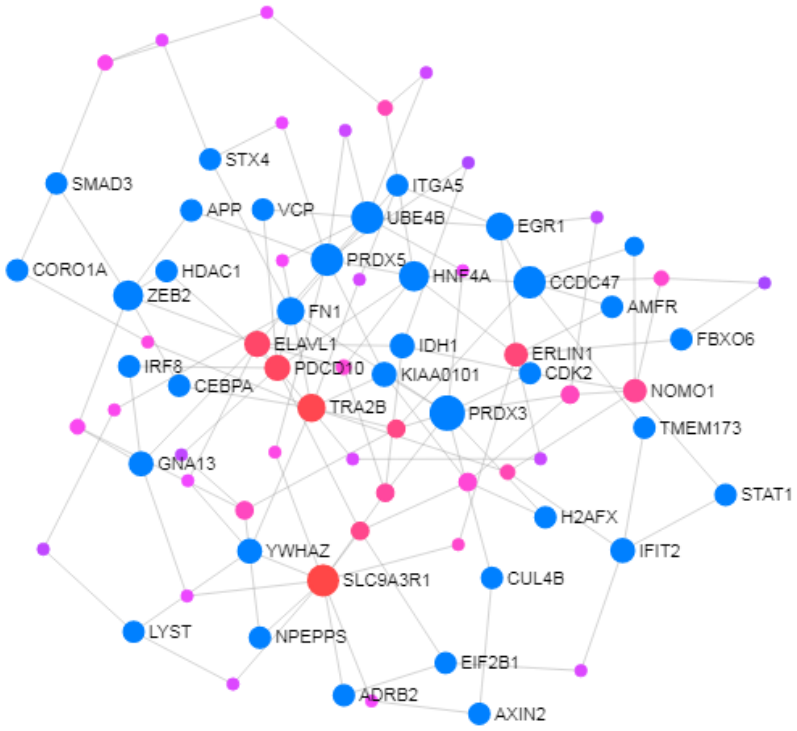

(C) Response to stress (*P*-value 0.00121)

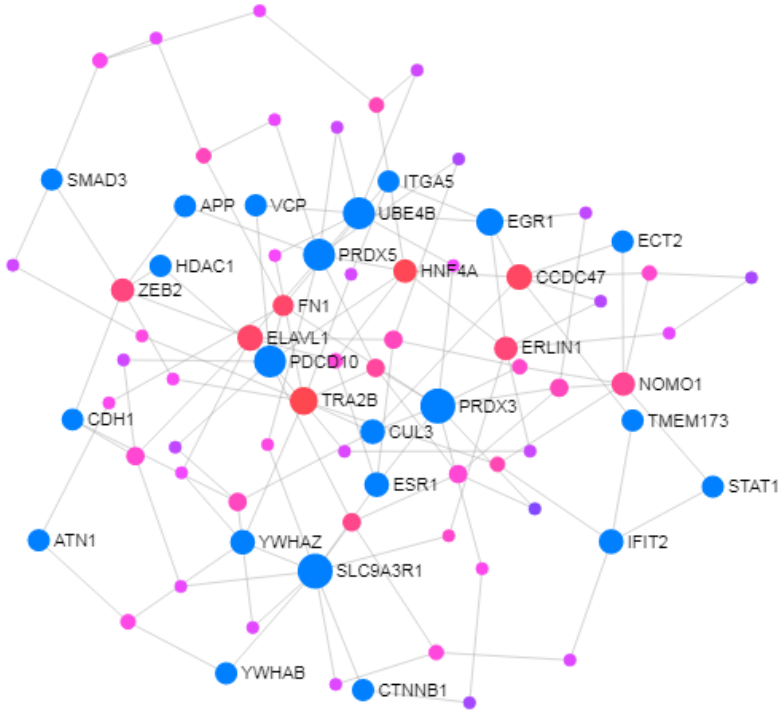

(D) Apoptosis (*P*-value 0.00124)

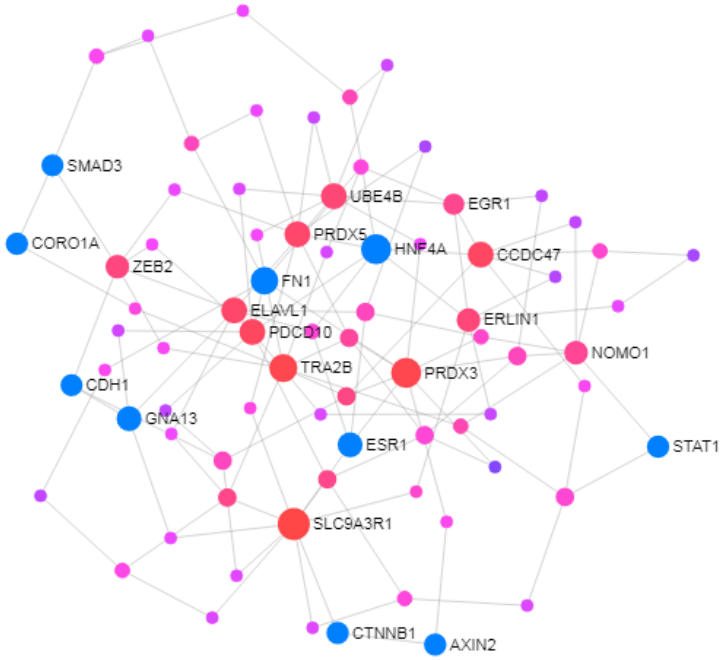

(E) Anatomical Structure Morphogensis (*P*-value 0.00391)

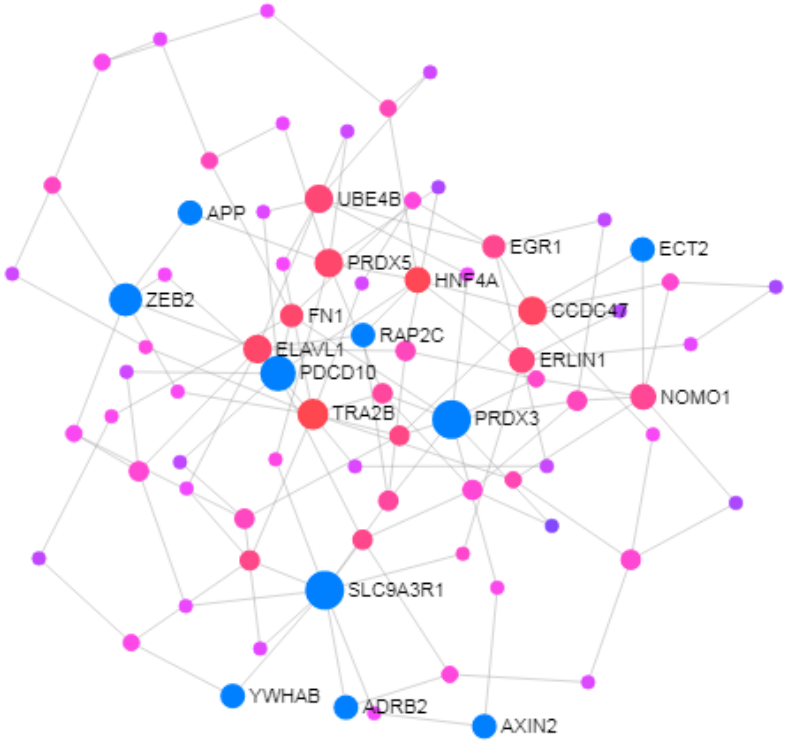

(F) Regulation of kinase activity (*P*-value 0.00581)

CHAPTER 6: DISCUSSION

6.1. Mutation Study

Regulation of HA levels is required for normal development, and to maintain normal tissue homeostasis. Degradation of HA by HYALs is important to maintaining these levels. Characterization of HYAL2 KO mice revealed craniofacial abnormalities; cardiac dysfunction, hearing loss, renal agenesis and mild anemia which indicated HYAL2 had a role in the regulation of HA homeostasis during organ development[100, 107]. The molecular etiology of CL/P is poorly understood even being one of the most frequent congenital craniofacial anomalies in humans. HYAL2 was identified as a novel cause of syndromic CLP in two unique human populations and submucous cleft palate (SMCP) in mice[100]. Facial dysmorphism, thickened valves, cortriatrium sinister, myopia, hearing loss and pectus excavatum were found to be associated with HYAL2 deficiency. Transient expression of the two HYAL2 mutants- p.K148R and p.P250L, identified in the in the study, showed an 11 and 20 fold reduction in HYAL2 levels respectively when compared to WT HYAL2. In this study, we compared and evaluated the expression levels of seven novel variants reported to us by clinicians after exome-sequencing from patients of mixed ethnicities.

The impact of each variant on the processing of HYAL2 was evaluated by examining the steady state levels of intracellular and cell surface HYAL2. Immunoblot analysis of HYAL2 in total cell lysates and immunofluorescence examining intracellular HYAL2 showed that the G204A and delAC mutations resulted in a level of HYAL2 protein similar to that of the WT HYAL2 protein. The remaining F425V, L238R and R277C substitution mutations resulted in a low level of stable HYAL2 protein with a complete absence of HYAL2 expression from S65X and R295X. While these shorter peptides (S65X and R295X) were likely unstable in this transient overexpression system, in the endogenous situation they would almost certainly result in nonsense mediated decay of the mRNA, resulting in no HYAL2 protein. Nonsense mediated decay impacts almost all mRNA species when the nonsense codon precedes the final intron.

Our IF and PI-PLC analyses showed parity in the analyses of the variants. Immunolocalization and PI-PLC cleavage both revealed very little cell-surface HYAL2 with L238R and G204A variants. As for all the other variants no cell-surface HYAL2 was detected with either PI-PLC or IF under non-permeabilized conditions. Permeabilization of cells with detergent showed stable

intracellular HYAL2 in all variants except S65X and R295X which we presume result in short peptides that are unstable or not detectable with our existing anti-HYAL2 antibody.

Our results show that the seven variants we have analyzed herein cause a deficiency of mature cell surface HYAL2. HYAL2 undergoes complex co-translational modification before achieving its final topology as a mature GPI-anchored cell surface glycoprotein. The co-translational steps required to generate mature HYAL2 begin in the endoplasmic reticulum and like other glycoproteins, even small amino acid changes can result in ER-associated degradation and HYAL2 deficiency. Indeed, all of the seven changes resulted in a reduced level of HYAL2 at the plasma membrane surface and are therefore mutations.

HA shows a size-dependent spatiotemporal regulation and alteration of HA level and size has been identified in kidney disease, cancer, lung injury and stroke[113-115]. The turnover of HA and the involvement of HYAL2 in the process has been a matter of investigation in several laboratories. The localization of HYAL2 and HA distribution in the early embryonic (E8.5 -12.5) mouse heart suggested that these molecules were important during development. The new patients extend our phenotypic findings and validate the typical phenotype associated with HYAL2 deficiency. Previous studies have indicated that the removal of high molecular mass HA from the provisional extracellular matrix is critical to heart development[116], and that a failure to remove HA resulted in increased epithelial to mesenchymal transition (EMT) and decreased differentiation[91]. We reasoned that the increased HA in the absence of HYAL2 would result in excess EMT and decreased differentiation. Indeed in mice we have observed expanded valves and accessory tissues as well as increased numbers of mesenchymal cells in the heart. In this study, the patients heterozygous for F425V and S65X were reported to have atrial/ventricular (AV) septal defects, mitral atresia, pulmonary hypertension, patent ductus arterious and other defects that were not previously reported. The early deaths in these patients may be explained by the severe cardiac dysfunction observed due to reduced HYAL2 expression.

Cardiac dysfunction and craniofacial abnormalities that we observed with this set of HYAL2 mutations further suggests a significant role for HYAL2 at the cell-surface to remove HA in a time-dependent pattern to regulate normal organ development. This study increases and adds to the range of phenotypes typical to HYAL2 deficiency for a better diagnosis of diseases which may root from HYAL2 deficiency. It may be possible that there is active interplay between

HYAL2 and morphogens which regulate developmental signals and HYAL2 KO/mutated tissues are unable respond to those developmental cues to develop and proliferate. This possibility needs further investigation but it is clear from our study that the complete absence of HYAL2 activity leads to poor cardiac and craniofacial development and can threaten survival in humans.

6.2. HYAL2 binding partner study

All of the major functions regulated by HA including development, differentiation and wound-healing are presumed to be dependent on its size. In somatic tissues, HYAL1 and HYAL2 function as the major HA-degrading enzymes. Though, HYAL1 shows clear specificity towards HA removal, the specific activity of HYAL2 in degrading HA remains elusive. Overaccumulation of HA in *Hyal2-/-* tissues indirectly defines its function in HA turnover, but assaying the activity of HYAL2 directly has been challenging. Most proteins tend to function in the cell as a part of a large complex and an important way to assess function of the protein is by looking at possible binding partners of the protein. We hypothesized that establishing and validating a method to search for possible interacting protein partners of HYAL2 would lay the foundation of understanding the HYAL2 network which will aid in elucidating the mechanism of action and eventually designing an enzyme assay to understand the activity of HYAL2. In this study, we have used proximity-dependent biotinylation to identify novel partners of HYAL2. The protein pools of BioID2-only (control) and SS-BioID2-HYAL2 (experimental) have been compared to selectively sort the proteins unique to the interactome of HYAL2 and are consistent across all biological replicates.

BioID2 when fused to a bait protein (HYAL2 in this case) and supplemented with external biotin, promiscuously biotinylates proximate proteins. This leads to the biotinylation of direct interacting proteins (stable or transient) relevant to HYAL2 interactome as well as proteins present in the interactome by mere chance. Non-specific interactors including heat-shock proteins, keratins, tubulins, actins, elongation factors, histones, ribosomal proteins are often biotinylated with other proteins and identified by MS analysis. Though, the copurification of non-specific interactors cannot be entirely avoided, they can be ignored and excluded out of the PPI analysis using appropriate controls without fusion proteins and web-accessible resources like CRAPome, which can help filtering out common contaminants and proteins with high spectral counts usually obtained in with every pull-down. Here, we have used cells expressing only BioID2 only alongside SS-BioID2-HYAL2 to reduce the common proteins that BioID2 non-specifically biotinylated in both the control and experimental samples. We have also used the contaminant repository for affinity purification, CRAPome which is a web-accessible resource

where by querying one protein at a time, an user can identify the significance of that protein (if any) present in their pulled-down sample.

A total of 64 proteins were obtained as 'unique' to the HYAL2 sample though their association with HYAL2 is speculative. A spectrum of functions usually associated with HYAL2 and HA ranging from wound healing to morphogenesis were observed by GO and functional analysis of the genes. It will be interesting to validate the involvement of HYAL2 in all of the enriched biological pathways to confirm how the enriched proteins in each biological process obtained from our functional analysis is involved in the HYAL2 interactome. We have created a network map with the unique proteins and modules have been extracted from this network based on these key unique proteins which act as 'hubs' in the dataset. Studying the hubs and their interactions with the the non-hubs will be particularly useful to understand the functional complexity of HYAL2 if a hub is found to be signficant to HYAL2 when investigated experimentally.

One of the interesting partners in the dataset is SLC9A3R1 also known as Na(+)/H(+) exchange regulatory cofactor (NHE-RF1). The protein is present with a log (I) value of 7.06 among the 64 unique proteins across two replicates and is a common member identified in most of the functional clusters analyzed by DAVID. The protein also secures the place as a key hub with highest nodal degree of 76 in the entire dataset analyzed by NetworkAnalyst. Study by Bourguignon et al. have previously shown the interaction of HYAL2 with Na(+)/H(+)Exchanger (NHE1) [also known as SLC9A1] in association with cell surface receptor, CD44 in lipid rafts to induce a low-pH environment which enables the recruitment of HYAL2 for HA degradation[42]. NHERF1 is expressed in osteoblasts and plays a regulatory role in bone mineralization and matrix production[123] and NHEs are regulated by NHERF1 and NHERF2[124]. NHE1 and NHE6 which function in osteoblastogenesis showed reduced expression in NHERF1-null MSC in osteogenic medium[124]. NHERF1 was found to be associated in the disease pathways involving bone mineralization and bone anabolism when analyzed by NetworkAnalyst (**Supplementary Fig 2**). Muggenthaler et al. reported reduced ossification in the skull and underdeveloped viscerocranial bones in *Hyal2-/-* mice [100]. The signficant parity between HYAL2 and NHERF1 in bone development and the reported interaction between HYAL2 and NHE1, might suggest NHERF1 as a direct/indirect interactor of HYAL2 which should be investigated to provide experimental confirmation of the interaction.

Another potential interacting partner of HYAL2 which can be further investigated is Glypican 4 (GPC4) which is a conserved glypican across invertebrates and vertebrates. GPC4, a member of the heparin sulfate proteoglycan family is a GPI-anchored protein similar to HYAL2, belongs to the noncanonical Wnt/PCP pathway, controlling cellular migration and embryonic morphogenesis[125]. Studies have associated *gpc4* mutants in adult zebrafish with loss of chondrocyte organization, craniofacial defects and impaired palate morphogenesis[125-127]. Our gene-disease enrichment analysis revealed a spectrum of phenotypes associated with the loss of GPC4 which are similar to what we observed with the functional loss of HYAL2 (**Supplementary Fig 3**) which makes it a good candidate to consider for experimental verification.

Recent studies have indicated an association between the HYAL2 and RHOA in facilitating RHOA-dependent cell migration and attenuation of RHOA-dependent genes were observed post *HYAL2* knockdown in the fibroblasts[129]. GNA13 (Guanine nucleotide-binding protein subunit alpha-13), which acts as an effector of RHOA signaling mediating RhoGEFs activation and promoting RHOA/ROCK signaling pathway[130, 131] is present in our unique protein dataset with a good logI value of 6.935 and is one of the key hubs in the unique protein network with a nodal degree of 28. GNA13 is enriched in 7 major functional clusters analyzed by DAVID. Given the information we have on HYAL2-RHOA and RHOA-GNA13 signaling pathways, it would be interesting to verify experimentally if GNA13 regulates HYAL2 expression and is a binding partner.

Another candidate which can be further investigated is AXIN2 (AXIS Inhibition Protein 2), which is present in the dataset with high log (I) value of 7.175, enriched in the clusters associated with morphogenesis and is a hub in the network. AXIN2 belongs to the Wnt/β-catenin pathway that governs cell fates during craniofacial morphogenesis and studies have associated several AXIN2 polymorphisms with human oral clefting[132-134]. Members of the Wnt family are also associated with orofacial cleft susceptibility[133-135] and we have mapped Wnt pathway regulators including GPC4, AXIN2, SLC9A3R1 from our unique protein dataset and other non-hub Wnt regulators in our network modules. Wnt pathway genes might bear significant relevance to HYAL2 and it would be fascinating to study if HYAL2 coordinates or is a member of the cascade.

We have observed two major proteins known to be possible interactors of HA and HYAL2-CD44 and HMMR (RHAMM/CD168) in the control samples that were derived from captures of the BioID2-only sample. CD44 showed similar log (I) values 7.4 in both control and experimental samples across both biological replicates whereas HMMR is present in the control sample only of the 2nd biological replicate with a log (I) of 6.69. The presence of both proteins in the control samples, is indicative of the proteins being non-specific to HYAL2 which requires further investigation.

The main purpose of this study was to establish a method to search for novel proteins which are possible binding partners of HYAL2. We have provided a library of proteins which have been functionally clustered using bioinformatic resources and mapped to infer enriched PPI networks. These proteins can be experimentally validated using expression, co-localization or affinity purification studies in different models to reveal the biological meaning of their existence in the HYAL2 interactome. After experimental evaluation, the candidates which will stand as functionally associated with HYAL2, will be further investigated to determine how their loss impacts HYAL2 function. CRISPR/Cas9 can be used to KO the protein of interest in a cell line expressing HYAL2 to assess the impact.

CHAPTER 7: LIMITATIONS AND CONCLUSIONS

7.1. HYAL2 mutation study

HYAL2 is a constitutively expressed cell surface protein that is required for normal HA turnover. This is demonstrated by the increased size and levels of HA in the tissues and serum of *Hyal2-/-* mice[58, 99, 117] . Previous in vivo studies from our lab have demonstrated the importance of HYAL2 in cardiac and craniofacial development[95, 100]. These studies emphasized the presence of increased numbers of mesenchymal cells and decreased differentiation during development in *Hyal2-/-* mice which can be attributed to the excess accumulation of HA[95]. Analyzing two novel mutations in HYAL2, our lab has previously reported *HYAL2*-deficiency as a novel cause of syndromic CLP in humans, with other features including facial dysmorphism, septal defects, hearing loss, atrial dilations as common clinical phenotypes both in mice and humans[100]. Seven new variants reported in the *HYAL2* gene in patients with genetic disorders were biochemically analyzed here. We described an interference of the genetic variants with the the typical cellular expression and localization of HYAL2, which make these seven novel mutations of HYAL2 never reported before.

Though the availability of our *Hyal2-/-* mouse model gave us an excellent background for our experiments, transient expression of the cDNAs carrying the HYAL2 variants in MEFs, may not mimic the cellular milieu in which the real mutations exist. Protein overexpression in mammalian cell culture could overload the cellular environment and create toxicity by aggregation of the misfolded proteins impacting the level of protein production, folding and localization[118, 119]. Though in the present study we have demonstrated a clear functional change of HYAL2 due to the mutations, our inability to directly examine the enzymatic activity of HYAL2 hinders our understanding of the possible change in HA content due to these mutations in the patients.

In spite of the caveats in the study, we have been able to describe the functional importance of HYAL2 in maintaining the developmental homeostasis in humans. This study expands the molecular spectrum associated with pathogenic HYAL2 variants, and provides new insight into

the likely disease mechanism and functional roles of HYAL2. The report of the clinical features manifested in these patients will further help us in diagnosing disorders due to HYAL2 deficiency.

7.2. Interacting partners of HYAL2

In the seven years following its discovery, proximity labeling approaches like BioID have made significant contributions in mapping interactomes and is preferred over conventional affinity purification approaches due to its robustness in high-stringency protein capture. BioID labels both interacting (prey proteins) and non-interacting proteins (frequently occurring proteins) in the vicinity of the bait protein which gives valuable information on the cellular role of the bait protein. But, this is where one of the major limitations of using BioID lies. It is not easy to determine if a protein labelled by BioID is a direct interactor or if it bears any relevance to the bait protein[128]. Just being biotinylated does not prove the strength of an association of a prey protein with that of the bait. Systematic investigation and experimental validations thus become necessary to confirm a captured interaction. In our studies, analyzing the interactome of human HYAL2 by using of a human HYAL2 construct expressed in a mouse *Hyal2-/-* cell-line was also a major challenge. Some mouse proteins not expressed or with no homologues in humans become a limitation in data analysis and create confusion. Through this study we wanted to establish a interacting protein screening strategy for HYAL2 and *Hyal2-/-* MEFs have been an excellent cell-line for our study. But, repeating the experiment in a human *HYAL2-/-* cell-line would be ideal to develop a meaningful group of proteins for further study.

It will also be interesting to extend this study in tissues and cells demonstrating strong HYAL2 protein profile. Studies have suggested that proteins show distinct cell-type-specific expression and this dynamic regulation of protein-levels makes each tissue unique [140, 141]. Global expression patterns of proteins in all tissues and cells based on RNA expression, tissue microarrays, immunohistochemistry, and immunofluorescence, can be accessed by using resources like Human Protein Atlas (http://www.proteinatlas.org). Cell-types reported to produce abundant HYAL2 protein levels can be used to repeat these experiments to provide additional validation

on the candidate proteins analyzed in this study or to reveal novel candidates for further experimentation. The PPI study in a different cell-line may help in resolving the complexity around HYAL2 function and delineate precise functions of the protein in human growth and development.

MS data from BioID studies which allow identification of potential interacting partners of a bait protein is indispensable in interactome mapping. But, one of the major challenges in this is simplifying the MS data. Extensive lists of protein partners sometimes become challenging to sort and characterize. Semi-quantitative approaches like- abundance and ion intensities become important to choose signficant proteins. In that case, if a prey protein is expressed in low concentrations, MS may miss the candidate and it can be considered as a false-negative[128]. We have selected a combination of semi-quantitative, functional clustering, network mapping and statistical parameters to elucidate the enriched biological process and proteins involved in those processes. Another important step while analyzing the MS data is eliminating nonspecifically biotinylated proteins (eg. Mitochondrial proteins, matrix proteins, ion transporters) from experimental set by considering appropriate controls and our *Hyal2-/-* MEFs was an excellent choice for this. The availability of a control with no HYAL2 in the background, helped us in sorting proteins. We have provided the data of two biological replicates of BioID, but more replicates will bring more credibility to the data.

Our PPI study presented a list of unique protein partners which bears relevance to HYAL2 function. The study also revealed that several essential pathways involving morphogenesis and cell migration were significantly enriched. It can be derived from the PPI network that these essential biological processes are functionally connected. These reported genes will help in dissecting HYAL2 regulation in the future and may be considered as potential drug targets for diseases stemming from lack of HYAL2. The identity of the interacting proteins could also lead us to develop new assays for HYAL2 function and to consider other mechanisms of action.

SUPPLEMENTARY FIGURES

Figure 1: PNGase F treatment of Flag-HYAL2

Lysates of *Hyal2-/-* MEFs transfected with *Flag-HYAL2* were incubated with (+) or without (-) PNGase F to monitor the deglycosylation and reduction in size. Treated Flag-HYAL2 (+) showed reduction in a few kilodaltons when compared to untreated Flag-HYAL2 (-) and coincided with the cross-reacting band (*). *Hyal2-/-* MEFs transfected with WT-HYAL2 without PNGase F treatment showed no reduction in size (~53.6 kDa). Cross-reacting bands are observed in all lanes including control (*) with anti-HYAL2 antibody.

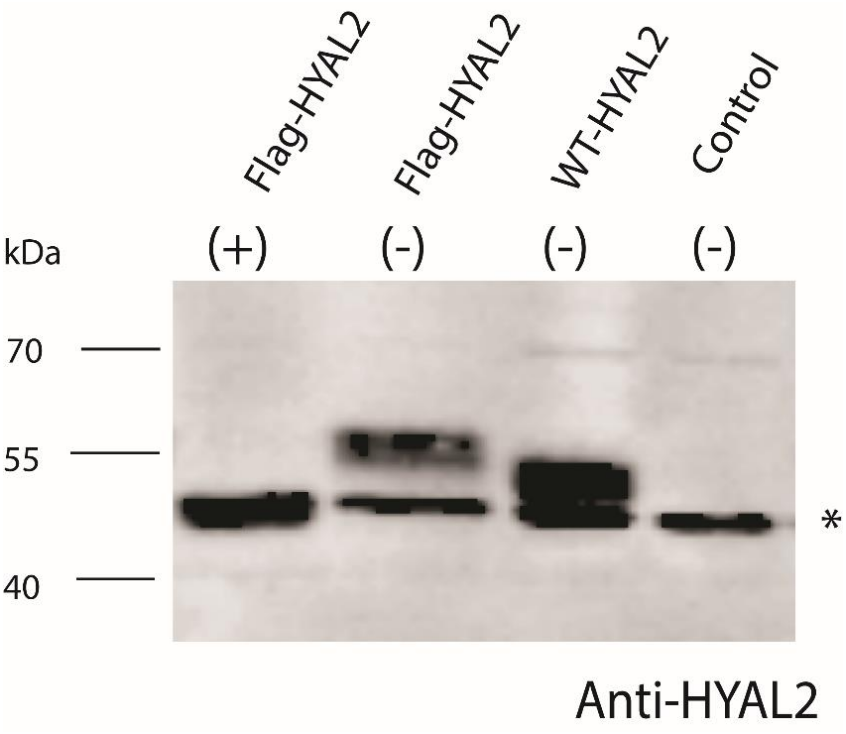

Figure 2: Gene-disease association for SLC9A3R1 (NHERF1).

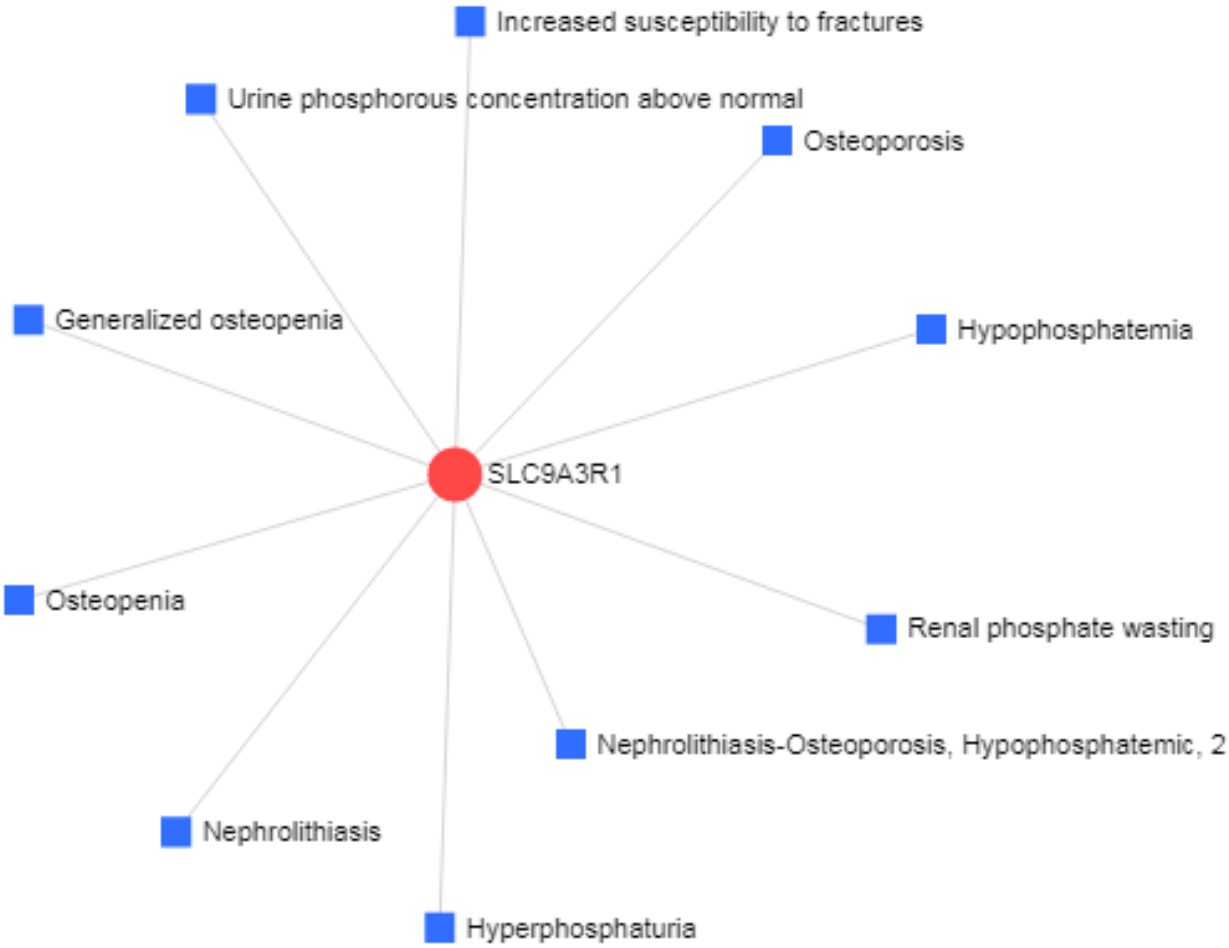

Figure 3: Gene-disease association for GPC4

GPC4 has a disease pathway consisting 135 disease. The phenotypes which bear significant resemblance to HYAL2 phenotypic spectrum has been selected.

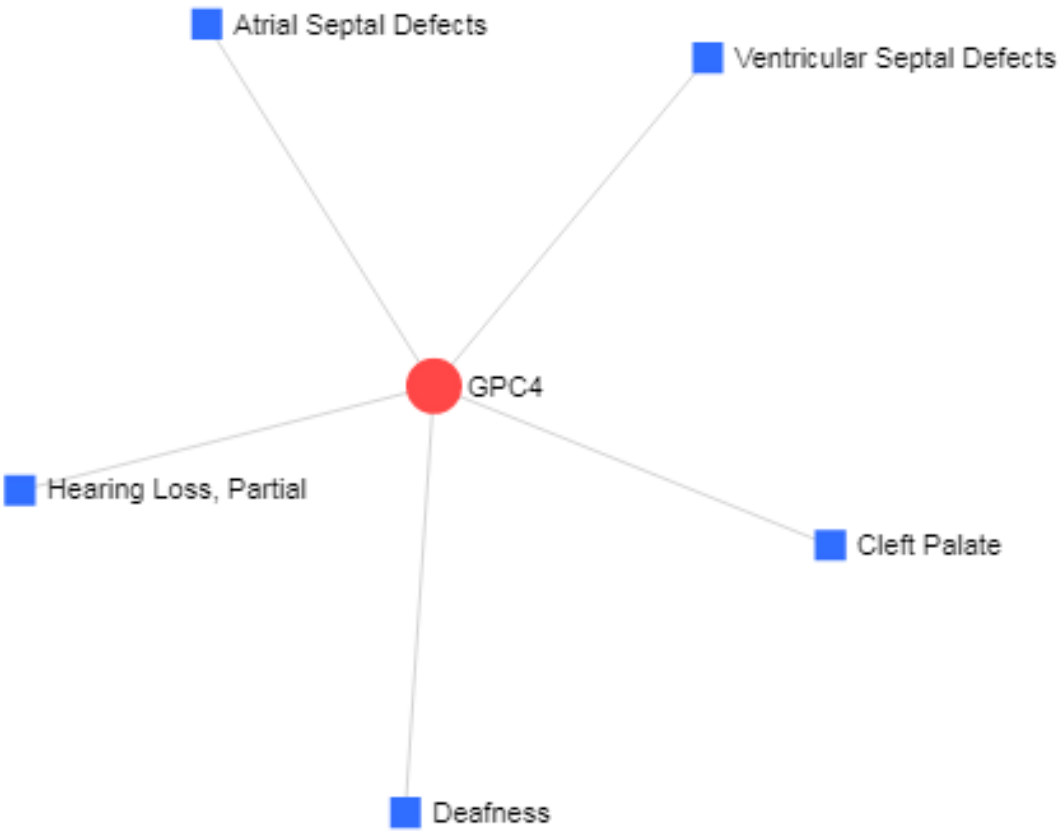

SUPPLEMENTARY METHODS

Method I: Electrocompetent *E. Coli* DH5α cell preparation

Day 1

1. Frozen glycerol stock of bacterial cells (Top 10, DH5α, etc.) was streaked onto an LB plate (no antibiotics) and was grown overnight at 37°C.

Day 2

1. Autoclaving:
    - 2 L of ddH2O
    - 100 mL of 10% v/v glycerol (molecular biology grade)
    - 1 L LB (or your preferred media)
    - 4 centrifuge bottles and caps
    - Lots of microfuge tubes
2. Chilled overnight at 4°C:
    - ddH2O
    - 10% glycerol
    - Centrifuge rotor
3. Starter culture of cells were prepared

A single colony of *E. coli* from fresh LB plate was selected and inoculated in a 10 mL starter culture of LB and was grown at 37°C in shaker overnight.

Day 3

1. 1 L of LB media was inoculated with 10 mL starter culture and grown in 37°C shaker. The OD600 was measured every hour, then every 15-20 minutes when the OD reached > 0.2.
2. When the OD600 reached 0.35-0.4, the cells were immediately put on ice. The culture was chilled for 20-30 minutes, swirled occasionally to ensure even cooling and centrifuge bottles were placed on ice at this time.

3. (Spin #1) 1 L culture was split into four parts by pouring about 250 mL into ice cold centrifuge bottles. The cells are harvested by centrifugation at 1000*g* (~2400 rpm) in the Beckman JA-10 rotor) for 20 minutes at 4°C.
4. The supernatant was decanted and each pellet was resuspended in 200 mL of ice cold ddH2O.
5. (Spin #2) The cells were harvested by centrifugation at 1000*g* (~2400 rpm in the Beckman JA-10 rotor) for 20 minutes at 4°C.
6. The supernatant was decanted and each pellet was resuspended in 100 mL of ice cold ddH2O.
7. (Spin #3) Resuspensions were combined into 2 centrifuge bottles (so each contains about 200 mL of cell suspension). The cells were harvested by centrifugation at 1000*g* (~2400 rpm in the Beckman JA-10 rotor) for 20 minutes at 4°C. At this step, two 50 mL conical tubes were rinsed with ddH2O and chill on ice.
8. The supernatant was decanted and each pellet was resuspended in 40 mL of ice cold 10% glycerol. Each suspension was transferred to a 50 mL conical tube.
9. The cells were harvested by centrifugation at 1000*g* (~2100 rpm in the Beckman GH-3.8 rotor) for 20 minutes at 4°C. 1.5 mL microfuge tubes were put on ice if not already chilled.
10. The supernatant was carefully aspirated with a sterile Pasteur pipette. Each pellet was resuspended in 1 mL of ice cold 10% glycerol by gently swirling. The final OD600 of the resuspended cells should be ~200-250.
11. The pellets were aliquoted into sterile 1.5 mL microfuge tubes and was frozen with liquid nitrogen. The frozen cells were stored in the -80°C freezer.

SOC Medium

20 ml of sterile 1 M glucose was added per liter of SOB medium immediately before use or frozen aliquots stored at -20 ºC can also be used.

SOB Medium

1. 900ml of distilled H2O
2. 20g BactoTryptone
3. 5g Bacto Yeast Extract
4. 2ml of 5M NaCl
5. 2.5ml of 1M KCl

6. 10ml of 1M MgCl2

7. 10ml of 1M MgSO4

8. pHwas adjusted to 7.0 with 10N NaOH and volume was adjusted to 1 L with distilled H2O.

2xYT Medium

1.900ml of distilled H2O.

2.16g BactoTryptone.

3.10g Bacto Yeast Extract.

4.5g NaCl.

5. pHadjusted to 7.0 with 5N NaOH.

6. Adjusted to 1L with distilled H2O.

7. Sterilized by autoclaving

Method II: PNGase F treatment for deglycosylation

Required:

- Glycoprotein Denaturing Buffer (10X)
- GlycoBuffer 2 (10X) (G7 buffer at -20℃
- 10% NP-40

Procedure:

1. 1-20 µg of glycoprotein is combined with 1 µl of denaturing buffer and water (if required) to make a 10 µl total reaction volume.

2. Glycoprotein is denatured by heating reaction at 100℃ for 10 mins.

3. The denatured glycoportein is chilled on ice and centrifuged for 10 secs.

4. A total reaction volume of 20 µl was made by adding 2 µl of glycobuffer, 2 µl of 10% NP-40 and 6 µl of water.

5. 1 µl of PNGase F (NEB P0704S) was added and mixed gently.

6. The reaction is incubated at 37℃ for 1 hour.

Method III: Making Biotin 1 mM (20X)stock

12.2 mg biotin (Sigma #B4501) was dissolved in 50 ml of serum-free DMEM and pipetted to allow complete dissolution in the media. The biotin solution was sterilized by passing through a 0.22-µm syringe-driven filter unit (Millex) and dispensed into a sterile 50-ml tube which can be stored up to 8 weeks at 4°C.

SUPPLEMENTARY TABLE

I. Global proteome machine (GPM) links to the experimental (SS-BioID2-HYAL2) and control (BioID2 only) samples of two biological replicates

Dataset	GPM link
BioID2 –Control Rep 1 GPM10000003571	http://hs2.proteome.ca/thegpm-cgi/plist.pl?npep=0&path=/gpm/archive/GPM10000003571.xml&proex=-1&ltype=0
BioID2 – HYAL2-Rep1 GPM10000003572	http://hs2.proteome.ca/thegpm-cgi/plist.pl?npep=0&path=/gpm/archive/GPM10000003572.xml&proex=-1&ltype=0
BioID2-Control Rep 2 GPM10000003676	http://hs2.proteome.ca/thegpm-cgi/plist.pl?npep=0&path=/gpm/archive/GPM10000003676.xml&proex=-1&ltype=0
BioID2 – HYAL2-Rep 2 GPM10000003677	http://hs2.proteome.ca/thegpm-cgi/plist.pl?npep=0&path=/gpm/archive/GPM10000003677.xml&proex=-1&ltype=0

II. Consistent unique proteins in HYAL2 interactome from two biological replicates with average (Avg) log I values ≥ 5 after background minimization

	Official Gene symbol	Avg log I value
1	AFG3L2	7.24
2	MCU	7.115
3	NOMO1	7.295
4	PTPRN2	6.735
5	SLC25A20	6.935
6	ARL6IP1	6.825
7	PTK7	6.52
8	GNA13	6.935
9	ERLIN1	6.885
10	TMED1	6.88
11	ITGA9	6.93
12	SLC6A6	6.67
13	MFSD1	6.345
14	TMED5	6.535
15	CLPTM1	6.39

16	TMX2	6.67
17	DNAJC3	7.06
18	ORMDL2	6.51
19	AXIN2	7.175
20	ERP29	6.285
21	PRDX5	6.58
22	CRTAP	6.51
23	FBLN2	6.575
24	DHCR7	6.32
25	PDCD10	6.18
26	TMX3	6.245
27	RAP2C	6.385
28	IFIT2	6.64
29	TOR1B	6.54
30	EIF2B1	6.27
31	IGFN1	6.22
32	YIPF3	6.205
33	TMEM97	6.52
34	FNDC3B	6.275
35	FAR1	6.155
36	STX4	6.255

37	SYNGR2	6.305
38	TMEM168	6.13
39	CD151	6.5
40	GPC4	6.135
41	MRC2	6.145
42	CORO1A	6.305
43	BCL2L13	6.19
44	ITGA5	6.425
45	MANBAL	6.26
46	CCDC47	6.54
47	HDDC2	6.205
48	VWA8	6.465
49	IDH1	6.69
50	PRORP	6.36
51	LYST	6.255
52	AGPAT3	6.075
53	CX3CL1	6.105
54	GPRC5A	6.555
55	MICAL3	6.575
56	NIPSNAP2	6.325
57	TRA2B	6.2

58	UBE4B	6.015
59	FITM2	5.885
60	PRDX3	5.92
61	SEC24D	6.125
62	RDH11	5.93
63	ZEB2	5.8
64	SLC9A3R1	7.06

REFERENCES

1. Dzamba, B., & DeSimone, D. (2018). Extracellular Matrix (ECM) and the Sculpting of Embryonic Tissues. Current Topics In Developmental Biology, 245-274. doi: 10.1016/bs.ctdb.2018.03.006
2. Meyer, K., & Palmer, J.W. THE POLYSACCHARIDE OF THE VITREOUS HUMOR.
3. Papakonstantinou, E., Roth, M., &Karakiulakis, G. (2012). Hyaluronic acid: A key molecule in skin aging. Dermato-Endocrinology, 4(3), 253-258. doi: 10.4161/derm.21923
4. Triggs-Raine, B. (2015). Biology of hyaluronan: Insights from genetic disorders of hyaluronan metabolism. World Journal Of Biological Chemistry, 6(3), 110. doi: 10.4331/wjbc.v6.i3.110
5. Bastow, E., Byers, S., Golub, S., Clarkin, C., Pitsillides, A., &Fosang, A. (2007). Hyaluronan synthesis and degradation in cartilage and bone. Cellular And Molecular Life Sciences, 65(3), 395-413. doi: 10.1007/s00018-007-7360-z
6. Fenderson, B., Stamenkovic, I., & Aruffo, A. (1993). Localization of hyaluronan in mouse embryos during implantation, gastrulation and organogenesis. Differentiation, 54(2), 85-98. doi: 10.1111/j.1432-0436.1993.tb00711.x
7. Gupta, R., Lall, R., Srivastava, A., & Sinha, A. (2019). Hyaluronic Acid: Molecular Mechanisms and Therapeutic Trajectory. Frontiers In Veterinary Science, 6. doi: 10.3389/fvets.2019.00192
8. Chowdhury, B., Hemming, R., Faiyaz, S., & Triggs-Raine, B. (2015). Hyaluronidase 2 (HYAL2) is expressed in endothelial cells, as well as some specialized epithelial cells, and is required for normal hyaluronan catabolism. HistochemistryAnd Cell Biology, 145(1), 53-66. doi: 10.1007/s00418-015-1373-8
9. Fallacara, A., Baldini, E., Manfredini, S., &Vertuani, S. (2018). Hyaluronic Acid in the Third Millennium. Polymers, 10(7), 701. doi: 10.3390/polym10070701
10. Fraser, J., Laurent, T., Pertoft, H., & Baxter, E. (1981). Plasma clearance, tissue distribution and metabolism of hyaluronic acid injected intravenously in the rabbit. Biochemical Journal, 200(2), 415-424. doi: 10.1042/bj2000415
11. SCHILLER, S., & DORFMAN, A. (1957). The metabolism of mucopolysaccharides in animals. IV. The influence of insulin. The Journal of biological chemistry, 227(2), 625–632

12. SIMKIN, P. (2000). Biology of the synovial joint. Annals Of The Rheumatic Diseases, 59(5), 330-330. doi: 10.1136/ard.59.5.330
13. Cyphert, J., Trempus, C., &Garantziotis, S. (2015). Size Matters: Molecular Weight Specificity of Hyaluronan Effects in Cell Biology. International Journal Of Cell Biology, 2015, 1-8. doi: 10.1155/2015/563818
14. Itano, N., Sawai, T., Yoshida, M., Lenas, P., Yamada, Y., &Imagawa, M. et al. (1999). Three Isoforms of Mammalian Hyaluronan Synthases Have Distinct Enzymatic Properties. Journal Of Biological Chemistry, 274(35), 25085-25092. doi: 10.1074/jbc.274.35.25085
15. Spicer, A., Seldin, M., Olsen, A., Brown, N., Wells, D., & Doggett, N. et al. (1997). Chromosomal Localization of the Human and Mouse Hyaluronan Synthase Genes. Genomics, 41(3), 493-497. doi: 10.1006/geno.1997.4696
16. Törrönen, K., Nikunen, K., Kärnä, R., Tammi, M., Tammi, R., & Rilla, K. (2013). Tissue distribution and subcellular localization of hyaluronan synthase isoenzymes. HistochemistryAnd Cell Biology, 141(1), 17-31. doi: 10.1007/s00418-013-1143-4
17. Camenisch, T., Spicer, A., Brehm-Gibson, T., Biesterfeldt, J., Augustine, M., &Calabro, A. et al. (2000). Disruption of hyaluronan synthase-2 abrogates normal cardiac morphogenesis and hyaluronan-mediated transformation of epithelium to mesenchyme. Journal Of Clinical Investigation, 106(3), 349-360. doi: 10.1172/jci10272
18. Bai, K. J., Spicer, A. P., Mascarenhas, M. M., Yu, L., Ochoa, C. D., Garg, H. G., & Quinn, D. A. (2005). The role of hyaluronan synthase 3 in ventilator-induced lung injury. American journal of respiratory and critical care medicine, 172(1), 92–98. https://doi.org/10.1164/rccm.200405-652OC
19. Spicer, A. P., Tien, J. L., Joo, A., & Bowling, R. A., Jr (2002). Investigation of hyaluronan function in the mouse through targeted mutagenesis. Glycoconjugate journal, 19(4-5), 341–345. https://doi.org/10.1023/A:1025321105691
20. Camenisch, T. D., Schroeder, J. A., Bradley, J., Klewer, S. E., & McDonald, J. A. (2002). Heart-valve mesenchyme formation is dependent on hyaluronan-augmented activation of ErbB2-ErbB3 receptors. Nature medicine, 8(8), 850–855. https://doi.org/10.1038/nm742
21. Matsumoto, K., Li, Y., Jakuba, C., Sugiyama, Y., Sayo, T., Okuno, M., Dealy, C. N., Toole, B. P., Takeda, J., Yamaguchi, Y., & Kosher, R. A. (2009). Conditional

inactivation of Has2 reveals a crucial role for hyaluronan in skeletal growth, patterning, chondrocyte maturation and joint formation in the developing limb. Development (Cambridge, England), 136(16), 2825–2835. https://doi.org/10.1242/dev.038505

22. Tien, J. Y., & Spicer, A. P. (2005). Three vertebrate hyaluronan synthases are expressed during mouse development in distinct spatial and temporal patterns. Developmental dynamics : an official publication of the American Association of Anatomists, 233(1), 130–141. https://doi.org/10.1002/dvdy.20328
23. Kobayashi, N., Miyoshi, S., Mikami, T., Koyama, H., Kitazawa, M., Takeoka, M., Sano, K., Amano, J., Isogai, Z., Niida, S., Oguri, K., Okayama, M., McDonald, J. A., Kimata, K., Taniguchi, S., &Itano, N. (2010). Hyaluronan deficiency in tumor stroma impairs macrophage trafficking and tumor neovascularization. Cancer research, 70(18), 7073–7083. https://doi.org/10.1158/0008-5472.CAN-09-4687
24. Adamia, S., Reichert, A. A., Kuppusamy, H., Kriangkum, J., Ghosh, A., Hodges, J. J., Pilarski, P. M., Treon, S. P., Mant, M. J., Reiman, T., Belch, A. R., &Pilarski, L. M. (2008). Inherited and acquired variations in the hyaluronan synthase 1 (HAS1) gene may contribute to disease progression in multiple myeloma and Waldenstrommacroglobulinemia. Blood, 112(13), 5111–5121. https://doi.org/10.1182/blood-2008-02-141770
25. Kuppusamy, H., Ogmundsdottir, H. M., Baigorri, E., Warkentin, A., Steingrimsdottir, H., Haraldsdottir, V., Mant, M. J., Mackey, J., Johnston, J. B., Adamia, S., Belch, A. R., &Pilarski, L. M. (2014). Inherited polymorphisms in hyaluronan synthase 1 predict risk of systemic B-cell malignancies but not of breast cancer. PloS one, 9(6), e100691. https://doi.org/10.1371/journal.pone.0100691
26. Arranz, A. M., Perkins, K. L., Irie, F., Lewis, D. P., Hrabe, J., Xiao, F., Itano, N., Kimata, K., Hrabetova, S., & Yamaguchi, Y. (2014). Hyaluronan deficiency due to Has3 knock-out causes altered neuronal activity and seizures via reduction in brain extracellular space. The Journal of neuroscience : the official journal of the Society for Neuroscience, 34(18), 6164–6176. https://doi.org/10.1523/JNEUROSCI.3458-13.2014
27. Rodén, L., Campbell, P., Fraser, J. R., Laurent, T. C., Pertoft, H., & Thompson, J. N. (1989). Enzymic pathways of hyaluronan catabolism. Ciba Foundation symposium, 143, 60–285. https://doi.org/10.1002/9780470513774.ch5

28. LINKER, A., MEYER, K., & WEISSMANN, B. (1955). Enzumatic formation of monosaccharides from hyaluronate. The Journal of biological chemistry, 213(1), 237–248.
29. Stern, R., &Jedrzejas, M. J. (2006). Hyaluronidases: their genomics, structures, and mechanisms of action. Chemical reviews, 106(3), 818–839. https://doi.org/10.1021/cr050247k
30. Csóka, A. B., Scherer, S. W., & Stern, R. (1999). Expression analysis of six paralogous human hyaluronidase genes clustered on chromosomes 3p21 and 7q31. Genomics, 60(3), 356–361. https://doi.org/10.1006/geno.1999.5876
31. Wei, M. H., Latif, F., Bader, S., Kashuba, V., Chen, J. Y., Duh, F. M., Sekido, Y., Lee, C. C., Geil, L., Kuzmin, I., Zabarovsky, E., Klein, G., Zbar, B., Minna, J. D., &Lerman, M. I. (1996). Construction of a 600-kilobase cosmid clone contig and generation of a transcriptional map surrounding the lung cancer tumor suppressor gene (TSG) locus on human chromosome 3p21.3: progress toward the isolation of a lung cancer TSG. Cancer research, 56(7), 1487–1492.
32. Frost, G. I., Csóka, A. B., Wong, T., & Stern, R. (1997). Purification, cloning, and expression of human plasma hyaluronidase. Biochemical and biophysical research communications, 236(1), 10–15. https://doi.org/10.1006/bbrc.1997.6773
33. Kim, E., Baba, D., Kimura, M., Yamashita, M., Kashiwabara, S., & Baba, T. (2005). Identification of a hyaluronidase, Hyal5, involved in penetration of mouse sperm through cumulus mass. Proceedings of the National Academy of Sciences of the United States of America, 102(50), 18028–18033. https://doi.org/10.1073/pnas.0506825102
34. Zhang, H., & Martin-Deleon, P. A. (2003). Mouse epididymal Spam1 (pH-20) is released in the luminal fluid with its lipid anchor. Journal of andrology, 24(1), 51–58.
35. Kaneiwa, T., Mizumoto, S., Sugahara, K., & Yamada, S. (2010). Identification of human hyaluronidase-4 as a novel chondroitin sulfate hydrolase that preferentially cleaves the galactosaminidic linkage in the trisulfatedtetrasaccharide sequence. Glycobiology, 20(3), 300–309. https://doi.org/10.1093/glycob/cwp174
36. Hemming, R., Martin, D. C., Slominski, E., Nagy, J. I., Halayko, A. J., Pind, S., & Triggs-Raine, B. (2008). Mouse Hyal3 encodes a 45- to 56-kDa glycoprotein whose

overexpression increases hyaluronidase 1 activity in cultured cells. Glycobiology, 18(4), 280–289. https://doi.org/10.1093/glycob/cwn006

37. Zhang, L., Bharadwaj, A. G., Casper, A., Barkley, J., Barycki, J. J., & Simpson, M. A. (2009). Hyaluronidase activity of human Hyal1 requires active site acidic and tyrosine residues. The Journal of biological chemistry, 284(14), 9433–9442. https://doi.org/10.1074/jbc.M900210200
38. REISSIG, J. L., STORMINGER, J. L., & LELOIR, L. F. (1955). A modified colorimetric method for the estimation of N-acetylamino sugars. The Journal of biological chemistry, 217(2), 959–966.
39. Frost, G. I., & Stern, R. (1997). A microtiter-based assay for hyaluronidase activity not requiring specialized reagents. Analytical biochemistry, 251(2), 263–269. https://doi.org/10.1006/abio.1997.2262
40. Guntenhöner, M. W., Pogrel, M. A., & Stern, R. (1992). A substrate-gel assay for hyaluronidase activity. Matrix (Stuttgart, Germany), 12(5), 388–396. https://doi.org/10.1016/s0934-8832(11)80035-1
41. Lepperdinger, G., Strobl, B., & Kreil, G. (1998). HYAL2, a human gene expressed in many cells, encodes a lysosomal hyaluronidase with a novel type of specificity. The Journal of biological chemistry, 273(35), 22466–22470. https://doi.org/10.1074/jbc.273.35.22466
42. Bourguignon, L. Y., Singleton, P. A., Diedrich, F., Stern, R., & Gilad, E. (2004). CD44 interaction with Na+-H+ exchanger (NHE1) creates acidic microenvironments leading to hyaluronidase-2 and cathepsin B activation and breast tumor cell invasion. The Journal of biological chemistry, 279(26), 26991–27007. https://doi.org/10.1074/jbc.M311838200
43. Vigdorovich, V., Strong, R. K., & Miller, A. D. (2005). Expression and characterization of a soluble, active form of the jaagsiekte sheep retrovirus receptor, Hyal2. Journal of virology, 79(1), 79–86. https://doi.org/10.1128/JVI.79.1.79-86.2005
44. Vigdorovich, V., Miller, A. D., & Strong, R. K. (2007). Ability of hyaluronidase 2 to degrade extracellular hyaluronan is not required for its function as a receptor for jaagsiekte sheep retrovirus. Journal of virology, 81(7), 3124–3129. https://doi.org/10.1128/JVI.02177-06

45. Harada, H., & Takahashi, M. (2007). CD44-dependent intracellular and extracellular catabolism of hyaluronic acid by hyaluronidase-1 and -2. The Journal of biological chemistry, 282(8), 5597–5607. https://doi.org/10.1074/jbc.M608358200
46. Shuttleworth, T. L., Wilson, M. D., Wicklow, B. A., Wilkins, J. A., & Triggs-Raine, B. L. (2002). Characterization of the murine hyaluronidase gene region reveals complex organization and cotranscription of Hyal1 with downstream genes, Fus2 and Hyal3. The Journal of biological chemistry, 277(25), 23008–23018. https://doi.org/10.1074/jbc.M108991200
47. Puissant, E., Gilis, F., Dogné, S., Flamion, B., Jadot, M., & Boonen, M. (2014). Subcellular trafficking and activity of Hyal-1 and its processed forms in murine macrophages. Traffic (Copenhagen, Denmark), 15(5), 500–515. https://doi.org/10.1111/tra.12162
48. Gasingirwa, M. C., Thirion, J., Mertens-Strijthagen, J., Wattiaux-De Coninck, S., Flamion, B., Wattiaux, R., & Jadot, M. (2010). Endocytosis of hyaluronidase-1 by the liver. The Biochemical journal, 430(2), 305–313. https://doi.org/10.1042/BJ20100711
49. Chao, K. L., Muthukumar, L., & Herzberg, O. (2007). Structure of human hyaluronidase-1, a hyaluronan hydrolyzing enzyme involved in tumor growth and angiogenesis. Biochemistry, 46(23), 6911–6920. https://doi.org/10.1021/bi700382g
50. Triggs-Raine, B., Salo, T. J., Zhang, H., Wicklow, B. A., & Natowicz, M. R. (1999). Mutations in HYAL1, a member of a tandemly distributed multigene family encoding disparate hyaluronidase activities, cause a newly described lysosomal disorder, mucopolysaccharidosis IX. Proceedings of the National Academy of Sciences of the United States of America, 96(11), 6296–6300. https://doi.org/10.1073/pnas.96.11.6296
51. Martin, D. C., Atmuri, V., Hemming, R. J., Farley, J., Mort, J. S., Byers, S., Hombach-Klonisch, S., Csoka, A. B., Stern, R., & Triggs-Raine, B. L. (2008). A mouse model of human mucopolysaccharidosis IX exhibits osteoarthritis. Human molecular genetics, 17(13), 1904–1915. https://doi.org/10.1093/hmg/ddn088
52. Strobl, B., Wechselberger, C., Beier, D. R., & Lepperdinger, G. (1998). Structural organization and chromosomal localization of Hyal2, a gene encoding a lysosomal hyaluronidase. Genomics, 53(2), 214–219. https://doi.org/10.1006/geno.1998.5472

53. Rai, S. K., Duh, F. M., Vigdorovich, V., Danilkovitch-Miagkova, A., Lerman, M. I., & Miller, A. D. (2001). Candidate tumor suppressor HYAL2 is a glycosylphosphatidylinositol (GPI)-anchored cell-surface receptor for jaagsiekte sheep retrovirus, the envelope protein of which mediates oncogenic transformation. Proceedings of the National Academy of Sciences of the United States of America, 98(8), 4443–4448. https://doi.org/10.1073/pnas.071572898
54. Andre, B., Duterme, C., Van Moer, K., Mertens-Strijthagen, J., Jadot, M., & Flamion, B. (2011). Hyal2 is a glycosylphosphatidylinositol-anchored, lipid raft-associated hyaluronidase. Biochemical and biophysical research communications, 411(1), 175–179. https://doi.org/10.1016/j.bbrc.2011.06.125
55. Marei, W. F., Salavati, M., & Fouladi-Nashta, A. A. (2013). Critical role of hyaluronidase-2 during preimplantation embryo development. Molecular human reproduction, 19(9), 590–599. https://doi.org/10.1093/molehr/gat032
56. Miller, A. D., Vigdorovich, V., Strong, R. K., Fernandes, R. J., & Lerman, M. I. (2006). Hyal2, where are you?. Osteoarthritis and cartilage, 14(12), 1315–1317. https://doi.org/10.1016/j.joca.2006.08.004
57. Lepperdinger, G., Müllegger, J., & Kreil, G. (2001). Hyal2--less active, but more versatile?. Matrix biology : journal of the International Society for Matrix Biology, 20(8), 509–514. https://doi.org/10.1016/s0945-053x(01)00170-6
58. Bourguignon, V., & Flamion, B. (2016). Respective roles of hyaluronidases 1 and 2 in endogenous hyaluronan turnover. FASEB journal : official publication of the Federation of American Societies for Experimental Biology, 30(6), 2108–2114. https://doi.org/10.1096/fj.201500178R
59. Chow, G., Knudson, C. B., & Knudson, W. (2006). Expression and cellular localization of human hyaluronidase-2 in articular chondrocytes and cultured cell lines. Osteoarthritis and cartilage, 14(9), 849–858. https://doi.org/10.1016/j.joca.2006.02.009
60. Duterme, C., Mertens-Strijthagen, J., Tammi, M., & Flamion, B. (2009). Two novel functions of hyaluronidase-2 (Hyal2) are formation of the glycocalyx and control of CD44-ERM interactions. The Journal of biological chemistry, 284(48), 33495–33508. https://doi.org/10.1074/jbc.M109.044362

61. Chang N. S. (2002). Transforming growth factor-beta1 blocks the enhancement of tumor necrosis factor cytotoxicity by hyaluronidase Hyal-2 in L929 fibroblasts. BMC cell biology, 3, 8. https://doi.org/10.1186/1471-2121-3-8
62. Hsu, L. J., Schultz, L., Hong, Q., Van Moer, K., Heath, J., Li, M. Y., Lai, F. J., Lin, S. R., Lee, M. H., Lo, C. P., Lin, Y. S., Chen, S. T., & Chang, N. S. (2009). Transforming growth factor beta1 signaling via interaction with cell surface Hyal-2 and recruitment of WWOX/WOX1. The Journal of biological chemistry, 284(23), 16049–16059. https://doi.org/10.1074/jbc.M806688200
63. de la Motte, C., Nigro, J., Vasanji, A., Rho, H., Kessler, S., Bandyopadhyay, S., Danese, S., Fiocchi, C., & Stern, R. (2009). Platelet-derived hyaluronidase 2 cleaves hyaluronan into fragments that trigger monocyte-mediated production of proinflammatory cytokines. The American journal of pathology, 174(6), 2254–2264. https://doi.org/10.2353/ajpath.2009.080831
64. Girish, K. S., & Kemparaju, K. (2007). The magic glue hyaluronan and its eraser hyaluronidase: a biological overview. Life sciences, 80(21), 1921–1943. https://doi.org/10.1016/j.lfs.2007.02.037
65. Vigetti, D., Karousou, E., Viola, M., Deleonibus, S., De Luca, G., & Passi, A. (2014). Hyaluronan: biosynthesis and signaling. Biochimica et biophysica acta, 1840(8), 2452–2459. https://doi.org/10.1016/j.bbagen.2014.02.001
66. Turley, E. A., Noble, P. W., & Bourguignon, L. Y. (2002). Signaling properties of hyaluronan receptors. The Journal of biological chemistry, 277(7), 4589–4592. https://doi.org/10.1074/jbc.R100038200
67. Toole B. P. (2004). Hyaluronan: from extracellular glue to pericellular cue. Nature reviews. Cancer, 4(7), 528–539. https://doi.org/10.1038/nrc1391
68. Mattheolabakis, G., Milane, L., Singh, A., & Amiji, M. M. (2015). Hyaluronic acid targeting of CD44 for cancer therapy: from receptor biology to nanomedicine. Journal of drug targeting, 23(7-8), 605–618. https://doi.org/10.3109/1061186X.2015.1052072
69. Masellis-Smith, A., Belch, A. R., Mant, M. J., Turley, E. A., & Pilarski, L. M. (1996). Hyaluronan-dependent motility of B cells and leukemic plasma cells in blood, but not of bone marrow plasma cells, in multiple myeloma: alternate use of receptor for hyaluronan-mediated motility (RHAMM) and CD44. Blood, 87(5), 1891–1899.

70. Lokeshwar, V. B., & Selzer, M. G. (2000). Differences in hyaluronic acid-mediated functions and signaling in arterial, microvessel, and vein-derived human endothelial cells. The Journal of biological chemistry, 275(36), 27641–27649. https://doi.org/10.1074/jbc.M003084200
71. Hirose, Y., Saijou, E., Sugano, Y., Takeshita, F., Nishimura, S., Nonaka, H., Chen, Y. R., Sekine, K., Kido, T., Nakamura, T., Kato, S., Kanke, T., Nakamura, K., Nagai, R., Ochiya, T., & Miyajima, A. (2012). Inhibition of Stabilin-2 elevates circulating hyaluronic acid levels and prevents tumor metastasis. Proceedings of the National Academy of Sciences of the United States of America, 109(11), 4263–4268. https://doi.org/10.1073/pnas.1117560109
72. del Fresno, C., Otero, K., Gómez-García, L., González-León, M. C., Soler-Ranger, L., Fuentes-Prior, P., Escoll, P., Baos, R., Caveda, L., García, F., Arnalich, F., & López-Collazo, E. (2005). Tumor cells deactivate human monocytes by up-regulating IL-1 receptor associated kinase-M expression via CD44 and TLR4. Journal of immunology (Baltimore, Md. : 1950), 174(5), 3032–3040. https://doi.org/10.4049/jimmunol.174.5.3032
73. Chang, E. J., Kim, H. J., Ha, J., Kim, H. J., Ryu, J., Park, K. H., Kim, U. H., Lee, Z. H., Kim, H. M., Fisher, D. E., & Kim, H. H. (2007). Hyaluronan inhibits osteoclast differentiation via Toll-like receptor 4. Journal of cell science, 120(Pt 1), 166–176. https://doi.org/10.1242/jcs.03310
74. Toole B. P. (2001). Hyaluronan in morphogenesis. Seminars in cell & developmental biology, 12(2), 79–87. https://doi.org/10.1006/scdb.2000.0244
75. Evanko, S. P., & Wight, T. N. (1999). Intracellular localization of hyaluronan in proliferating cells. The journal of histochemistry and cytochemistry : official journal of the Histochemistry Society, 47(10), 1331–1342. https://doi.org/10.1177/002215549904701013
76. Day, A. J., & Prestwich, G. D. (2002). Hyaluronan-binding proteins: tying up the giant. The Journal of biological chemistry, 277(7), 4585–4588. https://doi.org/10.1074/jbc.R100036200

77. Kultti, A., Rilla, K., Tiihonen, R., Spicer, A. P., Tammi, R. H., & Tammi, M. I. (2006). Hyaluronan synthesis induces microvillus-like cell surface protrusions. The Journal of biological chemistry, 281(23), 15821–15828. https://doi.org/10.1074/jbc.M512840200
78. Turley, E. A., & Roth, S. (1979). Spontaneous glycosylation of glycosaminoglycan substrates by adherent fibroblasts. Cell, 17(1), 109–115. https://doi.org/10.1016/0092-8674(79)90299-x
79. Turley, E. A., Bowman, P., & Kytryk, M. A. (1985). Effects of hyaluronate and hyaluronate binding proteins on cell motile and contact behaviour. Journal of cell science, 78, 133–145.
80. Turley, E. A., Austen, L., Vandeligt, K., & Clary, C. (1991). Hyaluronan and a cell-associated hyaluronan binding protein regulate the locomotion of ras-transformed cells. The Journal of cell biology, 112(5), 1041–1047. https://doi.org/10.1083/jcb.112.5.1041
81. Ruoslahti, E., & Yamaguchi, Y. (1991). Proteoglycans as modulators of growth factor activities. Cell, 64(5), 867–869. https://doi.org/10.1016/0092-8674(91)90308-l
82. Nieto M. A. (2001). The early steps of neural crest development. Mechanisms of development, 105(1-2), 27–35. https://doi.org/10.1016/s0925-4773(01)00394-x
83. Shukla, S., Nair, R., Rolle, M. W., Braun, K. R., Chan, C. K., Johnson, P. Y., Wight, T. N., & McDevitt, T. C. (2010). Synthesis and organization of hyaluronan and versican by embryonic stem cells undergoing embryoid body differentiation. The journal of histochemistry and cytochemistry : official journal of the Histochemistry Society, 58(4), 345–358. https://doi.org/10.1369/jhc.2009.954826
84. Zoltan-Jones, A., Huang, L., Ghatak, S., & Toole, B. P. (2003). Elevated hyaluronan production induces mesenchymal and transformed properties in epithelial cells. The Journal of biological chemistry, 278(46), 45801–45810. https://doi.org/10.1074/jbc.M308168200
85. Kosaki, R., Watanabe, K., & Yamaguchi, Y. (1999). Overproduction of hyaluronan by expression of the hyaluronan synthase Has2 enhances anchorage-independent growth and tumorigenicity. Cancer research, 59(5), 1141–1145.
86. Markwald, R. R., Fitzharris, T. P., Bank, H., & Bernanke, D. H. (1978). Structural analyses on the matrical organization of glycosaminoglycans in developing endocardial

cushions. Developmental biology, 62(2), 292–316. https://doi.org/10.1016/0012-1606(78)90218-x

87. Morris-Wiman, J., & Brinkley, L. (1992). An extracellular matrix infrastructure provides support for murine secondary palatal shelf remodelling. The Anatomical record, 234(4), 575–586. https://doi.org/10.1002/ar.1092340413
88. Weston, J. A., Pintar, J. E., Derby, M. A., & Nichols, D. H. (1977). The morphogenesis of spinal ganglia from neural crest cells. Progress in clinical and biological research, 15, 217–226.
89. von Gise, A., & Pu, W. T. (2012). Endocardial and epicardial epithelial to mesenchymal transitions in heart development and disease. Circulation research, 110(12), 1628–1645. https://doi.org/10.1161/CIRCRESAHA.111.259960
90. Camenisch, T. D., Schroeder, J. A., Bradley, J., Klewer, S. E., & McDonald, J. A. (2002). Heart-valve mesenchyme formation is dependent on hyaluronan-augmented activation of ErbB2-ErbB3 receptors. Nature medicine, 8(8), 850–855. https://doi.org/10.1038/nm742
91. Rodgers, L. S., Lalani, S., Hardy, K. M., Xiang, X., Broka, D., Antin, P. B., & Camenisch, T. D. (2006). Depolymerized hyaluronan induces vascular endothelial growth factor, a negative regulator of developmental epithelial-to-mesenchymal transformation. Circulation research, 99(6), 583–589. https://doi.org/10.1161/01.RES.0000242561.95978.43
92. Nandadasa, S., Foulcer, S., & Apte, S. S. (2014). The multiple, complex roles of versican and its proteolytic turnover by ADAMTS proteases during embryogenesis. Matrix biology : journal of the International Society for Matrix Biology, 35, 34–41. https://doi.org/10.1016/j.matbio.2014.01.005
93. Toole B., Banerjee S., Turner R., Munaim S., Knudson C. (1991) Hyaluronan-Cell Interactions in Limb Development. In: Hinchliffe J.R., Hurle J.M., Summerbell D. (eds) Developmental Patterning of the Vertebrate Limb. NATO ASI Series (Series A: Life Sciences), vol 205. Springer, Boston, MA. https://doi.org/10.1007/978-1-4615-3310-8_30
94. Maleski, M. P., & Knudson, C. B. (1996). Hyaluronan-mediated aggregation of limb bud mesenchyme and mesenchymal condensation during chondrogenesis. Experimental cell research, 225(1), 55–66. https://doi.org/10.1006/excr.1996.0156

95. Chowdhury, B., Xiang, B., Liu, M., Hemming, R., Dolinsky, V. W., & Triggs-Raine, B. (2017). Hyaluronidase 2 Deficiency Causes Increased Mesenchymal Cells, Congenital Heart Defects, and Heart Failure. Circulation. Cardiovascular genetics, 10(1), e001598. https://doi.org/10.1161/CIRCGENETICS.116.001598
96. Taneyhill, L. A., & Bronner-Fraser, M. (2005). Recycling signals in the neural crest. Journal of biology, 4(3), 10. https://doi.org/10.1186/jbiol31
97. Etchevers, H. C., Amiel, J., & Lyonnet, S. (2006). Molecular bases of human neurocristopathies. Advances in experimental medicine and biology, 589, 213–234. https://doi.org/10.1007/978-0-387-46954-6_14
98. Bernanke, D. H., & Orkin, R. W. (1984). Hyaluronate binding and degradation by cultured embryonic chick cardiac cushion and myocardial cells. Developmental biology, 106(2), 360–367. https://doi.org/10.1016/0012-1606(84)90234-3
99. Chowdhury, B., Hemming, R., Hombach-Klonisch, S., Flamion, B., & Triggs-Raine, B. (2013). Murine hyaluronidase 2 deficiency results in extracellular hyaluronan accumulation and severe cardiopulmonary dysfunction. The Journal of biological chemistry, 288(1), 520–528. https://doi.org/10.1074/jbc.M112.393629
100. Muggenthaler, M. M., Chowdhury, B., Hasan, S. N., Cross, H. E., Mark, B., Harlalka, G. V., Patton, M. A., Ishida, M., Behr, E. R., Sharma, S., Zahka, K., Faqeih, E., Blakley, B., Jackson, M., Lees, M., Dolinsky, V., Cross, L., Stanier, P., Salter, C., Baple, E. L., … Chioza, B. A. (2017). Mutations in HYAL2, Encoding Hyaluronidase 2, Cause a Syndrome of Orofacial Clefting and Cor Triatriatum Sinister in Humans and Mice. PLoS genetics, 13(1), e1006470. https://doi.org/10.1371/journal.pgen.1006470
101. Burk D. T. (1983). Distribution of glycosaminoglycans in the developing facial region of mouse embryos. Journal of craniofacial genetics and developmental biology, 3(4), 339–349.
102. Knudsen, T. B., Bulleit, R. F., & Zimmerman, E. F. (1985). Histochemical localization of glycosaminoglycans during morphogenesis of the secondary palate in mice. Anatomy and embryology, 173(1), 137–142. https://doi.org/10.1007/BF00707312
103. Galloway, J. L., Jones, S. J., Mossey, P. A., & Ellis, I. R. (2013). The control and importance of hyaluronan synthase expression in palatogenesis. Frontiers in physiology, 4, 10. https://doi.org/10.3389/fphys.2013.00010

104. Toole, B. P., & Trelstad, R. L. (1971). Hyaluronate production and removal during corneal development in the chick. Developmental biology, 26(1), 28–35. https://doi.org/10.1016/0012-1606(71)90104-7
105. Haddon, C. M., & Lewis, J. H. (1991). Hyaluronan as a propellant for epithelial movement: the development of semicircular canals in the inner ear of Xenopus. Development (Cambridge, England), 112(2), 541–550.
106. Pohl, M., Sakurai, H., Stuart, R. O., & Nigam, S. K. (2000). Role of hyaluronan and CD44 in in vitro branching morphogenesis of ureteric bud cells. Developmental biology, 224(2), 312–325. https://doi.org/10.1006/dbio.2000.9783
107. Jadin, L., Wu, X., Ding, H., Frost, G. I., Onclinx, C., Triggs-Raine, B., & Flamion, B. (2008). Skeletal and hematological anomalies in HYAL2-deficient mice: a second type of mucopolysaccharidosis IX?. FASEB journal : official publication of the Federation of American Societies for Experimental Biology, 22(12), 4316–4326. https://doi.org/10.1096/fj.08-111997
108. Chowdhury, B., Xiang, B., Muggenthaler, M., Dolinsky, V. W., & Triggs-Raine, B. (2016). Hyaluronidase 2 deficiency is a molecular cause of cor triatriatum sinister in mice. International journal of cardiology, 209, 281–283. https://doi.org/10.1016/j.ijcard.2016.02.072
109. Fenderson, B. A., Stamenkovic, I., & Aruffo, A. (1993). Localization of hyaluronan in mouse embryos during implantation, gastrulation and organogenesis. Differentiation; research in biological diversity, 54(2), 85–98. https://doi.org/10.1111/j.1432-0436.1993.tb00711.x
110. Danilkovitch-Miagkova, A., Duh, F. M., Kuzmin, I., Angeloni, D., Liu, S. L., Miller, A. D., & Lerman, M. I. (2003). Hyaluronidase 2 negatively regulates RON receptor tyrosine kinase and mediates transformation of epithelial cells by jaagsiekte sheep retrovirus. Proceedings of the National Academy of Sciences of the United States of America, 100(8), 4580–4585. https://doi.org/10.1073/pnas.0837136100
111. Zurzolo, C., & Simons, K. (2016). Glycosylphosphatidylinositol-anchored proteins: Membrane organization and transport. Biochimica et biophysica acta, 1858(4), 632–639. https://doi.org/10.1016/j.bbamem.2015.12.018

112. Mellacheruvu, D., Wright, Z., Couzens, A. L., Lambert, J. P., St-Denis, N. A., Li, T., Miteva, Y. V., Hauri, S., Sardiu, M. E., Low, T. Y., Halim, V. A., Bagshaw, R. D., Hubner, N. C., Al-Hakim, A., Bouchard, A., Faubert, D., Fermin, D., Dunham, W. H., Goudreault, M., Lin, Z. Y., … Nesvizhskii, A. I. (2013). The CRAPome: a contaminant repository for affinity purification-mass spectrometry data. Nature methods, 10(8), 730–736. https://doi.org/10.1038/nmeth.2557
113. Al'Qteishat, A., Gaffney, J., Krupinski, J., Rubio, F., West, D., Kumar, S., Kumar, P., Mitsios, N., & Slevin, M. (2006). Changes in hyaluronan production and metabolism following ischaemic stroke in man. Brain : a journal of neurology, 129(Pt 8), 2158–2176. https://doi.org/10.1093/brain/awl139
114. Turino, G. M., & Cantor, J. O. (2003). Hyaluronan in respiratory injury and repair. American journal of respiratory and critical care medicine, 167(9), 1169–1175. https://doi.org/10.1164/rccm.200205-449PP
115. Toole, B. P., Wight, T. N., & Tammi, M. I. (2002). Hyaluronan-cell interactions in cancer and vascular disease. The Journal of biological chemistry, 277(7), 4593–4596. https://doi.org/10.1074/jbc.R100039200
116. Camenisch, T. D., Spicer, A. P., Brehm-Gibson, T., Biesterfeldt, J., Augustine, M. L., Calabro, A., Jr, Kubalak, S., Klewer, S. E., & McDonald, J. A. (2000). Disruption of hyaluronan synthase-2 abrogates normal cardiac morphogenesis and hyaluronan-mediated transformation of epithelium to mesenchyme. The Journal of clinical investigation, 106(3), 349–360. https://doi.org/10.1172/JCI10272
117. Higuchi, Y., Nishida, Y., Kozawa, E., Zhuo, L., Arai, E., Hamada, S., Morita, D., Ikuta, K., Kimata, K., Ushida, T., & Ishiguro, N. (2017). Conditional knockdown of hyaluronidase 2 in articular cartilage stimulates osteoarthritic progression in a mice model. Scientific reports, 7(1), 7028. https://doi.org/10.1038/s41598-017-07376-5
118. Gibson, T. J., Seiler, M., & Veitia, R. A. (2013). The transience of transient overexpression. Nature methods, 10(8), 715–721. https://doi.org/10.1038/nmeth.2534
119. Moriya H. (2015). Quantitative nature of overexpression experiments. Molecular biology of the cell, 26(22), 3932–3939. https://doi.org/10.1091/mbc.E15-07-0512
120. Boyle, E. I., Weng, S., Gollub, J., Jin, H., Botstein, D., Cherry, J. M., & Sherlock, G. (2004). GO::TermFinder--open source software for accessing Gene Ontology information

and finding significantly enriched Gene Ontology terms associated with a list of genes. Bioinformatics (Oxford, England), 20(18), 3710–3715. https://doi.org/10.1093/bioinformatics/bth456

121. Huang, d., Sherman, B. T., & Lempicki, R. A. (2009). Systematic and integrative analysis of large gene lists using DAVID bioinformatics resources. Nature protocols, 4(1), 44–57. https://doi.org/10.1038/nprot.2008.211
122. Xia, J., Gill, E. E., & Hancock, R. E. (2015). NetworkAnalyst for statistical, visual and network-based meta-analysis of gene expression data. Nature protocols, 10(6), 823–844. https://doi.org/10.1038/nprot.2015.052
123. Liu, L., Alonso, V., Guo, L., Tourkova, I., Henderson, S. E., Almarza, A. J., Friedman, P. A., & Blair, H. C. (2012). Na+/H+ exchanger regulatory factor 1 (NHERF1) directly regulates osteogenesis. The Journal of biological chemistry, 287(52), 43312–43321. https://doi.org/10.1074/jbc.M112.422766
124. Shenolikar, S., Voltz, J. W., Cunningham, R., & Weinman, E. J. (2004). Regulation of ion transport by the NHERF family of PDZ proteins. Physiology (Bethesda, Md.), 19, 362–369. https://doi.org/10.1152/physiol.00020.2004
125. LeClair, E. E., Mui, S. R., Huang, A., Topczewska, J. M., & Topczewski, J. (2009). Craniofacial skeletal defects of adult zebrafish Glypican 4 (knypek) mutants. Developmental dynamics : an official publication of the American Association of Anatomists, 238(10), 2550–2563. https://doi.org/10.1002/dvdy.22086
126. Sisson, B. E., Dale, R. M., Mui, S. R., Topczewska, J. M., & Topczewski, J. (2015). A role of glypican4 and wnt5b in chondrocyte stacking underlying craniofacial cartilage morphogenesis. Mechanisms of development, 138 Pt 3, 279–290. https://doi.org/10.1016/j.mod.2015.10.001
127. Rochard, L., Monica, S. D., Ling, I. T., Kong, Y., Roberson, S., Harland, R., Halpern, M., & Liao, E. C. (2016). Roles of Wnt pathway genes wls, wnt9a, wnt5b, frzb and gpc4 in regulating convergent-extension during zebrafish palate morphogenesis. Development (Cambridge, England), 143(14), 2541–2547. https://doi.org/10.1242/dev.137000
128. Mehus, A. A., Anderson, R. H., & Roux, K. J. (2016). BioID Identification of Lamin-Associated Proteins. Methods in enzymology, 569, 3–22. https://doi.org/10.1016/bs.mie.2015.08.008

129. Midgley, A. C., Woods, E. L., Jenkins, R. H., Brown, C., Khalid, U., Chavez, R., Hascall, V., Steadman, R., Phillips, A. O., & Meran, S. (2020). Hyaluronidase-2 Regulates RHOA Signaling, Myofibroblast Contractility, and Other Key Profibrotic Myofibroblast Functions. The American journal of pathology, 190(6), 1236–1255. https://doi.org/10.1016/j.ajpath.2020.02.012
130. O'Hayre, M., Inoue, A., Kufareva, I., Wang, Z., Mikelis, C. M., Drummond, R. A., Avino, S., Finkel, K., Kalim, K. W., DiPasquale, G., Guo, F., Aoki, J., Zheng, Y., Lionakis, M. S., Molinolo, A. A., & Gutkind, J. S. (2016). Inactivating mutations in GNA13 and RHOA in Burkitt's lymphoma and diffuse large B-cell lymphoma: a tumor suppressor function for the Gα13/RHOA axis in B cells. Oncogene, 35(29), 3771–3780. https://doi.org/10.1038/onc.2015.442
131. Suzuki, N., Nakamura, S., Mano, H., & Kozasa, T. (2003). Galpha 12 activates Rho GTPase through tyrosine-phosphorylated leukemia-associated RhoGEF. Proceedings of the National Academy of Sciences of the United States of America, 100(2), 733–738. https://doi.org/10.1073/pnas.0234057100
132. Letra, A., Bjork, B., Cooper, M. E., Szabo-Rogers, H., Deleyiannis, F. W., Field, L. L., Czeizel, A. E., Ma, L., Garlet, G. P., Poletta, F. A., Mereb, J. C., Lopez-Camelo, J. S., Castilla, E. E., Orioli, I. M., Wendell, S., Blanton, S. H., Liu, K., Hecht, J. T., Marazita, M. L., Vieira, A. R., … Silva, R. M. (2012). Association of AXIN2 with non-syndromic oral clefts in multiple populations. Journal of dental research, 91(5), 473–478. https://doi.org/10.1177/0022034512440578
133. Letra, A., Menezes, R., Granjeiro, J. M., & Vieira, A. R. (2009). AXIN2 and CDH1 polymorphisms, tooth agenesis, and oral clefts. Birth defects research. Part A, Clinical and molecular teratology, 85(2), 169–173. https://doi.org/10.1002/bdra.20489
134. Mostowska, A., Hozyasz, K. K., Wójcicki, P., Lasota, A., Dunin-Wilczyńska, I., & Jagodziński, P. P. (2012). Association of DVL2 and AXIN2 gene polymorphisms with cleft lip with or without cleft palate in a Polish population. Birth defects research. Part A, Clinical and molecular teratology, 94(11), 943–950. https://doi.org/10.1002/bdra.23056
135. Rafighdoost, H., Hashemi, M., Danesh, H., Bizhani, F., Bahari, G., & Taheri, M. (2017). Association of single nucleotide polymorphisms in AXIN2, BMP4, and IRF6 with Non-Syndromic Cleft Lip with or without Cleft Palate in a sample of the southeast Iranian

population. Journal of applied oral science : revista FOB, 25(6), 650–656. https://doi.org/10.1590/1678-7757-2017-0191

136. Kim, D. I., Jensen, S. C., Noble, K. A., Kc, B., Roux, K. H., Motamedchaboki, K., & Roux, K. J. (2016). An improved smaller biotin ligase for BioID proximity labeling. Molecular biology of the cell, 27(8), 1188–1196. https://doi.org/10.1091/mbc.E15-12-0844

137. Varnaitė, R., & MacNeill, S. A. (2016). Meet the neighbors: Mapping local protein interactomes by proximity-dependent labeling with BioID. Proteomics, 16(19), 2503–2518. https://doi.org/10.1002/pmic.201600123

138. Balakrishnan, R., Harris, M. A., Huntley, R., Van Auken, K., & Cherry, J. M. (2013). A guide to best practices for Gene Ontology (GO) manual annotation. Database : the journal of biological databases and curation, 2013, bat054. https://doi.org/10.1093/database/bat054

139. Harris, M. A., Clark, J., Ireland, A., Lomax, J., Ashburner, M., Foulger, R., Eilbeck, K., Lewis, S., Marshall, B., Mungall, C., Richter, J., Rubin, G. M., Blake, J. A., Bult, C., Dolan, M., Drabkin, H., Eppig, J. T., Hill, D. P., Ni, L., Ringwald, M., … Gene Ontology Consortium (2004). The Gene Ontology (GO) database and informatics resource. Nucleic acids research, 32(Database issue), D258–D261. https://doi.org/10.1093/nar/gkh036

140. Pontén, F., Gry, M., Fagerberg, L., Lundberg, E., Asplund, A., Berglund, L., Oksvold, P., Björling, E., Hober, S., Kampf, C., Navani, S., Nilsson, P., Ottosson, J., Persson, A., Wernérus, H., Wester, K., & Uhlén, M. (2009). A global view of protein expression in human cells, tissues, and organs. Molecular systems biology, 5, 337. https://doi.org/10.1038/msb.2009.93

141. Pontén, F., Schwenk, J. M., Asplund, A., & Edqvist, P. H. (2011). The Human Protein Atlas as a proteomic resource for biomarker discovery. Journal of internal medicine, 270(5), 428–446. https://doi.org/10.1111/j.1365-2796.2011.02427.x

142. Roux, K. J., Kim, D. I., Burke, B., & May, D. G. (2018). BioID: A Screen for Protein-Protein Interactions. Current protocols in protein science, 91, 19.23.1–19.23.15. https://doi.org/10.1002/cpps.51